

**Data Report for  
Video Plankton Recorder Cruise  
R/V Peter W. Anderson, March 12-14, 1998**

---

Massachusetts Water Resources Authority

Environmental Quality Department  
ENQUAD Report 1998-22



**Data Report for Video Plankton Recorder Cruise  
R/V *Peter W. Anderson*, March 12-14, 1998**

**Cabell S. Davis  
and  
Scott M. Gallager**

**Consultants to:  
SeaScan Inc., 346 Gifford St., Falmouth, MA 02540  
(Under Subcontract with Battelle Ocean Sciences,  
397 Washington St., Duxbury, MA 02332)**

**Submitted to**

**Massachusetts Water Resources Authority  
Environmental Quality Department  
100 First Avenue  
Charlestown Navy Yard  
Boston, MA 02129**

Davis CS and Gallager SM. 1998. Data Report for Video Plankton Recorder Cruise R/V Peter W Anderson, March 12-14, 1998. Boston: Massachusetts Water Resources Authority. Report 1998-22. 118 p.

## EXECUTIVE SUMMARY

Plankton population abundance varies over a broad range of temporal and spatial scales. Due to technological limitations, this variability has been largely undersampled, and as a result, we have a limited understanding of both the variations in population size as well as the underlying processes controlling it. In Massachusetts and Cape Cod Bays, there is an important societal need to understand the variations in the plankton, as this region is becoming increasingly impacted by anthropogenic sources of contaminants. The Bays provide a rich source of seafood and serve as a principal feeding habitat for the endangered northern right whale.

In preparation for the relocation of the Boston Harbor Sewer Outfall 15 km offshore into western Massachusetts Bay, considerable effort has been mounted to monitor many ecological components of Bays system including the plankton, benthos, and fishes. The zooplankton monitoring has consisted of 12 stations sampled 6 times per year, and there now exists several years of baseline data. Although the sampling is sparse by design, these data are thought to provide adequate baseline information for determining possible changes in the zooplankton populations after the new outfall comes on line. Detecting change however will not necessarily provide insights into the causes of the change or what remedial action may be needed.

In order to augment the baseline plankton data with high-resolution distributional data on plankton and associated environmental variables, we conducted a Video Plankton Recorder survey covering the entire region of Massachusetts and Cape Cod Bays during March 12-14, 1998. These data will help provide insights into how and why the plankton is distributed in the Bays over a broad range of scales. This report describes the methods used during the cruise as well as the post-cruise data processing, visualization, and analysis.

Data were collected continuously for 58 hours covering an along track distance of 350 nautical miles, with a spatial resolution of centimeters. Data were obtained for temperature, salinity, fluorescence, beam attenuation, downwelling light, and abundance of dominant zooplankton and large phytoplankton taxa (rod-shaped diatoms, *Chaetoceros* chains, *Oithona*, *Oithona* w/ eggs, unidentified copepods, ostracod/barnacle cyprids, larvaceans, barnacle nauplii, and pteropods). Plankton data were obtained from automatic identification of ~300,000 high-magnification images of plankton captured during the survey.

Two main water types were found in the Bays, and we have termed these Massachusetts Bay Bottom Water (MBBW) and Cape Ann Plume Water (CAPW). The colder-fresher CAPW was present in the upper part of the water column throughout the northern and western parts of the Bays, while the warmer-saltier MBBW was present throughout the lower part of the water column in Massachusetts Bay and in northern central Cape Cod Bay. The T-S diagram indicates that the water in Cape Cod Bay was a mixture of these two main water types. The T-S plot also suggested that a pronounced warm plume, which was observed in eastern Cape Cod Bay, was a result of local heating in this area. It is speculated that the warm surface plume was being driven out of Cape Cod Bay around Provincetown by strong wind forcing.

Characteristic spatial distributions were found for both phytoplankton and zooplankton taxa. The different planktonic taxa were found to have different affinities for the different water types, thus providing some insights into their origins. Dominant features of the phytoplankton included an intense bloom of rod-shaped diatoms in eastern Cape Cod Bay, which corresponded to very large fluorescence values and was associated with the warm surface plume in this region. Fluorescence was high in Cape Cod Bay as determined from both the VPR fluorometry data as well as from SeaWifs data. The region of the CAPW had lower fluorescence and plankton abundance values. By

contrast a less intense but broader distribution of chain-forming diatoms of the genus *Chaetoceros* was found throughout southern Massachusetts Bay and was associated with the MBBW, suggesting an offshore origin.

For zooplankton, the dominant copepod was *Oithona*, which, like *Chaetoceros*, was distributed throughout southern Massachusetts Bay, but it extended further into northern Massachusetts Bay. Egg-bearing adult female *Oithona* were found to be more abundant and more patchy at depth. Another group that was dominant in this region was ostracods/cyprids, which were substantially more abundant at depth. These groups were associated with the warmer-saltier MBBW. Other zooplankton groups were associated with both the Cape Cod Bay waters and the MBBW. Zooplankton abundance was generally much lower in the CAPW.

The correlation length scales for the various taxa and for the environmental variables were also computed. The correlograms (normalized covariance of abundance values plotted versus lagged distance) revealed several interesting features. First, all of the plankton taxa, except for rod-shaped diatoms and unidentified copepods, exhibited a sharp loss in correlation over very short distances (~2-4 km). Such a decline was not observed in the physical variables or in fluorescence or attenuation, implying taxa-specific small-scale patchiness. Second, for the environmental variables, as well as for most plankton taxa, a large negative correlation was found at the largest length scales (40-60 km). This trend was due to the large-scale gradient in values across the entire region due to the intrusions of the CAPW and MBBW. The shapes of the correlograms varied among the different taxa and environmental variables, reflecting their different distributional patterns.

The data provide insights into the characteristic spatial distribution of dominant phytoplankton and zooplankton taxa as a function of their physical environment. The data suggest that the CAPW serves to dilute the plankton in the northern and western parts of the Bays but also contributes significantly to the formation of Cape Cod Bay water. This CAPW water flows from Cape Ann along the western side of the Bays and into Cape Cod Bay. Cape Cod Bay appears to act as a cul-de-sac in which local surface heating may be important in initiating phytoplankton blooms during spring. The dominant hydrographic patterns observed together with the associated plankton distributions can be viewed as characteristic of the spring period in the bays. These characteristic patterns yield large scale correlations that are likely to be observable during any spring period. Dense small-scale copepod patches were not observed, nor were feeding right whales. This was likely due to the high winds, which act to dissipate plankton patches.

Further study of heat flux, wind forcing, and moored T-S data, prior to and during our cruise, is needed to support these concepts. Analysis of longer time series (eg. moored T-S data) is needed to place this March 1998 data in a seasonal and interannual context. Further statistical analysis of subsets of VPR data, e.g., treating each tow as a separate plankton net tow, is needed for quantification of the underlying statistical distributions and for comparison with the MWRA net tow data. Comparison of the data presented in this report with other VPR data from March, 1996, March, 1997, and June 1998 is currently in progress.

## TABLE OF CONTENTS

EXECUTIVE SUMMARY .....	2
LIST OF TABLES .....	6
LIST OF FIGURES .....	6
1.0 INTRODUCTION .....	9
2.0 OBJECTIVES .....	11
3.0 METHODS .....	11
3.1 The VPR.....	11
3.1.1 Underwater Unit.....	11
3.1.2 Cable and Winch.....	11
3.1.3 Deployment/Retrieval.....	12
3.1.4 Environmental Data Logging, Processing, and Display .....	12
3.1.5 Video Recording, Processing, and Display.....	12
3.2 Survey Design and Tow Pattern .....	13
3.3 Post-Cruise Data Processing, Display, and Analysis.....	13
3.3.1 Video Processing / Focus Detection .....	13
3.3.2 Plankton Identification.....	14
3.3.3 Classification accuracy .....	16
3.3.4 Data visualization.....	17
3.3.5 Correlation Length Scales.....	18
3.3.6 Temperature-Salinity-Plankton Plots.....	18
3.3.7 Satellite Imagery .....	18
4.0 RESULTS AND DISCUSSION .....	19
4.1 Overview.....	19
4.2 Distributional Patterns of Environmental Variables .....	19
4.2.1 Temperature .....	19
4.2.2 Salinity .....	20
4.2.3 Seawater Density .....	21
4.2.4 Temperature-Salinity Relationships.....	21
4.2.5 Down-welling Light.....	23
4.2.6 Fluorescence .....	23
4.2.7 Attenuation.....	24
4.3 Distributional Patterns in Plankton Taxa .....	25
4.3.1 General Abundance Values.....	25
4.3.2 Rod-Shaped Diatoms .....	25
4.3.3 Temperature-Salinity-Plankton Relationships .....	26
4.3.4 Chaetoceros Chains.....	27

4.3.5 Oithona.....	28
4.3.6 Oithona with Eggs.....	29
4.3.7 Unidentified Copepods .....	30
4.3.8 Barnacle Larvae .....	30
4.3.9 Larvaceans .....	31
4.3.10 Ostracods / Barnacle Cyprids.....	32
4.3.11 Pteropods.....	33
4.3.12 Total Plankton.....	33
4.3.13 Summary of Plankton Patterns.....	33
4.4 Correlation Length Scales.....	34
4.4.1 Physical Variables.....	34
4.4.2 Fluorescence and Attenuation.....	34
4.4.3 Planktonic Taxa .....	36
4.4.3.1 Rod-Shaped Diatoms .....	36
4.4.3.2 Chaetoceros Chains.....	36
4.4.3.3 Oithona.....	37
4.4.3.4 Oithona with Eggs.....	38
4.4.3.5 Unidentified Copepods .....	38
4.4.3.6 Barnacle Nauplii .....	39
4.4.3.7 Larvaceans .....	39
4.4.3.8 Ostracods/Cyprids.....	40
4.4.3.9 Pteropods.....	40
LITERATURE CITED .....	41

## LIST OF TABLES

Table 1. Plankton taxa observed in video.

Table 2. Abundance of plankton observed during the 10-s time-bins.

## LIST OF FIGURES ([Access all figures by clicking here](#))

Figure 1. VPR Survey Track – R/V *Peter W. Anderson*,  
March 12 (0230) to March 14 (1415), 1998 (EST)

Figure 2A. Temperature (°C): Along-track curtain plot of VPR data.

Figure 2B. Temperature (°C): AVHRR Satellite Image

Figure 2C. Temperature (°C): Stacked kriging plots of VPR data at 10m depth layers.

Figure 3A. Salinity (psu): Along-track curtain plot of VPR data.

Figure 3B. Salinity (psu): Stacked kriging plots of VPR data at 10m depth layers.

Figure 4A. Density ( $\sigma_t$ ): Along-track curtain plot of VPR data.

Figure 4B. Density ( $\sigma_t$ ): Stacked kriging plots of VPR data at 10m depth layers.

Figure 5A. Color-coded Temperature – Salinity Plot

Figure 5B. 3-D dot-plot of data locations, with T-S color coded as in Fig. 5A.

Figure 6. Downwelling Light ( $W/m^2$ ): Along-track curtain plot of VPR data.

Figure 7A. Fluorescence ( $\mu g$  Chl a / liter): Along-track curtain plot of VPR data.

Figure 7B. Fluorescence ( $\mu g$  Chl a / liter): SeaWifs Image, March 11, 1998 (1650 GMT)

Figure 7C. Fluorescence ( $\mu g$  Chl a / liter): Stacked kriging plots of VPR data at 10m layers.

Figure 7D.  $\log_{10}$ [Fluorescence ( $\mu g$  Chl a / liter)]: Along-track curtain plot of VPR data.

Figure 7E.  $\log_{10}$ [Fluorescence ( $\mu g$  Chl a / liter)]: SeaWifs, March 11, 1998 (1650 GMT)

Figure 7F.  $\log_{10}$ [Fluorescence ( $\mu g$  Chl a / liter)+1]: Stacked kriging plots of VPR data

Figure 8A. Attenuation (beam-C): Stacked kriging plots of VPR data at 10m depth layers

Figure 8B.  $\log_{10}$ [Attenuation (beam-C)]: Stacked kriging plots of VPR data at 10m layers

Figure 9A. Rod-Shaped Diatoms: Sample of images used for training automatic classifier.

Figure 9B. Rod-Shaped Diatoms (Bloom conditions): Sample of images use for training.

Figure 9C. Rod-Shaped Diatoms (#/liter): Along-track curtain plot of VPR data.

Figure 9D. Rod-Shaped Diatoms (#/liter): Stacked kriging plots of VPR data at 10m layers

Figure 9E. Rod-Shaped Diatoms ( $\log_{10}$ [(#/liter)+1]): Along-track curtain plot.

Figure 9F. Rod-Shaped Diatoms ( $\log_{10}$ [(#/liter)+1]): Stacked kriging plots.

Figure 10A,B. Temperature-Salinity-Plankton Plots (Plankton abundance in #/liter)  
Figure 10C,D. Temperature-Salinity-Plankton Plots (Plankton abundance in  $\log_{10}[\#/liter]$ )

Figure 11A. *Chaetoceros* Chains: Sample of images used for training  
Figure 11B. *Chaetoceros* Chains (#/liter): Along-track curtain plot of VPR data.  
Figure 11C. *Chaetoceros* Chains (#/liter): Stacked kriging plots at 10m layers  
Figure 11D. *Chaetoceros* Chains ( $\log_{10}[(\#/liter+1)]$ ): Stacked kriging plots of VPR data

Figure 12A. *Oithona*: Sample of images used for training the automatic classifier.  
Figure 12B. *Oithona* (#/liter): Along-track curtain plot of VPR data.  
Figure 12C. *Oithona* (#/liter): Stacked kriging plots of VPR data at 10m depth layers  
Figure 12D. *Oithona* ( $\log_{10}[(\#/liter+1)]$ ): Stacked kriging plots of VPR data

Figure 13A. *Oithona* with eggs: Sample of images used for training  
Figure 13B. *Oithona* with eggs (#/liter): Along-track curtain plot of VPR data.  
Figure 13C. *Oithona* with eggs (#/liter): Stacked kriging plots of VPR data at 10m layers.  
Figure 13D. *Oithona* with eggs ( $\log_{10}[(\#/liter+1)]$ ): Stacked kriging plots of VPR data

Figure 14A. Unidentified Copepods: Sample of images used for training.  
Figure 14B. Unidentified Copepods (#/liter): Along-track curtain plot of VPR data.  
Figure 14C. Unidentified Copepods (#/liter): Stacked kriging plots at 10m layers.  
Figure 14D. Unidentified Copepods ( $\log_{10}[(\#/liter+1)]$ ): Stacked kriging plots.

Figure 15A. Barnacle Nauplii: Sample of images used for training the automatic classifier.  
Figure 15B. Barnacle Nauplii (#/liter): Along-track curtain plot of VPR data.  
Figure 15C. Barnacle Nauplii (#/liter): Stacked kriging plots of VPR data at 10m layers.  
Figure 15D. Barnacle Nauplii ( $\log_{10}[(\#/liter+1)]$ ): Stacked kriging plots of VPR data

Figure 16A. Larvaceans: Sample of images used for training the automatic classifier.  
Figure 16B. Larvaceans (#/liter): Along-track curtain plot of VPR data.  
Figure 16C. Larvaceans (#/liter): Stacked kriging plots of VPR data at 10m depth layers.  
Figure 16D. Larvaceans ( $\log_{10}[(\#/liter+1)]$ ): Stacked kriging plots of VPR data

Figure 17A. Ostracods/Cyprids: Sample of images used for training  
Figure 17B. Ostracods/Cyprids (#/liter): Along-track curtain plot of VPR data.  
Figure 17C. Ostracods/Cyprids (#/liter): Stacked kriging plots of VPR data at 10m layers.  
Figure 17D. Ostracods/Cyprids ( $\log_{10}[(\#/liter+1)]$ ): Stacked kriging plots of VPR data

Figure 18A. Pteropods: Sample of images used for training the automatic classifier.  
Figure 18B. Pteropods (#/liter): Along-track curtain plot of VPR data.  
Figure 18C. Pteropods (#/liter): Stacked kriging plots of VPR data at 10m depth layers.  
Figure 18D. Pteropods ( $\log_{10}[(\#/liter+1)]$ ): Stacked kriging plots of VPR data.

Figure 19A. Total Plankton (#/liter): Stacked kriging plots of VPR data at 10m layers.  
Figure 19B. Total Plankton ( $\log_{10}[(\#/liter+1)]$ ): Stacked kriging plots of VPR data.

Figure 20A. Correlograms for Temperature  
Figure 20B. Correlograms for Salinity

- Figure 21A. Correlograms for Fluorescence  
Figure 21B. Correlograms for Attenuation
- Figure 22A. Correlograms for Rod-Shaped Diatoms  
Figure 22B. Correlograms for *Chaetoceros* Chains  
Figure 22C. Correlograms for *Oithona*  
Figure 22D. Correlograms for *Oithona* with eggs  
Figure 22E. Correlograms for Unidentified Copepods  
Figure 22F. Correlograms for Barnacle Nauplii  
Figure 22G. Correlograms for Larvaceans  
Figure 22H. Correlograms for Ostracods/Barnacle Cyprids  
Figure 22I. Correlograms for Pteropods

## 1.0 INTRODUCTION

Understanding the processes controlling plankton populations in the sea requires high-resolution data on plankton abundance and associated environmental variables over a wide range of spatial scales (Haury et al., 1978). The patchy nature of plankton necessitates multi-scale sampling. Spatial heterogeneity in plankton abundance has been observed for over a century (Haeckel, 1890) and was quantified formally over 50 years ago (Hardy and Gunther, 1935; Hardy, 1936). Numerous subsequent studies have been conducted to quantify plankton spatial structure and relate it to associated environmental variables (see reviews in Cushing, 1975; Fasham, 1978; Haury et al., 1978; Okubo, 1980; Longhurst, 1981; Angel and Fasham, 1983; Mackas et al., 1985; Owen, 1989; Davis et al., 1991; Denman, 1992; Denman and Gargett, 1995). It has been well established that plankton patchiness is strongly correlated with physical variability (e.g., Cassie, 1959a,b, 1960) over a broad range of scales (e.g., Gallagher et al., 1996a) and that many mechanisms are responsible for the observed patterns (Haury et al., 1978).

In Massachusetts and Cape Cod Bays, the spatial scales of plankton variability remain poorly understood. Historical data on plankton abundance are primarily from widely spaced discrete samples which do not provide adequate multi-scale information (Bigelow, 1926; Toner et al., 1984; Horst et al., 1984; Bridges et al., 1984; Jossi and Goulet, 1990; Turner, 1994). High-resolution acoustical sampling on Stellwagen Bank revealed a close association of acoustical backscatter and internal waves (Haury et al. 1983), but the extent to which the backscatter was due to plankton, detritus, or physical microstructure remains uncertain, and this study was limited to a small region near the bank.

Due to technological limitations, extensive, bay-wide, high-resolution sampling of plankton taxonomic composition and associated environmental variables has not yet been possible. Since the bays have high socioeconomic value, are inhabited by endangered plankton-feeding right whales, and are being impacted by various sources of anthropogenic contamination, it is important understand the underlying factors controlling plankton abundance in this area.

Concern that relocation of the MWRA sewer outfall from Boston Harbor to Massachusetts Bay may impact the ecology of the bays prompted an extensive Harbor Outfall Monitoring (HOM) program from 1992-present. As part of this program, zooplankton net hauls have been made 6 times per year at 12 stations spread throughout the bays. Differences between post-discharge and baseline data will be determined statistically using the (HOM) data set. Although the MWRA HOM plankton data are sparse, they are thought to be sufficient for testing for relocation effects, assuming the underlying assumptions about the statistical distributions of the plankton are correct, i.e. that the plankton are effectively lognormally distributed. The true distribution of the plankton then will affect the statistical power of the tests. High-resolution spatial sampling can provide an estimate of the true statistical distribution of plankton in the bays.

Analysis of variance in the HOM data reveals that the variability is divided approximately evenly between interannual, seasonal, and spatial effects (Cibik et al., 1998). Thus, although high-resolution spatial sampling will increase the statistical power of the tests to

a certain extent, natural interannual variability may require that several years of post-relocation data be collected to achieve high enough statistical power for detecting outfall-related changes in the plankton populations.

Even when the power is sufficient, given the sparse nature of the HOM data, understanding causal relationships between significant changes in plankton abundance and the outfall may be difficult or impossible. High-resolution sampling may provide needed insights into the spatial relationships between plankton and associated environmental variables, so that strong inferences can be made about causes of observed post-discharge plankton patterns, even during the first year post-discharge.

In sum, high-resolution sampling can help to provide:

- a better estimate of the underlying statistical distribution of the plankton in the bays,
- increased statistical power by quantifying better the plankton spatial variability
- insights into the association of plankton and environmental variables and causes of observed plankton patterns

Toward this end, in March 1997, a broadscale Video Plankton Recorder survey of the bays was made. The objective of this cruise was to characterize the distribution of plankton with particular reference to the scales of copepod patchiness in the bays as related to whale foraging. A dense *Phaeocystis* bloom occurred in Cape Cod Bay at that time, no dense copepod patches were observed, and whale foraging in the region was the most limited on record. These events made 1997 a poor year to characterize the plankton distributions in the bays, and it was decided that another VPR survey was needed in March 1998.

A VPR survey was conducted between March 12-14, 1998 using the EPA research vessel *Peter W. Anderson*. The survey consisted of VPR towed transect lines covering the two bays. The objectives of the survey were to:

- 1) determine the distributional patterns (and dominant length scales of variation) of zooplankton and large phytoplankton taxa and
- 2) determine the relationship of plankton distributions to associated environmental variables over a broad range of scales in order to better understand the causes of the observed plankton patterns and to provide a broadscale context within which to interpret the MWRA HOM data

## **2.0 OBJECTIVES**

The objectives of this report are to:

- 1) present high-resolution distributional data on the plankton and environmental variables from the VPR survey in March 12-14, 1998.
- 2) quantify the correlation length scales of the plankton and environmental variables
- 3) examine the spatial relationships between plankton and environmental variables in an effort to understand the causes of the plankton distributional patterns.

## **3.0 METHODS**

### ***3.1 The VPR***

#### ***3.1.1 Underwater Unit***

The Video Plankton Recorder is a towed underwater video microscope that images plankton and seston in the size range from 0.1 - 20 mm (Davis et al., 1992a,b, 1996; Gallagher et al., 1996). The VPR included two video cameras, high and low magnification, with fields of view of 7 and 25 mm, respectively. The cameras were synchronized at 60HZ with a xenon strobe (~1  $\mu$ s pulse duration). The VPR system also included a CTD (Seabird), fluorometer (Wetlabs), transmissometer (Wetlabs), light sensor (Licor 192SA), flow meter (General Oceanics), altimeter, and pinger. The VPR sensors including cameras were mounted on a steel frame attached to the underside of a 3.5' V-fin.

#### ***3.1.2 Cable and Winch***

The data were telemetered to the surface via 0.68" armored fiber optic tow cable. Fiber optic receivers in the winch drum converted the signals back to analog electric (coax for video, and copper conductors for other data) which were sent through copper slip-rings to the ship's main lab. The winch (Dynacon with level wind) was placed on the starboard quarter of the fantail facing toward port, and the tow cable was fair-led through a steel block (30" sheave) suspended from the end of the crane boom.

### ***3.1.3 Deployment/Retrieval***

The VPR was towed from the crane boom off the port side of the ship to avoid sampling in the ship's wake. A detailed account of deployment/retrieval methods is given in the cruise report (Davis and Gallager, 1998). Note that on 3/12 at 1800 (EST) the VPR impacted the bottom and changed the strobe-camera alignment, affecting the image processing protocol (see section 3.1.5 and the Survey Report).

### ***3.1.4 Environmental Data Logging, Processing, and Display***

Environmental data from the VPR underwater unit together with GPS data (position, date, time in GMT), bottom depth data from the ship and time of day (GMT) from a video time-code generator were input to a data-logging PC (486) via multiple serial ports. A C++ program was used to read and parse the incoming data and write it to files on a Zip drive as well as on a hard drive of a Silicon Graphics Inc (SGI) workstation (Indigo2) via network file system mount at 10Mbit. The SGI also was linked to the image processing system (a 200MHZ Dual-processor Pentium-Pro running MS Windows NT workstation 4.0 and a Sun Sparc20 workstation) via a 100 megabit local area network. A 10-100Mbit switching box was used to allow the SGI to communicate at 10 and 100Mbit.

Environmental data was processed and displayed in real time on the SGI using C and Matlab routines. The C routine (called from within the main Matlab controlling program) was used to read and parse data from the active logging file and output the data to a binary Matlab (.mat) file. This file then was loaded into Matlab and the data processed. The environmental data were displayed as 3-D color dot plots using latitude, longitude, and VPR depth as the axes. Dot color was proportional to the value of the variable using a blue-red color map to represent low-high values, respectively.

### ***3.1.5 Video Recording, Processing, and Display***

The raw video coming from the slip rings via coaxial cables was time-stamped with time code from the time-code generator, displayed on video monitors, and recorded on SVHS tape recorders. Video from the high magnification camera also was sent to the image processing system. Image processing consisted of focus detection, feature extraction, and classification.

The high magnification video was input into the Imaging Technologies Inc. Model 150/40 image processing board contained in the Pentium-Pro computer. A C++ program running on this computer was used for focus detection. On average, about 1-6 in-focus objects (i.e. regions of interest, ROI) were observed per second (out of 60 video fields per second).

These ROIs were saved to disk as tagged image format (TIF) files using time of day in milliseconds as the filename. The ROI files were saved in subdirectories corresponding to

hour and year-day (with Jan 1 = day 0). To avoid differences in time of day between the computer clock and the time code generator, time code was sent to the computer's serial port. When the focus detection program was started, it read the initial time code and then incremented this time, in milliseconds, (using the computer clock) as the ROIs were extracted. Tens of thousands of these ROI files were generated during the course of the cruise. A Matlab program running on the Sun SS20 extracted diagnostic features from the ROIs. These features were saved in files corresponding to each ROI file.

Before automatic identification of the plankton could be done, the neural net classification program needed to be trained. This training is typically performed at the beginning of each cruise to accommodate cruise-specific illumination conditions resulting from camera/strobe alignment and general water clarity. (The potential for using an archived set of classifiers for different cruises is presently being explored.) An initial training data set was created by copying 3 hours of ROIs into a training directory and manually sorting representative ROIs into the proper taxonomic categories. The neural net training program then was run on this set of training ROIs to develop the parameter values needed for classification. The classifier then was used to begin automatically sorting ROIs into taxonomic categories. Normally, a program on the SGI would read in the filenames (= time codes) for a given taxon, bin them into the same time bins as the physical data, and plot their distributions using 3-D dot plots. However, at this point in the cruise, the VPR hit bottom and the high magnification camera head was rotated slightly toward the strobe, changing the lighting conditions. The focus detection parameters had to be changed, and a new training set of ROIs needed to be created. Due to the rough seas, it was decided to do this analysis after the cruise from the video tapes (see below).

### ***3.2 Survey Design and Tow Pattern***

It was originally planned to conduct a series of orthogonal transect lines running the length and width of the bays. Due to high winds (20-40 knots) and seas (4-10') and the narrow width of the ship, we had to adjust our track lines so that we were no more than 30 degrees from a line orthogonal to the wave troughs. We initially attempted to steam along parallel track lines but were forced into a zigzag type of survey track. Nonetheless, the entire area was surveyed. The VPR was towed from near surface to near bottom at a ship's speed of 6 knots. The R/V Anderson technicians operated the winch while the VPR team monitored and controlled the VPR system from the main lab (using 4 hour shifts). The VPR was towed continuously during the 3 survey days.

### ***3.3 Post-Cruise Data Processing, Display, and Analysis***

#### ***3.3.1 Video Processing / Focus Detection***

Video recorded after the VPR hit bottom was reprocessed in the laboratory in order to use the optimal parameter values for focus detection. Since the post-impact video was brighter than the original video, the focus detection parameters had to be adjusted. The adjustments made at sea were approximate so that ROI extraction had to be redone for the

post-impact video. To maintain consistency in pre- and post-impact ROI extraction, the segmentation threshold (brightness threshold) was adjusted such that the number of ROIs extracted per minute immediately pre- and post-impact were equal. Manual scrolling through the video also was performed to make sure there were no sudden shifts in actual abundance during this time. Once the proper threshold setting was determined, all of the post-impact video was processed using this setting. The post-impact ROIs were saved as a separate VPR tow number since the features and neural network classifiers would be different for the pre- and post-impact image sets.

### ***3.3.2 Plankton Identification***

Once the ROIs were generated, image features were extracted as described above for the real-time system. A large subset of post-impact ROIs was copied to corresponding training directories for manual sorting. Additional pre-impact ROIs also were copied to augment those sorted during the cruise and increase the training image set. The training ROIs were sorted manually into the various taxonomic groups. Representative ROIs were sorted into a given taxon until that taxon contained a sizable number of ROIs.

The list of taxa identified, the corresponding number of ROIs manually sorted, and the taxa selected for automatic identification are shown in Table 1.

**Table 1. Plankton taxa observed in video.**

TAXON	Number of ROIs Manually Sorted		Used in Training for Automatic Identification
	Pre-impact	Post-impact	
Barnacle nauplii	41	158	✓
<i>Calanus</i>	35	75	
Copepod, nauplii	135	18	
Copepod, unidentified	293	646	✓
Ctenophore, cidipid	124	87	
Ctenophore, lobate	56	58	✓
Diatom, rod-shaped, A	756	1234	
Diatom, rod-shaped, B	24	738	
Diatom, rod-shaped, C	0	198	
Diatom, <i>Chaetoceros</i> chain	150	863	✓
Fish Larva	0	2	
Larvacean	306	480	✓
Marine snow A	0	363	
Marine snow B	0	117	
Medusa	0	10	
<i>Oithona</i>	400	320	✓
<i>Oithona</i> w/ eggs	133	161	✓
Ostracod/barnacle cyprid	435	194	✓
Out-of-focus	700	1341	✓
<i>Phaeocystis</i>	250	236	
Polychaete	0	5	
Pteropod	104	153	✓
Surface	30	48	
Teardrop	8	41	
Total ROIs sorted	3979	7544	

Only those taxa having a relatively large number of training ROIs were selected for automatic identification. Lobate ctenophores were included in the training despite the lower number of training ROIs because of their distinct morphology and texture. By contrast *Phaeocystis* colonies were not included, despite the large number of training ROIs, because of their overall low abundance during the cruise. Only *Oithona* could be readily distinguished from the other copepods, so all other copepods were grouped together as unidentified copepods. There were also a significant number of ROIs that were out of focus due to imperfections in the focus detection/ROIs extraction program. The latter program was designed to be conservative in its focus detection so as not to miss in-focus objects. This results in some out of focus ROIs being generated. The neural network classifier was able to effectively sort out the remaining out of focus ROIs.

### 3.3.3 Classification accuracy

For the 10 taxonomic groups shown in Table 1, the neural network classifier was found to be 93% accurate for pre-impact ROIs and 86% accurate for the post-impact ROIs. Higher accuracy could be obtained by combining taxa (e.g. grouping the grazers) into 6 groups, but it was felt that the accuracy for the 10 taxa was acceptable and allowed important distributional data on these taxa to be obtained.

A region of reduced accuracy occurred in an area around the tip of Cape Cod where an intense bloom of rod-shaped diatoms was encountered. The vast number of images generated for rod-shaped diatoms in this area caused the relative error in abundance estimates to increase for some of the other taxa. Although rod-shaped diatoms were identified with very high accuracy (~95%), in bloom conditions these organisms constituted ~95% of the total plankton imaged. Thus, although the percent misidentification of this taxon was small, the absolute number of images incorrectly identified (as other taxa) was large relative to the true number of other taxa. A rough statistical correction was made to the abundance data to compensate for this error. Since our original abundance estimate,  $Y_{1,est}$ , for taxon<sub>1</sub> is given by:

$$Y_{1,est} = p_1Y_1 + (1 - p_2)Y_2 + (1 - p_3)Y_3 + \dots + (1 - p_n)Y_n \quad (1)$$

where  $Y_i$  is the true abundance of the  $i$ th taxon,  $p_i$  is the probability of correct identification of the  $i$ th taxon, and  $n$  is the total number of taxa. Ideally we would like to have probabilities,  $p_1$  to  $p_n$ , for taxa 1 to  $n$ , but this would require significant effort (i.e. manually sorting a second set of ROIs for accuracy analysis) and is beyond the scope of this data report. As an approximation, we will use:

$$Y_{1,est} = p_1Y_1 + (1 - p_2)Y_2 \quad (2)$$

where  $Y_2$  and  $p_2$  are abundance and probability of correct identification, respectively, for all other taxa combined (2 through  $n$ ). Rearranging this equation to find the true abundance,  $Y_1$ , for taxon<sub>1</sub> gives:

$$Y_1 = (Y_{1,est} - Y_2 + p_2Y_2) / p_1 \quad (3)$$

Since  $Y_2 = Y_{Total} - Y_1$ , where  $Y_{Total}$  is total abundance of all taxa combined ( $i = 1$  through  $n$ ), for ease of computation we used:

$$Y_1 = (Y_{1,est} - Y_{Total} + p_2Y_{Total}) / (p_1 - 1 + p_2) \quad (4)$$

to adjust the abundance data, with  $p_1 = 0.9$  and  $p_2 = 0.995$ . These values were chosen so that the scheme would be positive-definite (i.e. negative concentrations not allowed). This restriction causes only small corrections to the abundance values. For this reason, the abundance values remain biased for those taxa that are confused with the blooming rod-shaped diatoms.

This error was not a problem for those taxa that were clearly distinct in morphology from these diatoms (i.e., *Chaetoceros*, *Oithona*, *Oithona* with eggs, Ostracods/cyprids, and unidentified copepods) but caused artificially high abundance estimates of other taxa in the area of this bloom (i.e., larvaceans, barnacle nauplii, and pteropods).

### 3.3.4 Data visualization

The distributional data are displayed in two types of plots. Curtain plots were used to show the along-track vertical distribution of the different variables, while kriging was used to show the horizontal distributional patterns at fixed depths using stacked plots.

The curtain plots were generated by first obtaining the values of a given variable at 10-second intervals along the VPR tow path. The corresponding latitude, longitude, and depth of these data points then were found from the navigational and pressure-sensor data.

For plankton, the number of individuals in a given taxon observed during each 10-s interval was divided by the volume imaged during the interval in liters to obtain abundance in #/liter. The volume imaged per video field by the high magnification camera was 0.5 ml, as given by the product of the field width (0.7 cm), field height (0.55 cm), and depth of field (1.3 cm). Since video fields were acquired at 60 Hz, the volume imaged per 10 s was 0.3 liters.

Once the values in each 10-s interval were obtained, the cumulative distance traveled along the cruise track (in kilometers) was determined from the latitude and longitude. The values then were interpolated to a regular grid ( $x,z$ ) using the NCAR graphics routine, ZGRID, which uses a cubic spline fit and Laplacian smoothing. The gridded data then was mapped to a surface defined by latitude, longitude, depth, and variable value using the Matlab surf.m function.

Kriging was performed on the VPR data for each of the five environmental variables (temperature, salinity, density, fluorescence, and attenuation) as well as for the ten plankton taxa. Software developed in Matlab by Denzang Chu (WHOI) was used for kriging, and the results were saved to disk for subsequent customized plotting. Data first were prepared for use in the kriging program by separating the 10-s data into five 10m depth intervals: 0-10, 10-20, 20-30, 30-40, and >40. Data were saved in depth-specific

files with columns for longitude, latitude, and variable value. Each of these data files for each variable was read into the kriging program one at a time. After loading a given data file, the data were transformed using a 10-point running average and then decimated by a factor of 10 to speed up the computation. A variogram then was generated and a function fit via least squares to the variogram (inverse of correlogram). Standard kriging then was performed and the kriged data, together with the parameter values and correlogram data were saved to disk as a Matlab binary file. For a given variable, the five 10m-depth files were loaded into a Matlab program written to create the stacked plots. The stack plots used the same color map as the curtain plots. The locations of the decimated data points used in the kriging were overlaid as white dots on the kriging plots.

### ***3.3.5 Correlation Length Scales***

In addition to the distributional plots, the correlograms for each variable are presented so that the correlation scales of environmental data and plankton abundance can also be seen. Data for these plots were obtained from the kriging analysis for each species. A program was written to plot all correlograms for a given variable on one page.

### ***3.3.6 Temperature-Salinity-Plankton Plots***

To further examine the association of the plankton with the different water mass types in the Bays, temperature-salinity-plankton (T-S-P) plots are presented. These plots were generated directly from the 10-s binned data by plotting plankton abundance as a colored dot at each temperature-salinity point. Dot diameter and color was linearly related to abundance.

### ***3.3.7 Satellite Imagery***

Satellite data from AVHRR and SeaWifs were obtained from Andrew Thomas' remote sensing group at U. Maine. The data were received in the form of byte-formatted images and were loaded into Matlab and plotted using the same color map as the curtain plots. Plots of the Bays' region were from the larger area imagery provided by U. Maine (200x200km). The spatial resolution is 0.5 km/pixel, which was interpolated by Thomas' group from the original 1.1 km/pixel satellite data (Thomas, pers. comm.).

## 4.0 RESULTS AND DISCUSSION

### 4.1 Overview

This data report presents distributional patterns and correlograms of plankton and environmental variables as determined from a VPR survey that took place from March 12 (0230) to March 14 (1415), 1998. The survey covered the entire region of Cape Cod and Massachusetts Bays, beginning off Gloucester (Fig. 1). The VPR was towed nearly continuously for 58 hours covering a total along-track distance of about 350 nautical miles. Maximum tow depth was 100 m. Also presented in this report are satellite data of sea surface temperature and chlorophyll a from AVHRR and SeaWiFS (generously provided by Andrew Thomas, U. Maine). R. Geyer and R. Beardsley (WHOI) kindly provided help with the interpretation of the temperature-salinity data and corroborated our initial water-type characterizations.

### 4.2 Distributional Patterns of Environmental Variables

#### 4.2.1 Temperature

Seawater temperature over the entire region ranged from 2.94 – 4.49 °C. A cold plume of fresh water with low density was observed from Cape Ann toward the southwest and into Cape Cod Bay near Plymouth (Fig. 2A). The southeastern portion of the region was warmer with highest temperatures observed in a plume around the tip of Cape Cod near Provincetown. A cold plume was observed well offshore northeast of Provincetown.

The surface temperature patterns determined from the VPR are similar in a relative sense to the distribution of sea surface temperature (SST) observed from the AVHRR satellite (compare Figs. 2A and 2B). The absolute range in the AVHRR data was scaled to match the range of the VPR data in an effort to ground-truth the satellite data. This calibration was needed because the lower range of satellite SST values was 1.0 – 1.5 °C whereas no values less than 2.94 °C were observed in the VPR data. Generally, SST was warmer on the southeastern part of the region and colder to the northwest (Fig. 2B). Warmest SST values were observed in eastern Cape Cod Bay and in the warm plume around the tip of Cape Cod. The offshore cold plume northeast of Provincetown also was observed in the SST data. On a line from this cold plume to Gloucester Harbor, the SST is seen to be low then higher and then lower again, agreeing with the VPR data (Figs. 2A,2B).

The kriged VPR temperature data (Fig. 2C) also shows this pattern of surface temperature distribution, although the values over the southern portion of Stellwagen Bank are lower than the AVHRR SST data for this region. Nonetheless, the cold plume northeast of Provincetown can be seen, and the surface temperature along the line from this plume toward Gloucester Harbor first increases then decreases, as was observed in the satellite

data. The kriging also shows clearly the general increase in temperature with depth, except that the warm plume around Provincetown is surface intensified.

Despite the strong winds, the VPR data reveal that the water column was thermally stratified throughout most of the area (Figs. 2A,C). In the northwestern half of the region, temperature generally was colder at the surface and warmer at depth. Over southern Stellwagen Bank and in eastern Cape Cod Bay, the temperatures were higher in the surface than at depth.

#### ***4.2.2 Salinity***

The surface plume from Cape Ann is especially evident in the salinity data (Fig. 3A). The plume was found to be narrowest near Cape Ann and broadened out to the southwest in the subsequent two transects where it was present in the surface water throughout most of the lengths of these transects.

Fresher water also was observed at the near-shore apices of subsequent transects off the South Shore. This lower salinity water appears to be contiguous with the Cape Ann plume which extends inshore south of Boston Harbor and appears to follow the coast down to Plymouth (Fig. 3A). This pattern is consistent with the pattern for temperature as observed in both the VPR and satellite data.

The highest salinity water was observed in Stellwagen Basin and offshore (Fig. 3A). This higher salinity water was observed in the lower half of the water column beginning in the second transect south of Gloucester and extending southeastward into the bottom waters of central Cape Cod Bay. The higher salinity water also extended eastward in the third and fourth transects south of Gloucester.

The total range of salinity values observed during the survey was 29.83 – 32.04 psu.

The kriging results for salinity clearly show the freshwater plume extending from Cape Ann to the South Shore north of Plymouth (Fig. 3B). The water along the South Shore however is much fresher (~0.5 psu) than the water in the broad plume south of Gloucester, and the lower salinity along the South Shore water may therefore result from local freshwater input. The freshwater plume occurs primarily in the upper 20 m of the water column (i.e. first two layers in Fig. 3B) and it become progressively weaker with depth.

The kriging results also show relatively fresh water (~31.0 psu) along the coast next to Plymouth Harbor extending south into western Cape Cod Bay. The entire region of Cape Cod Bay is generally fresher than southern Massachusetts Bay and offshore regions.

A large tongue of relatively salty water was extended westward from offshore locations into the southern part of Massachusetts Bay to near Plymouth Harbor (Fig. 3B, upper three layers). This higher salinity water can be clearly observed in the upper 30 m of the water column. This plume also appears to extend southward through the middle of Cape Cod Bay, with the eastern and western parts of the bay having relatively lower salinity.

Salinity generally increases with depth throughout the region (Fig. 3B). In some areas, the water column was more isohaline. A higher salinity region northeast of Plymouth Harbor (the tip of the higher salinity tongue) persists with depth (Figs. 3A,3B). Likewise salinity in the apices of the two transects north of Provincetown varied little with depth.

#### ***4.2.3 Seawater Density***

Seawater density ( $\sigma_t$ ) also mirrored the SST patterns, with less dense surface waters in the northwestern half of the region and denser water to the southwest (Fig. 4A). The Cape Ann surface plume is seen to be continuous over a broad area off the northwestern half of the region. Highest density was observed in the middle part of the survey area with intermediate and low density in Cape Cod Bay (Fig. 4A). High density water from this middle region did extend into the bottom waters of northern central Cape Cod Bay (Fig. 4A).

The total range of seawater density observed during the survey was 23.75 – 25.42  $\sigma_t$ .

Kriging results clearly show the high salinity/density tongue extending into the southern half of Massachusetts Bay (Fig. 4B). The higher density water also appears to extend southward through the middle of Cape Cod Bay, with both eastern and western regions of the bay having relatively lower density. Density generally increased with depth throughout the survey region.

#### ***4.2.4 Temperature-Salinity Relationships***

Based on temperature-salinity (T-S) relationships, several distinct water types can be defined. Using an arbitrarily color-coded T-S plot (Fig. 5A) as a guide, the 3-D distributional patterns of the different water masses is revealed (Fig. 5B). Two dominant water types can be observed in the data, with local warming and freshening contributing to the other water types.

First, warmer-saltier water (blue ‘finger’ in upper right on T-S plot; Fig. 5A) is located in bottom waters of Massachusetts Bay (Fig. 5B). In this report, this water-type will be termed Massachusetts Bay Bottom Water (MBBW), and it is characterized by salinity greater than about 31.5 psu and temperature greater than about 3.5 °C. This deep water extends shoreward from the offshore Gulf of Maine area into the bottom waters of the

near-field region (note blue layer on bottom half of the 2<sup>nd</sup> and 3<sup>rd</sup> transects south of Gloucester, Fig. 5B). This bottom water also extends southward into the middle region of southern Massachusetts Bay, filling Stellwagen Basin and extending into north central Cape Cod Bay (Fig. 5B).

The other dominant water-type is the Cape Ann Plume Water (CAPW). In contrast to the warmer and saltier MBBW, the plume of colder fresher water from Cape Ann appears as a horizontal 'finger' in the lower left portion of the T-S plot (red area in Fig. 5A). The CAPW is characterized by salinity less than 31.0 psu and temperature less than 3.4 °C. This plume extends throughout the surface waters of northwestern Massachusetts Bay including the near-field region and along the south shore (Fig. 5B). This cold plume also was observed in the satellite SST data and in the curtain and kriging plots for temperature and salinity. The T-S properties identify this water mass as distinct from the warmer-saltier bottom water (MBBW).

Another prominent region on the T-S plot corresponds to the warmer water surface plume in eastern Cape Cod Bay which extends around the tip of Cape Cod. This water was of intermediate salinity (31.0-31.25 psu) appears as the dark green 'finger' in the T-S plot (Fig. 5A) with temperature ranging from 4.0 up to 4.5 °C. This water-type is termed Cape Cod Bay Plume Water (CCBPW) and extends from the two easternmost transects in Cape Cod Bay northward around Provincetown (Fig. 5B).

From the T-S plot, it is evident that this CCBPW is continuous with cooler water of intermediate salinity (base of green 'finger' in Fig. 5A). This cooler water extends throughout Cape Cod Bay (except in the northwest part) and is termed Cape Cod Bay Central Water (CCBCW). CCBCW is characterized by salinity of 31.0-31.25 psu and temperature of 3.6-4.0 °C. Two small side-lobes occur off of the base of this "finger" and correspond to regions of lower salinity (<31.0 psu) in the transect adjacent to the Cape Cod Canal entrance.

An explanation for the formation of the Cape Cod Bay water-types can be found by considering the mixing of the two main water types CAPW and MBBW. Such mixing would occur along the line from the red to blue regions in the T-S diagram (Fig. 5A). The CCBCW appears to be a mixture of the two main water types, MBBW and CAPW. The freshwater plume coming around Cape Ann is known to be episodic in nature and is driven in spring by river discharge from the north. The CCBCW observed during the cruise therefore could have been the result of MBBW mixing with a remnant of CAPW that had entered Cape Cod Bay on a previous date. The CCBCW is warmer than would be expected by mixing MBBW and CAPW and this warming likely resulted from local heating in Cape Cod Bay.

Likewise, the warmer plume of CCBPW appears to have formed by local heating of the CCBCW, since the salinity is the same for these two water-types (Fig. 5A). Cape Cod Bay typically has weaker circulation than Massachusetts Bay and forms a “cul-de-sac” that is subject to local heating because of the weak flow through the area. The strong winds that occurred during the cruise could have been responsible for driving horizontal transport of this warm surface water, thus forming the observed plume around Provincetown. Further study of heating and wind forcing are required to support this hypothesis.

Another interesting smaller ‘finger’ on the T-S plot is observed at 3.6 °C and 30.6 psu (small yellow-green finger on T-S plot, Fig. 5A). This water was located at the near-shore end of the 1<sup>st</sup> and 4<sup>th</sup> transects south of Gloucester Harbor, and may be part of a warmer coastal band of low to intermediate salinity water extending from Gloucester around the mouth of Boston Harbor (Fig. 5B). This water-type is termed Boston Harbor Water (BHW).

#### ***4.2.5 Down-welling Light***

The down-welling light patterns are shown (Fig.6) to provide spatial reference for the day/night sampling periods. As can be seen, the survey covered three daylight periods including the 2<sup>nd</sup> to 4<sup>th</sup> transects south of Gloucester, the middle and eastern part of Cape Cod Bay, and the central part of Massachusetts Bay. The total range of down-welling light values observed during the survey was 0-104 W/m<sup>2</sup>.

#### ***4.2.6 Fluorescence***

Fluorescence was highest in southern and eastern Cape Cod Bay where extremely high values (up to 27.3 µg Chl a / liter) were observed (see curtain plot, Fig. 7A). The fluorescence throughout Massachusetts Bay was much lower (~1.0 µg Chl a / liter) (Fig. 7A). The relative distribution of chlorophyll-a is in general agreement with satellite data collected on the day before the VPR survey began (Fig. 7B). The satellite data also show very high chlorophyll values in Cape Cod Bay and much lower values in Massachusetts Bay. The absolute magnitude of the highest satellite data values (62 µg Chl a / liter) are much higher than the highest values in the VPR data. (27.3 µg Chl a / liter). This discrepancy may be due to saturation of the VPR’s fluorometer or to a known problem with the SeaWiFS chlorophyll data above 2.0 µg Chl a / liter (Subramaniam, A., unpublished data). Nonetheless, there is a remarkable similarity in the relative patterns generated by the VPR and satellite sensors (Figs. 7A, 7B). One noticeable difference is the relatively high SeaWiFS fluorescence in western Cape Cod Bay that was not observed by the VPR two days later.

The VPR data show that the high fluorescence around the tip of Cape Cod is associated with the high temperature plume (CCBPW) in that region (compare Figs. 2A, 5B, and

7A). Note that the spatial curvature of the temperature plume corresponds closely with the distributional pattern of fluorescence in this area.

Kriging results for VPR fluorescence data also show the high values in southern and eastern Cape Cod Bay and low values elsewhere (Fig. 7C). The high fluorescence in the plume off Provincetown decreases in intensity with depth, as was seen in the curtain plot.

To examine fluorescence patterns in Massachusetts Bay, the VPR data also were  $\log_{10}$ -transformed. This curtain plot (Fig. 7D) reveals higher fluorescence in southern Massachusetts Bay than in the northern half of the bay. The region over southern Stellwagen Bank is relatively higher in fluorescence than elsewhere in the bay.

The  $\log_{10}$ -transformed SeaWiFS data (from March 11) do not show the same patterns as the VPR survey for Massachusetts Bay (Fig. 7E). Instead of higher fluorescence in the southern part of the bay, the SeaWiFS data show lower fluorescence in the central and southern regions of the bay and higher values to the north. The reason for this discrepancy is not clear at present, but the SeaWiFS data match more closely the attenuation data (seen below).

The kriged  $\log$ -transformed VPR data (Fig. 7F) also reveals higher fluorescence in southern than northern Massachusetts Bay. The relatively higher fluorescence in the southern half of the bay extends throughout the water column. An area of very low fluorescence is revealed in the vicinity of Plymouth Harbor.

#### ***4.2.7 Attenuation***

Attenuation patterns appear generally similar to those for fluorescence, with high values in Cape Cod Bay and lower values elsewhere (Fig. 8A). An exception is that intermediate attenuation values were observed in the Cape Ann plume region, which did not correspond to higher values of fluorescence (compare Figs. 7C and 8A). The  $\log_{10}$ -transformed attenuation data show this plume clearly (Fig. 8B). Unlike the fluorescence data,  $\log_{10}$ -transformed attenuation data reveals lowest attenuation in southern/central Massachusetts Bay and higher values to the north. Interestingly, this pattern of attenuation is more consistent with the SeaWiFS “chlorophyll-a” data than is the VPR fluorescence data (compare Figs. 7E and 8B). Both figures show relatively high values in the coastal areas and low values in the deeper regions (compare the very high values in Cape Cod Bay and the intermediate values in coastal areas and near Cape Ann. Also compare the dark blue region in Fig. 8B with the green region in Fig. 7E.) The total range of beam-C values was  $-0.99$  to  $1.25$ .

### 4.3 Distributional Patterns in Plankton Taxa

#### 4.3.1 General Abundance Values

The abundance (number/liter) observed in the 10-s time-bins for each taxon is shown in Table 2. Maximum, mean, and median values are given for each taxon. (note that a median value of 0.0 occurred for a taxon when no individuals were observed in more than half of the 10-s intervals). Rod-shaped diatoms clearly dominated the plankton. Although these diatoms were identified with a high degree of accuracy (~95%), the remaining 5% were mistakenly identified as other taxa. During the bloom conditions near Provincetown (see below), the number of misidentified rod-shaped diatoms could exceed the number of other taxa. For this reason, the maximum abundance values shown in Table 2 for the affected taxa (i.e., barnacle nauplii, larvaceans, and pteropods) are artificially high.

**Table 2. Abundance of plankton observed during the 10-s time-bins.**

TAXON	Abundance (#/liter)		
	Max	Mean	Median
Diatom, rod-shaped	336.0	20.784	12.785
Ostracod/barnacle cyprid	61.3	3.791	2.801
Larvacean	45.6	2.110	0.514
Copepod, unidentified	42.8	4.576	3.096
Diatom, <i>Chaetoceros</i>	38.1	3.750	1.991
<i>Oithona</i>	25.5	3.538	2.940
Barnacle nauplii	18.5	0.715	0.000
Pteropod	18.3	0.962	0.000
<i>Oithona</i> w/ eggs	15.4	0.816	0.000
Ctenophore, lobate	14.1	0.124	0.000

#### 4.3.2 Rod-Shaped Diatoms

A subset of the training images for rod-shaped diatoms is shown in Figs. 9A and 9B. Highest abundance observed for these organisms was 336 per liter in bloom conditions (Table 2). These abundance estimates are undoubtedly very low however, since orientation of the rods relative to the strobe-camera axis caused only those rods in a specific orientation to be captured (Figs. 9A). Moreover, in bloom conditions, multiple rods were observed in each ROI but each ROI is counted as one organism. Also, the extremely high abundance in bloom conditions could potentially have overloaded the image processing system causing some in-focus diatom-rods to be missed.

The rod-shaped diatoms could have been *Thalassiosira rotula* or perhaps *Rhizosolenia alata*. It was not possible for us to identify the genus of this group from the video. Three

subsets of these diatoms were manually sorted (Table 1), but these subsets were combined for training. In two of the subsets the rods occurred as single strands in the ROIs (e.g. Fig. 9A), while in the third subset, multiple strands were often present due to the bloom conditions (e.g. Fig. 9B).

The bloom conditions occurred in the warm, high-fluorescence plume in eastern Cape Cod Bay, which extended around the tip of the Cape (Fig. 9C). *The spatial pattern of the diatoms in this area coincides closely with the temperature/fluorescence plume (compare Figs. 2A, 7A, and 9C).* This is an interesting finding because it demonstrates a close association between the hydrography and plankton. The kriging results for this group also indicate that the bloom is contained primarily in the upper 10 m of the water column (Fig. 9D).

The  $\log_{10}$ -transformed abundance data for diatom rods (Figs. 9E-F) reveals that their abundance extends throughout the southern half of Massachusetts Bay, and that very low abundance occurred in the freshwater plume extending from Cape Ann southward along the South Shore coastal region. These data are similar to the kriged  $\log_{10}$ -transformed fluorescence data (cf. Figs. 7F and 9F). The region of low fluorescence off Plymouth also has low abundance of diatom rods. This general correspondence implies that these diatoms may be responsible for a large fraction of the observed fluorescence signal. The distributional patterns of rod-shaped diatoms and fluorescence differ in the region along the South Shore where fluorescence is intermediate in magnitude but rod-shaped diatom abundance is very low. Diatom abundance was relatively high along the offshore region of Massachusetts Bay, whereas fluorescence values were low in this area. A strong east/west gradient was observed in abundance of diatom rods along a north/south line from Barnstable Harbor northward through the middle of Cape Cod Bay (Fig. 9F). The corresponding gradient in fluorescence was restricted to northern Cape Cod Bay and did not extend inshore to Barnstable (Fig. 7F).

### ***4.3.3 Temperature-Salinity-Plankton Relationships***

The association of a given taxon to a particular water type is revealed in the temperature-salinity-plankton (T-S-P) diagrams (Figs. 10A-D). Before discussing the relationships of individual taxa to T-S properties, it is instructive to examine the T-S-P diagrams for fluorescence and beam attenuation.

The T-S-P diagrams show clearly that the highest fluorescence and attenuation values are associated with the “finger” of Cape Cod Bay water (CCBPW and CCBCW) (Figs. 10A). High fluorescence values are found in both Cape Cod Bay water types, but lower values were found in the two lower-salinity side lobes corresponding to the region off the Cape Cod Canal. Although highest fluorescence occurred in both water types, highest attenuation was found in the CCBCW. The low-intermediate attenuation values observed

near Cape Ann in the kriging plots (Figs. 8A,B) appear as a light blue region overlaying the region of CAPW in the T-S-P diagram (Fig. 10A).

Association of lower values of fluorescence and attenuation with T-S properties can be better examined in  $\log_{10}$ -transformed T-S-P plots (Fig. 10C). Here again, we find high fluorescence throughout the Cape Cod Bay water types, but now we see that intermediate values are present throughout the transition region between the MBBW and the CAPW, this region being colder than the Cape Cod Bay water types. The lowest fluorescence values were associated with the Boston Harbor Water (BHW). The intermediate values of attenuation in the CAPW are clearly seen in the  $\log_{10}$ -transformed data. It is interesting to note that a line of intermediate attenuation values runs from the CAPW to the tip of the finger of MBBW.

The T-S-P plot for rod-shaped diatoms shows that the bloom of this organism is restricted almost entirely to the CCBPW (Fig. 10A). It is likely that this diatom was blooming in the warm surface water of eastern Cape Cod Bay as it was transported around Provincetown in the CCBPW. The  $\log_{10}$ -transformed data shows the gradient in abundance along the line from the CAPW to the MBBW, with the lowest levels found in the lower salinity waters (Fig. 10C).

Other T-S-P relationships will be discussed below in the sections for each taxon.

#### **4.3.4 *Chaetoceros* Chains**

Another abundant phytoplankton group observed in the video were chain-forming *Chaetoceros* species (Fig. 11A). This group was readily identified since their long spines scattered light effectively giving them a feather-like appearance. Maximum abundance in a 10-s interval was 38/liter with mean and median values of 3.750 and 1.991/liter, respectively (Table 2).

Unlike the diatom-rods, which occurred primarily in the warm plume near Provincetown, *Chaetoceros* chains were most abundant in the middle of the survey region, i.e. the southern half of Massachusetts Bay (Fig 11B). Very low abundance was found in western and southern Cape Cod Bay and in the freshwater plume in northern Massachusetts Bay.

Kriging results show these patterns clearly (Fig 11C). Abundance along the coast is very low except near Provincetown where moderate numbers were seen. The surface waters along the south shore had low abundance of *Chaetoceros*, but their numbers increased with depth in this region.  $\log_{10}$ -transformed abundance (Fig 11D) also reveals the high concentrations in the central part of the surveyed area and highlights the very low abundance in northern Massachusetts Bay, in the surface waters along the South Shore, and in southwest Cape Cod Bay.

T-S-P diagrams for *Chaetoceros* chains reveal a primary association with the MBBW and little association with CAPW (Fig. 10A). The abundance of this group follows the mixing line toward the CAPW, but low abundance is reached well before the region of CAPW. This gradient suggests an offshore origin for this taxon. The log<sub>10</sub>-transformed abundance data (Fig. 10C) show that *Chaetoceros* chains also were present in the Cape Cod Bay waters from eastern CCBCW into the warmer CCBPW.

#### 4.3.5 *Oithona*

This copepod genus was readily distinguished from other copepod taxa in the video (Fig. 12A). The majority of *Oithona* were found to be oriented in a head-down posture as described in Davis et al. (1992a). This posture is thought to be a predator avoidance behavior. The maximum abundance of *Oithona* was 25.5 /liter and mean and median abundance was 3.538 and 2.940 /liter, respectively (Table 2).

As was the case for *Chaetoceros* chains, *Oithona* abundance was highest in the center of the surveyed region (Fig. 12B). They were more abundant in the upper 30m of the water column and were less abundant in the deeper regions of northern Massachusetts Bay and offshore areas. This genus occurred in very low abundance in the warm-plume near Provincetown and generally had lower abundance in Cape Cod Bay. Relative to *Chaetoceros*, they were more abundant in the northern part of the survey region and less abundant in the southern part

Kriging results show this pattern very clearly (Fig. 12C). The lower abundance areas are in northern Massachusetts Bay, the surface waters of the South Shore coastal region, and Cape Cod Bay. *Oithona* abundance was lowest in Cape Cod Bay as can be seen clearly in the log<sub>10</sub>-transformed abundance data (Fig. 12D).

*Oithona* abundance coincides most closely with the salinity distribution (compare Figs. 3B and 12C). The *Oithona* abundance is highest in the higher-salinity tongue that extends shoreward from the open waters of the Gulf of Maine to Plymouth through the middle of the domain. The correspondence of the *Oithona* distributional pattern with that of salinity (and density) is likely due to its offshore origins. This species is well known as a dominant member of the plankton community in the offshore waters of the Gulf of Maine and Georges Bank (e.g. Davis, 1987).

The T-S-P plot for *Oithona* reveals highest abundance along the mixing line from MBBW to CAPW, with very low abundance in CCBPW or CCBCW (Fig. 10A). This pattern is similar to that found for *Chaetoceros* chains except that *Oithona* abundance was relatively lower in Cape Cod Bay water-types and relatively higher in the CAPW. In essence, relatively high *Oithona* abundance extended into the CAPW and into the BHW as well.

The extent of this pattern is seen in the  $\log_{10}$ -transformed data (Fig. 10C), where the difference between the *Oithona* and *Chaetoceros* associations is clear. *Oithona* is relatively less abundant in the CCBPW but more abundant in the CAPW and BHW.

#### 4.3.6 *Oithona* with Eggs

Females of *Oithona* that carried egg sacs (attached to the base of the urosome) could be readily distinguished from the other plankton observed in the video (Fig. 13A). As was the case for the other *Oithona*, *Oithona* carrying eggs also were oriented primarily in a head-down posture. Such a posture may help protect the eggs from capture by a predator from below. The maximum abundance of *Oithona* with eggs was 15.4/liter with a mean value of 0.124/liter. (The median value was zero because no individuals were seen in over half of the 10-s intervals.)

The horizontal distributional pattern of *Oithona* with eggs was generally similar to that of the other *Oithona* (cf. Figs. 12C,D and 13C,D). This group was most abundant in the central part of the surveyed region, but moderate abundance also extended into Cape Cod Bay and into the near-field region of the new outfall site outside Boston Harbor. Very low abundance was found in an area off the mouth of the Cape Cod Canal and off of Cape Ann. The vertical distribution was distinctly different, however, with a general increase in abundance with depth (Fig. 13C). *Oithona* with eggs were most abundant below 20 m (Fig. 13C). The extension of the distributions into Cape Cod Bay and the near-field region is most evident in the  $\log_{10}$ -transformed abundance data (Fig. 13D). The distributional pattern for this group also appeared much more patchy than that for the other *Oithona*.

The pattern of *Oithona* with eggs matched the salinity and density patterns even more closely than did the other *Oithona* (compare Figs. 3B and 13D). The extensions of the distributions of *Oithona* with eggs into central Cape Cod Bay and into the near-field region off Boston Harbor are also seen in the salinity and density distributions. Since these relatively high salinity/density regions are contiguous with the warmer-saltier offshore water, it appears that the *Oithona* with eggs may be carried into these regions from a source offshore. The increasing abundance with depth corresponds to the increasing salinity with depth, lending further support to this view. The patchy distribution of this group also is evident in these kriging plots.

The T-S-P plot for *Oithona* with eggs was similar to that for *Oithona*, except that abundance in the CAPW was much lower (Fig. 10B). A ridge of relatively high abundance occurred along the mixing line from MBBW toward CAPW. Relatively high abundance also was observed in the CCBCW. The  $\log_{10}$ -transformed data (Fig. 10D) show the distribution extending into the CCBCW as well as in the BHW.

#### 4.3.7 Unidentified Copepods

Copepods other than *Oithona* were grouped together as unidentified copepods and comprised a mixture of *Calanus*, *Pseudocalanus*, and *Centropages* (Fig. 14A). These copepods were oriented in various directions with no obvious preferred direction. Individuals of the *Calanus* – *Pseudocalanus* genera were often observed to have oil sacs in their bodies (Fig. 14A). Unidentified copepods had a maximum abundance of 42.8 /liter and a mean and median abundance of 4.576 and 3.096 /liter, respectively (Table 2).

The curtain plot for unidentified copepods indicates that they were most abundant in southern Massachusetts Bay and Cape Cod Bay (Fig. 14B). Highest abundance was found in two areas: 1) the surface waters near the tip of Cape Cod and 2) deeper waters in the middle of Massachusetts Bay. Low abundance was observed throughout most of Cape Cod Bay, the South Shore coastal area, and in northern Massachusetts Bay.

Kriging plots for unidentified copepods also shows their bimodal spatial distribution, with heavy concentrations in surface waters near Provincetown and at depth in the middle of the survey area (Fig. 14C). The distributions appear patchy, with high concentrations in a few localized areas. Log<sub>10</sub>-transformed data show that the distribution of these copepods extends into the eastern half of Cape Cod Bay (Fig. 14D) as did the distribution of *Oithona* with eggs. Unidentified copepod abundance was much higher in the region of Provincetown. This distributional pattern contrasts with that of the other *Oithona* which had relatively low abundance throughout Cape Cod Bay.

The bimodal spatial distribution of unidentified copepods is reflected in their T-S-P diagram (Fig. 10B). Groups of high values can be seen in the MBBW and in the CCBPW with intermediate values in the intervening water types. Abundance falls off sharply along the mixing line from MBBW toward CAPW, with very low abundance observed in the CAPW itself. The log<sub>10</sub>-transformed data (Fig. 10D) show that lower concentrations do extend into the CAPW, and that the lowest values were found in the BHW and in the lowest salinity water (along the South Shore).

#### 4.3.8 Barnacle Larvae

Barnacle larvae could be distinguished by their bright light-scattering appendages and dark body (Fig. 15A). No obvious preferred orientation was observed for this taxon. Maximum abundance of barnacle larvae was 18.5 /liter and the mean was 0.715 /liter (Table 2). As was the case for larvaceans, the abundance of barnacle nauplii was biased by misidentification of rod-shaped diatoms in the bloom near Provincetown. The high abundance in this area is due to a mixture of these groups.

The curtain and kriging plots for barnacle nauplii show that the highest abundance occurred in eastern Cape Cod Bay and near Provincetown (Figs. 15B,C). Low-intermediate values (~2 /liter) extended into southern Massachusetts Bay. The  $\log_{10}$ -transformed kriging plot shows that the low-intermediate abundance values extend into central Cape Cod Bay and well into Massachusetts Bay as far as the nearfield and Boston Harbor regions (Fig. 15D). Lowest values occurred south of Gloucester Harbor and in western Cape Cod Bay. Comparison with the  $\log_{10}$ -transformed distributions of rod-shaped diatoms reveals a similar pattern (Fig. 9F), except that the diatoms were plentiful in western Cape Cod Bay and offshore in northern Massachusetts Bay, whereas barnacle nauplii had low abundance in these areas.

The T-S-P plots for barnacle nauplii show most of the high abundance values located in the CCBPW (Fig. 10B). The  $\log_{10}$ -transformed T-S-P plot (Fig. 10D) reveals that intermediate values run along the mixing line from MBBW to CAPW. This plot is similar to that for unidentified copepods. It is clear then that barnacle larvae are ubiquitous throughout the water types found in the survey area.

#### **4.3.9 Larvaceans**

Larvaceans were distinguished in the video by their head, tail, and mucous house, the latter being stippled with small particles (Fig. 16A). No preferred orientation was observed in this group. The larvaceans bodies scattered light quite well, giving them a bright shiny appearance and allowing them to be easily detected by the focus detection program. Larvaceans had a maximum abundance of 45.6 /liter and a mean and median abundance of 2.110 and 0.514 /liter, respectively (Table 2). Larvaceans were ubiquitous throughout the study area but were confused to an unknown extent with rod-shaped diatoms in the bloom near Provincetown. Thus the high abundance values in this area are a mixture of larvaceans and misidentified rod-shaped diatoms.

The linear curtain and kriging plots for this group show highest abundance in eastern Cape Cod Bay and in southern Massachusetts Bay (Figs. 16B,C), but, again, these patterns are biased to some as yet unknown extent by misidentified diatom rods. Comparing the distributions of larvaceans (Fig. 16C) and diatom rods (Fig. 9D) shows that low-intermediate abundance levels of larvaceans (~4-6 /liter) are found throughout much of the southern half of the survey area, while diatom rods are restricted to the region near the tip of Cape Cod.. The  $\log_{10}$ -transformed data reveal the widespread distribution of larvaceans (Fig. 16D) with low-intermediate values (~0.5-0.6) spread throughout the surveyed region. Lowest abundance occurred in the South Shore coastal surface waters, in southern Cape Cod Bay near Barnstable, and in the deepest layer near Cape Ann. The  $\log_{10}$ -transformed distributional patterns for diatom rods (Fig. 9F) also differs from that of the larvaceans (Fig. 16D). In terms of  $\log_{10}$ -transformed values, the diatoms have a moderate relative abundance in the offshore region of Massachusetts Bay while larvacean abundance is relatively low in this area. Likewise, although intermediate relative

abundance of larvaceans was found in the Cape Ann region, rod-shaped diatoms had relatively low abundance in this area.

The T-S-P plot for larvaceans appears similar to that for barnacle larvae, with most of the high abundance values occurring in the CCBPW (Fig. 10B). The  $\log_{10}$ -transformed T-S-P diagram appears similar to those for unidentified copepods and barnacle nauplii (Fig. 10D), except that low concentrations are found in the lowest salinity water off the south shore. Intermediate values run along a ridge from the MBBW to the CAPW.

#### **4.3.10 Ostracods / Barnacle Cyprids**

This group had a morphology that was very distinct from the other groups (Fig. 17A). The general ovoid body shape with a dark central portion indicates that these organisms are likely to be either ostracods or barnacle cyprids. No appendages were seen on any of the images however, so that positive identification was not possible. These organisms were usually oriented such that the hinge side of the valves was toward the surface. This group was not confused with rod-shaped diatoms in classification, and its abundance estimates therefore are not biased by misidentification of that group. Maximum abundance of this group was 61.3 /liter with mean and median values of 3.791 and 2.801 /liter, respectively.

The curtain plot ostracods/cyprids shows highest abundance occurring in the central portion of Massachusetts Bay (Fig. 17B). Abundance was found to be higher in the middle and lower portions of the water column creating distinct subsurface maxima for this group. The kriging plot for ostracods/cyprids reveals this pattern clearly (Fig. 17C). Highest abundance was found in the bottom layer in central Massachusetts Bay. Low abundance occurred in Cape Cod Bay and in the surface waters of the South Shore and off Gloucester Harbor. Low abundance also occurred in the bottom layer off Cape Ann. The  $\log_{10}$ -transformed data also show lowest abundance in these areas (Fig. 17D). Intermediate values were observed off Plymouth Harbor. These distributional patterns were similar to those seen for *Oithona* (cf. Figs. 12D,17D).

The T-S-P plot for ostracods/cyprids shows a strikingly close association with MBBW (Fig. 10B). The highest values were found exclusively in the MBBW region of the T-S diagram. Low abundance occurred in the other areas (CCBPW, CCBCW, CAPW, BHW). The  $\log_{10}$ -transformed data show that low-intermediate values do extend along the mixing curve from the MBBW into the CAPW (Fig. 10D). Lowest values were found in the CCBPW and in the low salinity water of the south shore. The T-S-P relationships for this group suggests a strong affinity for the warmer saltier MBBW.

#### **4.3.11 Pteropods**

Pteropods were easily identified by their bright parapodia and round bodies with dark centers (Fig. 18A). These organisms were nearly always oriented with their shells positioned below their parapodia. This group, like barnacle nauplii and larvaceans, was confused with the rod-shaped diatoms in the vicinity of the Provincetown bloom. Thus, the abundance estimates in this region reflect a combination of these two groups. Maximum abundance of pteropods was 18.3 /liter and the mean was 0.962 /liter.

The curtain plot for pteropods shows them to be patchily distributed with highest concentrations near Provincetown (Fig. 18B). Intermediate concentrations occurred in patches throughout a large portion of the survey area. The kriging plot is dominated by the high concentrations near Provincetown (Fig. 18C). The  $\log_{10}$ -transformed data show intermediate values occurring throughout the study area except for low abundance areas near Barnstable, the South Shore surface waters, and near Gloucester (Fig. 18D). Abundance in the bottom two layers is very patchy.

The T-S-P plot for pteropods shows high concentrations in the CCBPW and in the MBBW with concentrations falling off sharply along the mixing line toward the CAPW (Fig. 10B). The  $\log_{10}$ -transformed data show low-intermediate abundance throughout most of the water types reflecting the widespread nature of the pteropods (Fig. 10D).

#### **4.3.12 Total Plankton**

The kriging plot for total abundance of the above nine planktonic taxa taken together shows the overwhelming dominance of the rod-shaped diatoms in the surface bloom near Provincetown (Fig. 19A). Intermediate values (~100 /liter) occurred in southern Massachusetts Bay from surface to bottom. The  $\log_{10}$ -transformed data show high abundance extending from eastern Cape Cod Bay and Provincetown into southern Massachusetts Bay (Fig. 19B). Lowest values occurred in southern Cape Cod Bay, in the surface waters near the South Shore and Gloucester, and in the deepest layer off Cape Ann.

#### **4.3.13 Summary of Plankton Patterns**

The plankton taxa can be divided into four groups based on their distributional patterns. First, rod-shaped diatoms dominated the CCBPW which was also characterized by high fluorescence and beam attenuation. Second, *Chaetoceros* chains and Ostracods/cyprids were closely associated with the warmer saltier MBBW. Third, *Oithona* and *Oithona* with eggs also were most abundant in the MBBW, but their distributions extended north into the CAPW/BHW and *Oithona* with eggs extended south into CCBCW. Fourth, unidentified copepods, larvaceans, pteropods, and barnacle nauplii all had high abundance in both the CCBPW and in the MBBW, and the latter three taxa were ubiquitous throughout the study area.

## ***4.4 Correlation Length Scales***

The variograms computed for kriging the different depth layers for each variable were used to determine the corresponding correlograms. In this section, the correlograms are described for each variable at each of the five depths corresponding to the kriging plots.

### ***4.4.1 Physical Variables***

The correlograms for temperature varied as a function of depth (Fig. 20A). In the top two layers (0-10 m and 10-20m) the covariance fell off nearly linearly with the lagged distance. Negative correlations were found at length scales of 40-60 km. The covariance crossed the zero line at about 30 km for both of these surface layers. In contrast, the covariance function in the deeper layers decreased more abruptly with distance, with the covariance at a lag of 20 km having a value close to zero. Thus, in the upper layers, temperature was positively correlated over longer scales than it was in the deeper layers. In the lower two layers temperature values were uncorrelated at the longest length scales (~40 km), while in the upper layers a strong negative correlation was found at these scales.

In contrast to temperature, surface salinity values became uncorrelated over much shorter distances (Fig. 20B). The covariance function fell to zero sharply, reaching zero at 20 km and 12 km in the upper 0-30 and >30 m layers, respectively. In the layers between 10-30 m, negative correlation occurred at distances greater than 20 km with a minimum correlation occurring near 30 km.

An explanation for these patterns can be found by considering the underlying source of the variability. Temperature is forced over large spatial scales through surface heating. Salinity on the other hand is influenced by local discharge and runoff, so this forcing is operates over shorter spatial scales than does the forcing of temperature. The larger correlation length scales for temperature than for salinity in the surface layers then is likely due to the larger scale over which the temperature forcing operates. Correlograms for temperature and salinity are more similar to each other in the deeper layers, since surface heating has less influence at these depths.

### ***4.4.2 Fluorescence and Attenuation***

Correlograms for fluorescence (Fig. 21A) more closely match those for temperature than salinity. In the upper 0-20 m, the correlograms for temperature and fluorescence are quite similar with a generally linear decrease to a maximum negative correlation at 50-60 km. As for temperature, in the deeper layers, the covariance of fluorescence values falls off more sharply with distance, reaching zero at 20 km in the 20-30m layer. In the >40 m

layer, however, the covariance decreases less rapidly with distance, reaching a value 0.25 at 20 km.

The fluorescence also had a pronounced “shoulder” at about 20-30 km with a steeper negative slope at shorter and longer length scales. Temperature and salinity also had “shoulders” at 20-30 km, although these varied in magnitude. In most cases, the “shoulders” in the correlograms for fluorescence, temperature, and salinity occurred near the zero covariance line, signifying a lack of correlation at scales of 20-30 km. In the two deepest layers, the covariance value at 40 km was about -0.25 whereas at shallower depths it was near zero at this length scale. In general, whereas the covariance of temperature and salinity values tended to level off to near zero at distances above 20 km, the covariance of fluorescence values reached a shoulder 20-30 km and then continued to decrease, reaching a relatively large negative value at the largest length scales (Fig. 21A). Thus in the bottom three layers, fluorescence became strongly negatively correlated at the longest length scales, whereas covariance in temperature and salinity was near zero at scales greater than about 20 m.

The strong negative correlation for fluorescence is likely due to the high values in eastern Cape Cod Bay and southern Massachusetts Bay. Relatively high fluorescence values extended down in the water column, and, as seen in the log-transformed fluorescence data, a pronounced gradient in fluorescence was present across the survey area at all depths (Fig. 7F). This fluorescence pattern was likely due to a combination of *Chaetoceros* chains and rod-shaped diatoms, which together, yield an joint abundance pattern that is similar to that of fluorescence.

The correlograms for attenuation (Fig. 21B) were similar to those for fluorescence except that the “shoulders” were less pronounced and the covariance tended to fall off more sharply with distance, reaching negative values at shorter length scales. A sharper decline in covariance was observed in the deeper layers (>20 m), with this decline followed by a leveling off at a value near -0.25. In the upper layers the correlograms for attenuation and fluorescence were similar, but attenuation covariance values were more negative at the larger scales. The reason for this difference in correlation length scales for attenuation and fluorescence can be seen in the kriging plots for these variables (cf. Figs. 7F and 8B). It is clear from these plots that the distribution of fluorescence is broader than that of attenuation. The smaller scale of the attenuation distribution is reflected in its correlogram.

### 4.4.3 Planktonic Taxa

#### 4.4.3.1 Rod-Shaped Diatoms

Covariance for rod-shaped diatom abundance decreases to zero in the first 20 km at all depths (Fig. 22A). In the surface layer the covariance levels off and is slightly negative (-0.1). In the 10-30 m layers, a shoulder is reached at 20 km where the covariance is zero until about 30 km at which point the covariance become increasingly negative. In the two deepest layers, no shoulder is seen, and the covariance drops continuously to relatively large negative values at 40 km (-0.4).

The loss of correlation in the first 20 km reflects the localized nature of the rod-shaped diatom bloom (Fig. 9D). Strong negative correlation at large scales in the deeper layers may be attributed to very low abundance of these diatoms in the subsurface waters near Cape Ann (Fig. 9F). It is not clear why the covariance levels off at a slightly negative value in the surface layer yet becomes increasingly negative in the deeper layers.

#### 4.4.3.2 *Chaetoceros* Chains

The correlograms for *Chaetoceros* chains differ from the rod-shaped diatoms in that they decrease more gradually with distance (Fig. 22B). In the surface layer, the covariance remains positive until ~27 km, then decreases, reaching relatively large negative values (-0.4) by 40 km. These large negative covariance values, at large distances, were found at all depths.

Another interesting characteristic of the *Chaetoceros* correlograms is the sharp drop in covariance over the first 2 km (i.e. between the first and second data points). At distances of 2-20 km the decrease was gradual, but during the first 2 km, the correlation fell abruptly in the top three depth layers. This large drop in correlation reflects some degree of local patchiness on scales < 2 km. Such a sharp reduction over the first 2 km was not observed in any of the environmental variables (temperature, salinity, fluorescence, attenuation) or in rod-shaped diatoms.

The correlograms for rod-shaped diatoms had a more curvilinear shape than those for *Chaetoceros* (cf. Figs. 22A,B). Within the first 20 km, the spatial correlation for rod-shaped diatoms decreased more quickly than it did for *Chaetoceros*. For example, at 10 km, the covariance values were higher for *Chaetoceros* than for the rod-shaped diatoms. By contrast, at length scales greater than 20 km, the covariance decreased more sharply for *Chaetoceros* in the three upper layers (0-30 m). The shapes of the *Chaetoceros* correlograms did not match those for any of the other variables (but did match those of the unidentified copepods; see below).

The more gradual decrease in covariance with distance over the first 20 km reflects the larger size of the *Chaetoceros* “patch” compared to the rod-shaped diatom bloom (cf. Figs. 9D and 11C). At a 10 km scale the gradients in the vicinity of the rod-shaped diatom bloom are sharper than the gradients in the *Chaetoceros* “patch”. At larger scales, the strong negative correlation for *Chaetoceros* is due to its affinity for the southern Massachusetts Bay waters (eg. MBBW) and generally low abundance outside this region (Fig. 11D).

#### 4.4.3.3 *Oithona*

The correlograms for *Oithona* were highly linear in the two upper layers (0-20 m) but had a curvilinear shape in the deeper layers (>20 m) (Fig. 22C). As was the case for *Chaetoceros*, the covariance dropped sharply over the first 2-4 km, indicating some degree of local patchiness over these scales. In the upper 0-20 m, the covariance decreased linearly from 2-4 km to 58 km, reaching values of -0.4 to -0.5. Also, in the upper 0-20 m, at 20 km the covariance remained positive with a value of ~0.25, and covariance crossed the zero line at a distance of 30-35 km. In the deeper layers, the covariance decreased more quickly with distance over the first 20 km, reaching the zero line at 18-20 km. At larger scales, the covariance in the deeper layers (>20 m) leveled off at a value near -0.25 at a distance of ~30 km. Interestingly, in the 30-40 m layer, the correlation went back to zero at a distance of 50 km, indicating a dominant length scale of negative correlation at 30 km and lack of correlation at the 50 km scale.

The characteristics of these correlograms can be better understood by examining the distributional patterns of *Oithona*. The curtain plots for *Oithona* and *Chaetoceros* show the patchy nature of these organisms (Figs. 11B and 12B), which accounts for the sharp drop in correlation over the first 2-4 km. The kriging plots for *Oithona* show that its region of high-abundance in the upper 20 m is larger than that of either *Chaetoceros* or rod-shaped diatoms (Figs. 9D,11C,12C). This larger-scale distributional pattern causes the covariance values over the first 30 km in the upper 20 m to be greater for *Oithona* than for the other two groups.

It is interesting to note that the order of the “size of high-abundance region” for these three taxa is reflected in their correlograms. In the upper 20 m, *Oithona* had the largest region of high-abundance, followed, in order, by *Chaetoceros* and rod-shaped diatoms. Their corresponding correlograms reflect this trend, in that the correlation length scale (eg. the distance at which the covariance crosses the zero line) is greatest for *Oithona* (30-35 km), intermediate for *Chaetoceros* (25-30 km), and shortest for rod-shaped diatoms (~20 km). In general, the covariance decreased most sharply for rod-shaped diatoms, more gradually for *Chaetoceros*, and most gradually for *Oithona*.

At depths >20 m, the size of the high-abundance region for *Oithona* is reduced and the covariance decreased more sharply, reaching the zero line at 20 km. At these depths, the

size of the high-abundance region for *Oithona* is similar to that of *Chaetoceros*, whose covariance values also reach the zero line at 20 km.

At greater length scales (>40 km), the large negative correlation in the upper 20 m for *Oithona* was due to its low abundance in Cape Cod Bay relative to Massachusetts Bay. In deeper layers, the negative correlation at large scales tapers off due to the loss of data points in Cape Cod Bay (because it is shallow there). By contrast, for *Chaetoceros*, the correlation at these large length scales does not taper off at depths >20 m and instead remains as strongly negative at these depths as it is in the upper layers. This difference is due to the restriction of *Chaetoceros* to the southern Massachusetts Bay with very low abundance in the northern half, whereas *Oithona* is plentiful in both northern and southern halves of Massachusetts Bay. Thus a sharp gradient across the domain is maintained with increasing depth for *Chaetoceros* but not for *Oithona*.

#### 4.4.3.4 *Oithona* with Eggs

The patchy nature of *Oithona* with eggs is seen in the correlograms for this group (Fig. 22D). A very large loss of correlation occurs within the first 2-4 km in the upper 20 m. In these shallower layers, the covariance decreases very gradually, and linearly, from 0.2 to -0.25 between 10 and 60 km, with a zero crossing at 30 km. In deeper layers, there is a complete loss of correlation within the first 5-10 km and near zero correlation at larger scales, except in the deepest layer where a negative correlation at 40 km was found.

The curtain plot for this species reveals its patchy nature (Fig. 13B). Kriging plots show the widespread occurrence of this organism (Fig. 13C). The distribution in the upper 20 m appears less patchy than at depth. Patchiness in the deeper layers appears on scales <10 km and broad background distribution accounts for the lack of correlation at larger scales. The sharp drop in covariance over the first 2-6 km in the upper 20 m can be accounted for by small scale patchiness (<6 km). Also in the upper 20 m, the gradual, linear, decrease in correlation from 10-60 km can be explained by the lack of pronounced patchiness and the large scale gradient in abundance over the region (note the ridge of relatively high abundance that runs from eastern Cape Cod Bay into the nearfield region) (Figs. 13C,D).

#### 4.4.3.5 Unidentified Copepods

The other copepods also were patchy on the smallest scales as indicated by the sharp drop in correlation over the first 2 km (Fig. 22E). Unlike *Oithona* and *Oithona* with eggs, however, after this initial drop over the first 2 km, the covariance for the other copepods decreased gradually and quasi-linearly from 2 to 60 km. In the upper 20 m the covariance values reached zero at a distance of 25-30 km, while in the deeper layers, the zero line was crossed at 20 km. This decline resulted in a large negative correlation at larger length

scales (>40 km) at all depths. The correlogram for these copepods was very similar to that for *Chaetoceros* chains (Fig. 22B).

The gradual linear decrease in correlation can be explained by the relatively large region of high abundance, the lack of pronounced patchiness on scales of ~10 km (as was seen in *Oithona* with eggs), and the pronounced gradient across the survey region at all depths (Figs. 14C,D). The sharper decrease in correlation over the first 20 km in the deeper layers (>20 m) may be attributable to the patchiness on scales of 15-20 km observed in the kriging plots (Fig. 14C,D). The covariance values did not taper off with increasing distance as was the case for *Oithona* because of the pronounced north-south gradient in Massachusetts Bay (Fig. 14D) (as was seen for *Chaetoceros* chains).

#### 4.4.3.6 Barnacle Nauplii

As was the case for copepods and *Chaetoceros* the covariance dropped sharply for barnacle nauplii over a very short distance (2-4 km), signifying pronounced patchiness at these small scales (Fig. 22F). At larger scales the covariance fell gradually and linearly with distance, crossing the zero line at 25-30 km. Negative covariance values were found at the largest scales (40-60 km).

The gradual decline in covariance with distance is indicative of the generally broad distribution of this group (Fig. 15D). The localized region of high abundance, however, accounts for the relatively short distance over which the covariance reaches zero. The lack of pronounced patchiness at scales of 10-20 km and the large scale gradient in abundance across the surveyed region causes the linear decrease in covariance. The negative covariance at larger scales is due to the low abundance of barnacle nauplii in northeastern Massachusetts Bay and western Cape Cod Bay (Fig. 15D).

#### 4.4.3.7 Larvaceans

Covariance values for larvaceans decreased abruptly to zero within the first 20 km and remained at or near zero at larger scales (Fig. 22G). In the upper 20 m, the covariance fell sharply within the first 2-4 km and then more gradually to the zero crossing at 20 km. The correlation remained close to zero at all higher length scales. In the deeper layers, the covariance fell to near zero within the first 10 km. In the 20-30 m layer the covariance remained near zero at all higher length scales, while at depths >30 m a negative correlation was found at a distance of 40 km.

Correlograms for larvaceans reflect the widespread and patchy nature of this taxon (Fig. 16D). In the upper two layers, the localized region of high abundance (Fig. 16D) causes the correlation length scale of this group to be relatively short (~20 km zero crossing),

which was similar to the case for diatom rods. In the upper 30 m, no pronounced large scale gradient in abundance is observed (Fig. 16D) which accounts for the lack of negative correlation at large scales. At depths >30 m, low abundance values appear in the offshore and Cape Ann region, creating a large scale gradient that leads to the negative correlation observed at scales >40 km.

#### 4.4.3.8 *Ostracods/Cyprids*

Correlation length scales for Ostracods/Cyprids were greater than for any other taxon (Fig. 22H). After a small initial drop in covariance over the first 2 km, the covariance decreased gradually and nearly linearly over scales from 2-60 km. The zero crossings occurred at 35 km in the two upper layers, at 25-30 km in the 20-40 m layers, and at 19 km in the deepest layer. A strong negative correlation occurred at distances >40 km at all depths.

Although this taxon is most abundant in southern Massachusetts Bay, intermediate abundance occurs over a fairly broad area (Figs. 17B-D). The large region of relative abundance in each layer accounts for the correspondingly large correlation length scale for this group. The large scale gradient and lack of 10-20 km patchiness accounts for the gradual decrease in correlation with distance and the large negative correlation at scales >40 km.

#### 4.4.3.9 *Pteropods*

Correlograms for pteropods were nearly identical to those for larvaceans (Fig. 22I). Covariance values decreased abruptly to zero within the first 20 km and remained near zero at scales up to 40 m. Negative correlations did occur at scales of 50-60 km in the upper 20 m, and slightly negative values occurred at deeper depths as well. In the deeper layers, the covariance fell to near zero within the first 5-10 km.

As was the case for larvaceans, correlograms for pteropods reflect its widespread and patchy distribution (Fig. 18D). The localized region of high abundance in the upper two layers causes the covariance to fall to zero by 20 km. No pronounced large-scale gradient in abundance was observed in any depth layer (Fig. 18D), which accounts for the lack of negative correlation at large scales.

## LITERATURE CITED

Angel, M. V. and M. J. R. Fasham. 1983. Eddies and biological processes. pp. 492-524. in A. R. Robinson, ed., *Eddies in marine science*. Springer, Berlin.

Bigelow, H. B. 1926. Plankton of the offshore waters of the Gulf of Maine. *Bull. U. S. Bur. Fish.*, 40, 1-509.

Bridges, W. L., R. D. Anderson, J. D. Davis, and D. Merriman. 1984. A brief survey of Pilgrim Nuclear Power Plant effects upon the marine aquatic environment. Observations on the Ecology and Biology of Western Cape Cod Bay, Massachusetts., *Lect. Notes Coast. Estuar. Stud.*, 11, 263-271

Cassie, R. M. 1959a. An experimental study of factors inducing aggregation in marine plankton. *N.Z. J. Sci.*, 2, 339-365.

Cassie, R. M. 1959b. Some correlations in replicate plankton samples. *N.Z. J. Sci.*, 2, 473-484.

Cassie, R. M. 1960. Factors influencing the distribution pattern of plankton in the mixing zone between oceanic and harbor waters. *N.Z. J. Sci.*, 3, 26-50.

Cibik S. J., Lemieux K. B., Davis C. S., and D. M. Anderson. 1998. Massachusetts Bay plankton communities: characterization and discussion of issues relative to MWRA's outfall relocation. Boston: Massachusetts Water Resources Authority. Report ENQUAD 98-08. 140 p.

Cushing, D. H. 1975. *Marine Ecology and Fisheries*. Cambridge University Press, Oxford.

Davis, C. S. 1987. Components of the zooplankton production cycle in the temperate ocean. *J. Mar. Res.*, 45, 947-983.

Davis, C. S., G. R. Flierl, P. J. Franks and P. H. Wiebe. 1991. Micropatchiness, turbulence, and recruitment in plankton. *J. Mar. Res.*, 49, 109-151.

Davis, C. S., S. M. Gallager, M. S. Berman, L. R. Haury, and J. R. Strickler. 1992a. The Video Plankton Recorder (VPR): Design and initial results. *Arch. Hydrobiol. Beih.*, 36, 67-81.

Davis, C. S., S. M. Gallager, and A. R. Solow. 1992b. Microaggregations of oceanic plankton observed by towed video microscopy. *Science* 257, 230-232.

Davis, C. S., S. M. Gallagher, M. Marra, and W. K. Stewart. 1996. Rapid visualization of plankton abundance and taxonomic composition using the Video Plankton Recorder. *Deep Sea Res. II*, 43, 1947-1970.

Davis, C. S. and S. M. Gallagher. 1998. Cruise Report for R/V *Peter W. Anderson* cruise 9803, March, 11-14, 1998. MWRRA Report, 4/1998.

Denman, K. L. 1992. Scale-determining biological-physical interactions in oceanic food webs. In: Giller, P.S., A. G. Hildrew, and D. G. Raffaelli, (eds.), *Aquatic Ecology: Scale, Pattern, and Process*. Blackwell Scientific, Oxford, pp. 377-402 .

Denman, K. L., and A. E. Gargett. 1995. Biological-Physical interactions in the upper ocean: the role of vertical and small scale transport processes. *Ann. Rev. Fluid Mech.*, 27, 225-255.

Fasham, M.J.R. 1978. The statistical and mathematical analysis of plankton patchiness. *Oceanogr. Mar. Biol. Ann. Rev.*, 16, 43-79.

Gallagher, S. M., C. S. Davis, A. W. Epstein, A. Solow, and R. C. Beardsley. 1996. High resolution observations of plankton spatial distributions correlated with hydrography in the Great South Channel, Georges Bank. *Deep Sea Res. II*, 43, 1627-1664. Haeckel, E. 1890 *Plankton Studies*. [transl. by G.W. Field]. Rep. U.S. Comm. Fish Fish. 1889-1891, p. 565-631.

Hardy, A. C. 1936. Observations on the uneven distribution of the oceanic plankton. *Discovery Rep.*, 11, 511-538.

Hardy, A. C. and E. R. Gunther. 1935. The plankton of the South Georgia whaling grounds and adjacent waters, 1926-1927. *Discovery Rep.*, 11, 1-456.

Haury, L. R., J. A. McGowan and P. H. Wiebe. 1978. Patterns and processes in the time-space scales of plankton distributions, in *Spatial Patterns in Plankton Communities*, J. H. Steele, ed., Plenum Press, New York, 277-327.

Haury, L. R. P. H. Wiebe, M. H. Orr, and M. G. Briscoe. 1983. Tidally generated high-frequency internal wave packets and their effects on plankton in Massachusetts Bay. *J. Mar. Res.*, 41, 65-112.

Horst, T., R. Lawton, R. Toner, M. Scherer, J. D. Davis, and D. Merriman. 1984. Seasonal abundance and occurrence of some planktonic and ichthyofaunal communities in Cape Cod Bay: Evidence for biogeographical transition. *Observations on the Ecology and Biology of Western Cape Cod Bay, Massachusetts.*, *Lect. Notes Coast. Estuar. Stud.*, 11, 241-261.

Jossi, J.W. and J.R. Goulet. 1990. Zooplankton community abundance, coherence, and stability of the northeast shelf ecosystem. *ICES C.M.* 1990/L:93.

Longhurst, A. R., ed. 1981. Analysis of marine ecosystems. Academic Press, London. 741 pp.

Mackas, D. L., K. L. Denman, and M. R. Abbott. 1985. Plankton Patchiness: Biology in the physical vernacular. Bull. Mar. Sci., 37,652-674.

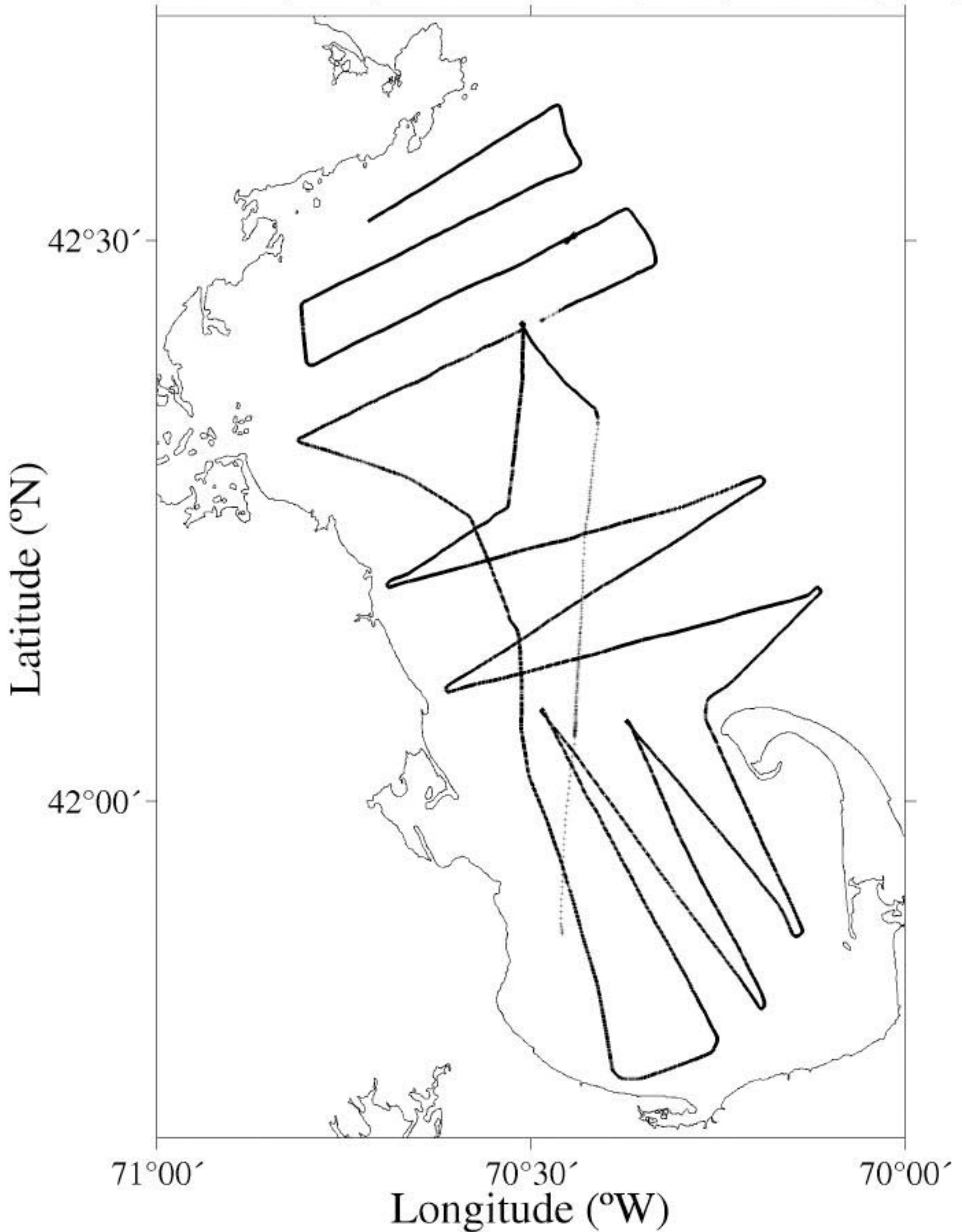
Okubo, A. 1980. Diffusion and ecological problems: mathematical models. Biomathematics, 10, Springer Verlag, NY.

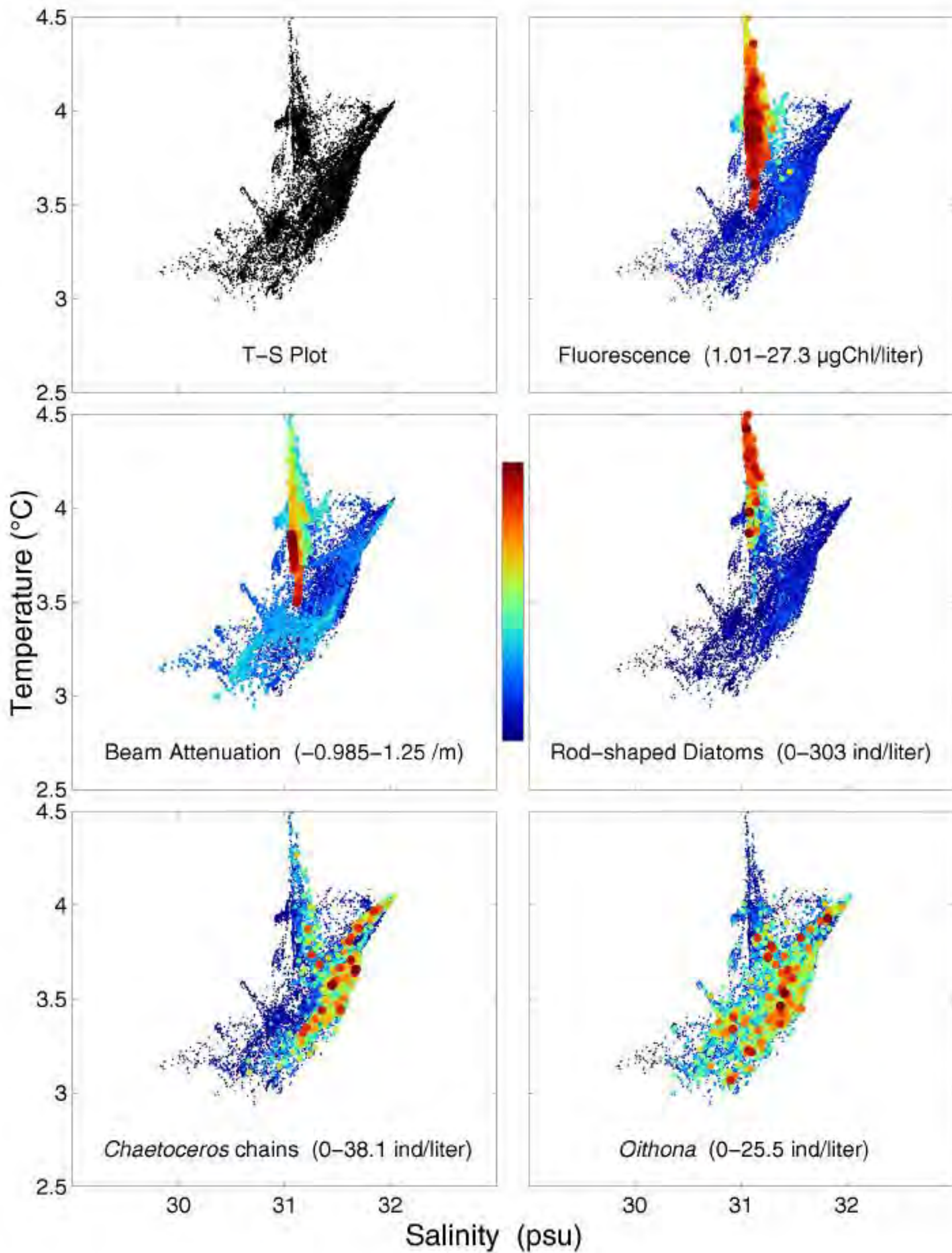
Owen, R. W. 1966. Small-scale horizontal vortices in the surface layer of the sea. J. Mar. Res., 24, 56-66.

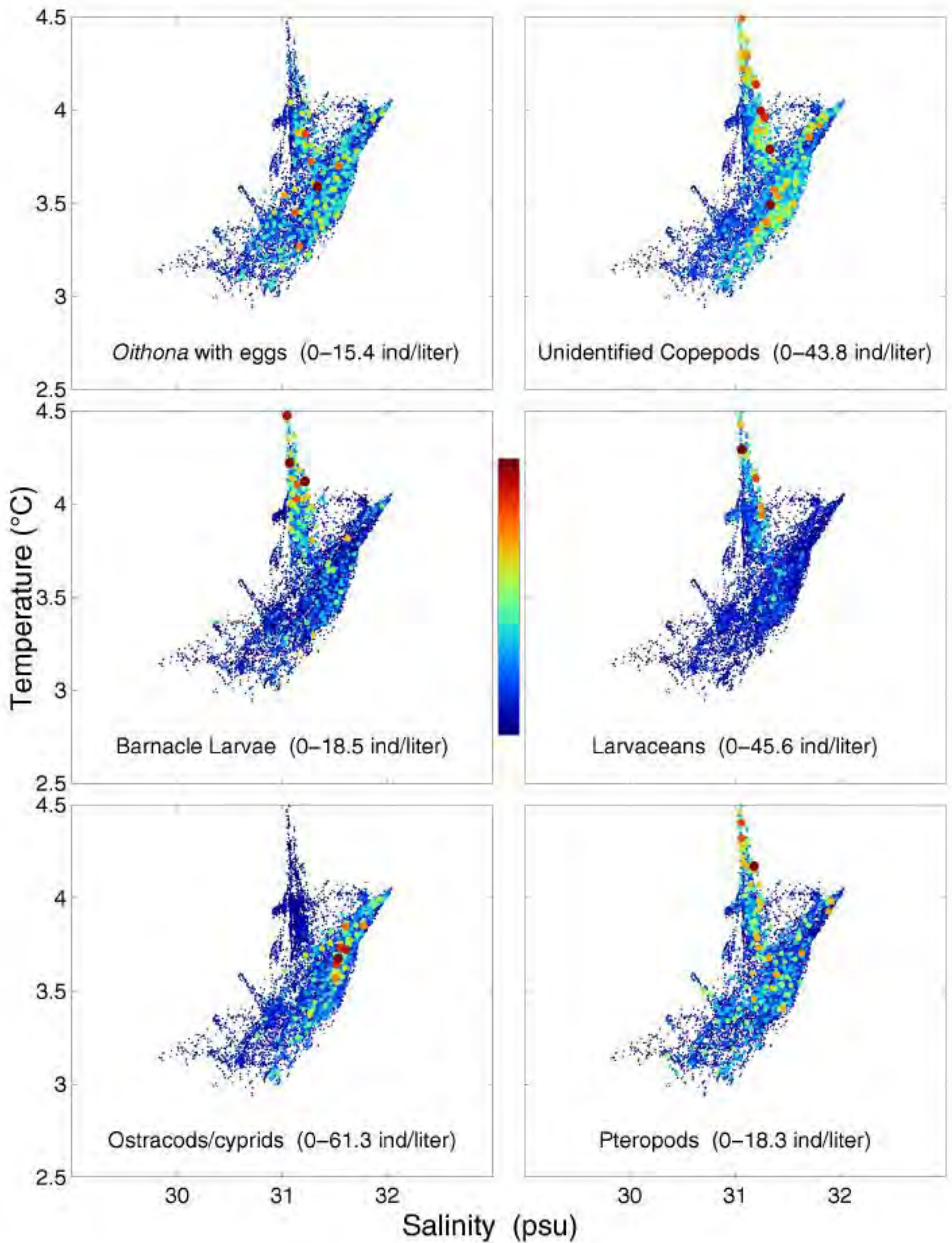
Toner, R.C. 1984. Zooplankton of Western Cape Cod Bay. In: Lecture notes on Coastal and Estuarine Studies 11. Observations on the Ecology and Biology of Western Cape Cod Bay, Massachusetts, J.D. Davis and D. Merriman, eds. pp. 65-76.

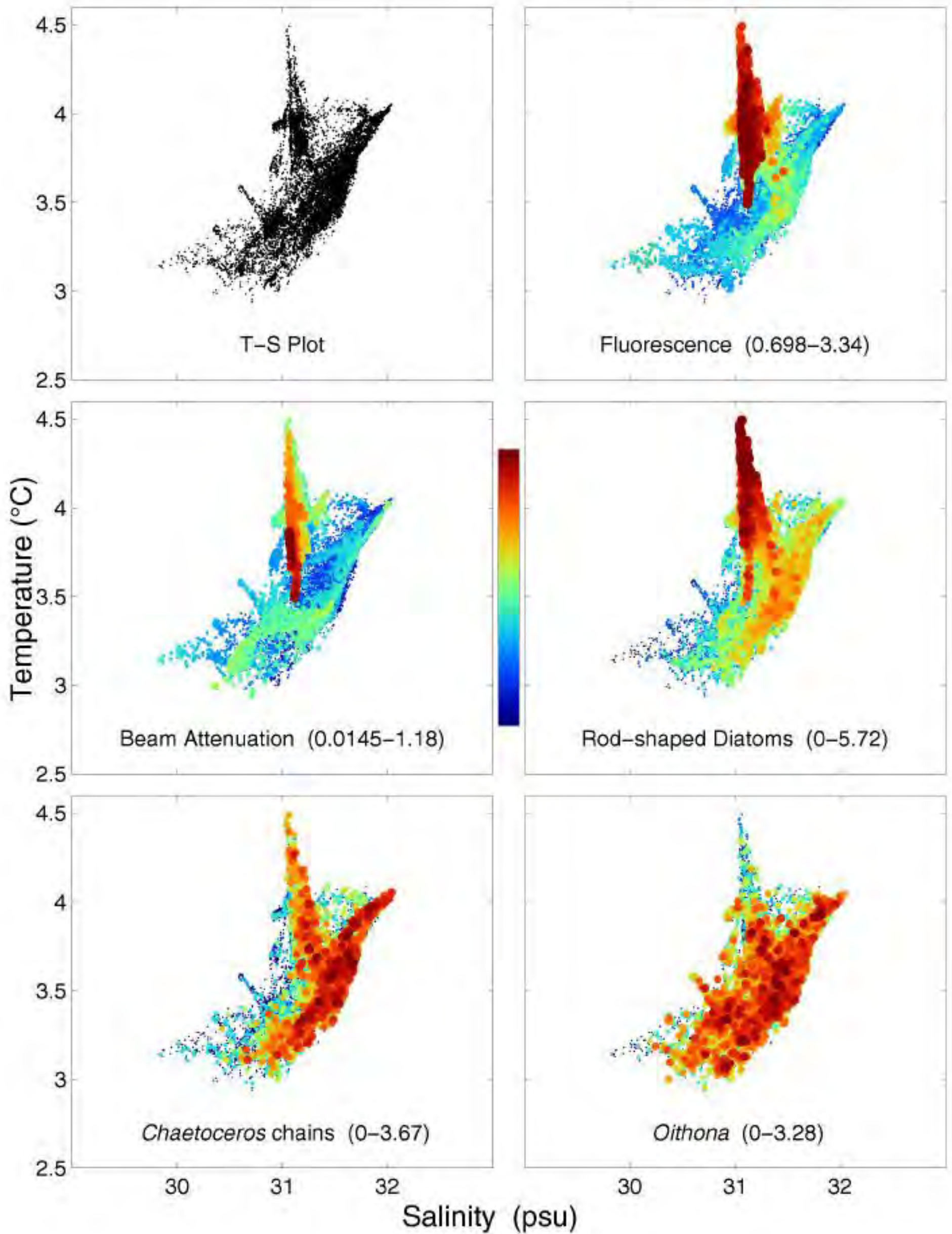
Turner, J.T. 1994. Planktonic Copepods of Boston Harbor, Massachusetts Bay, and Cape Cod Bay, 1992. Hydrobiologia, 292/293: 405-413.

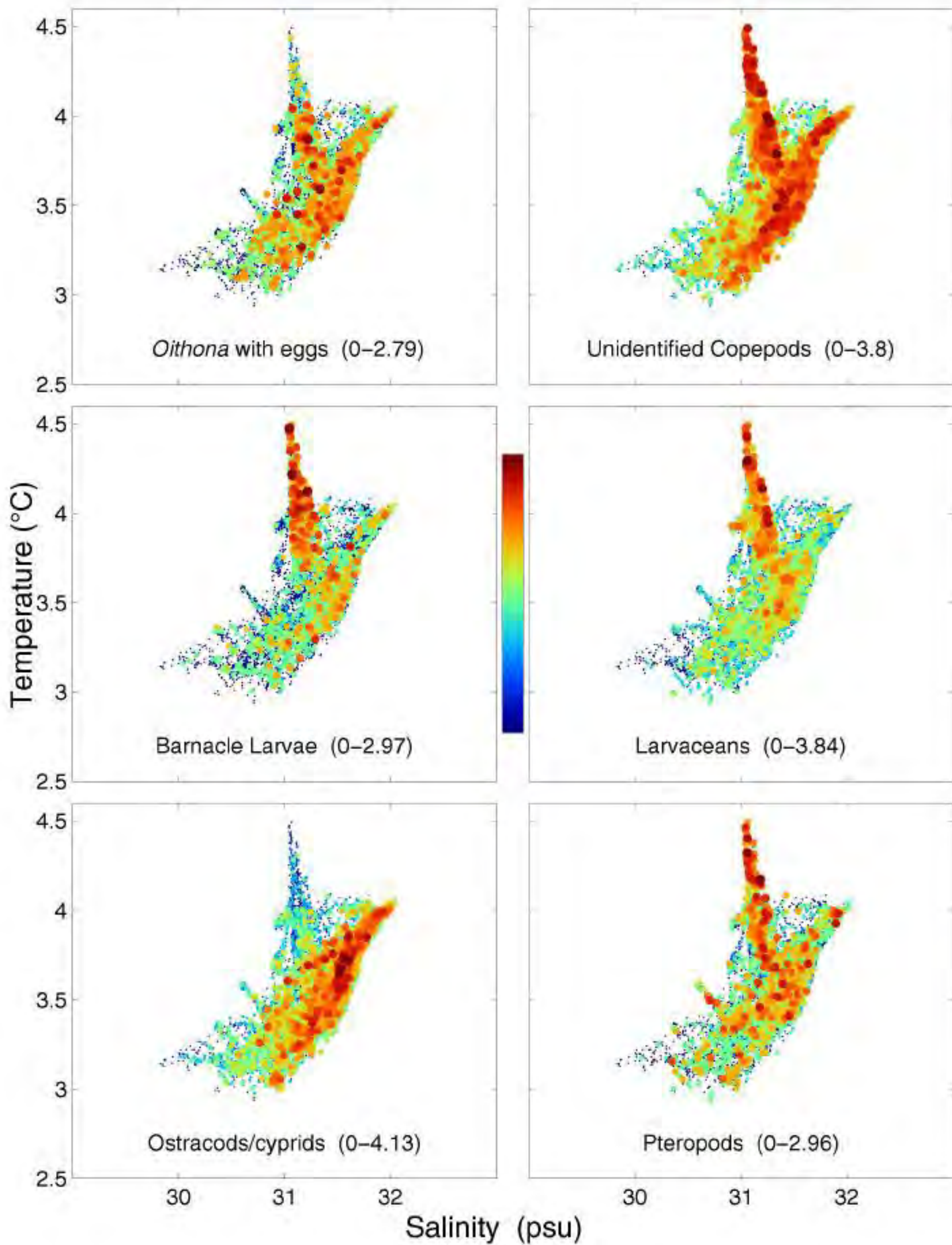
AN9803 – Positions of VPR Data  
March 12 (0230) – March 14 (1415), 1998 (EST)

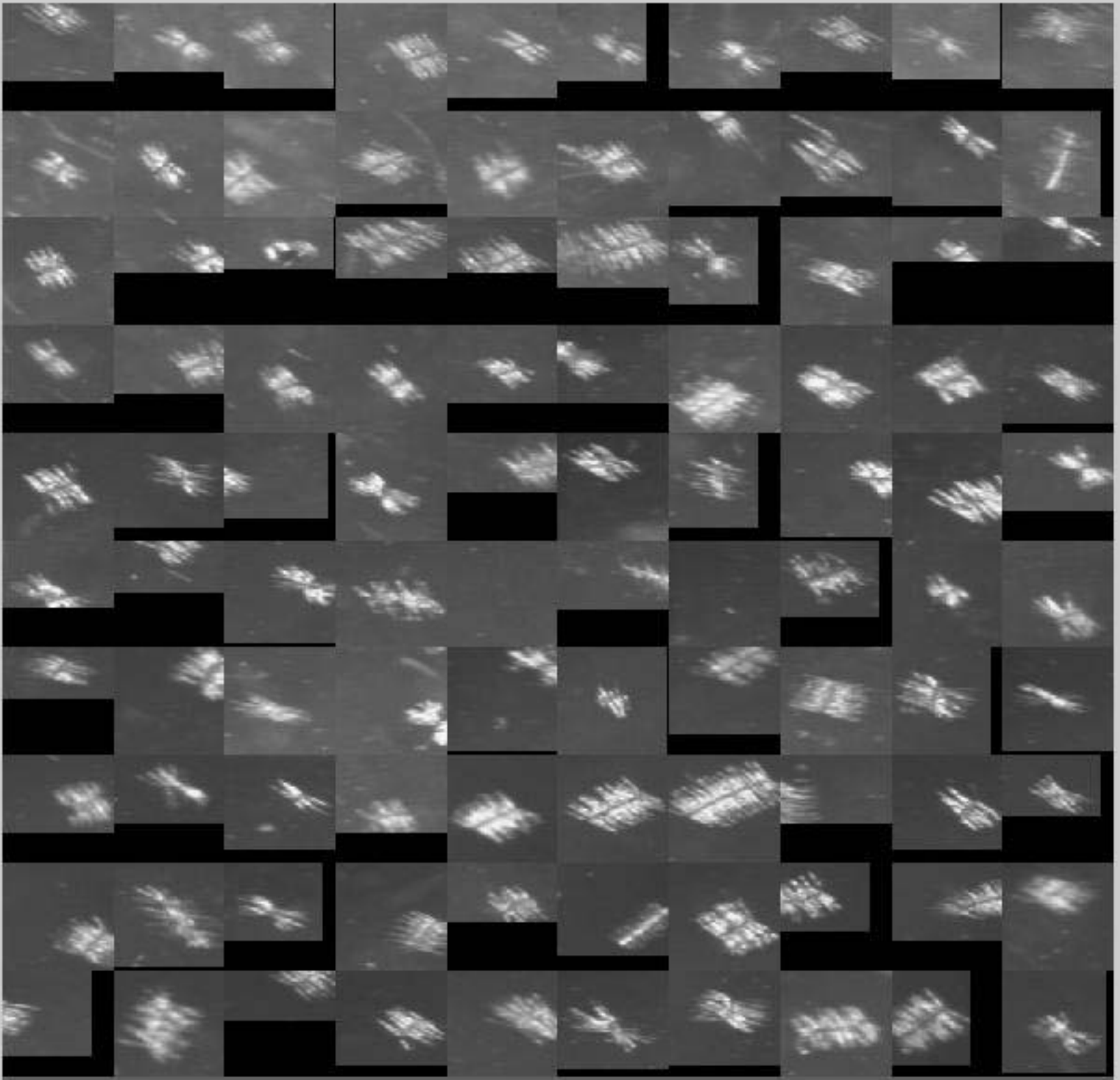








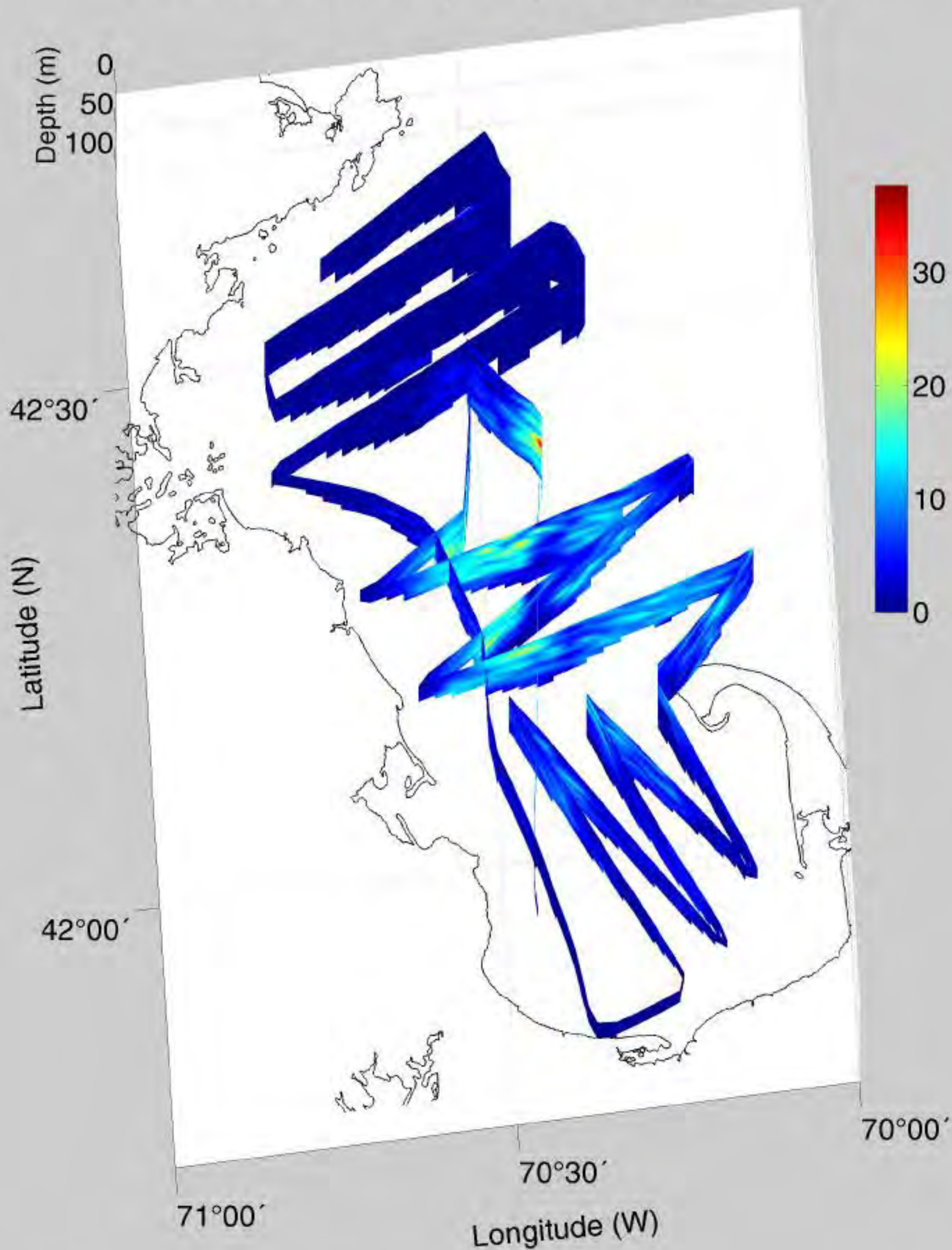




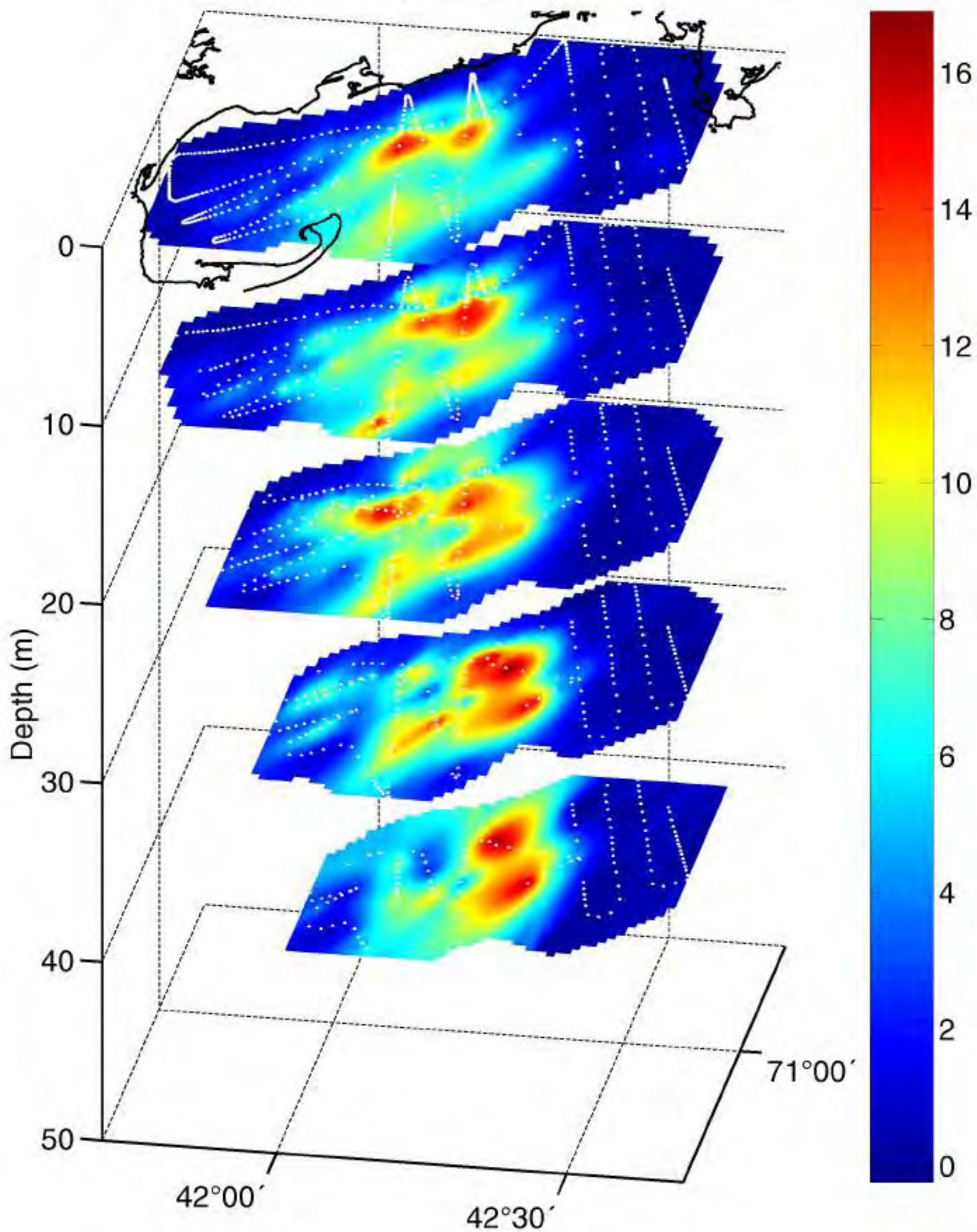
*Chaetoceros* chains

— ~ 1.0 mm

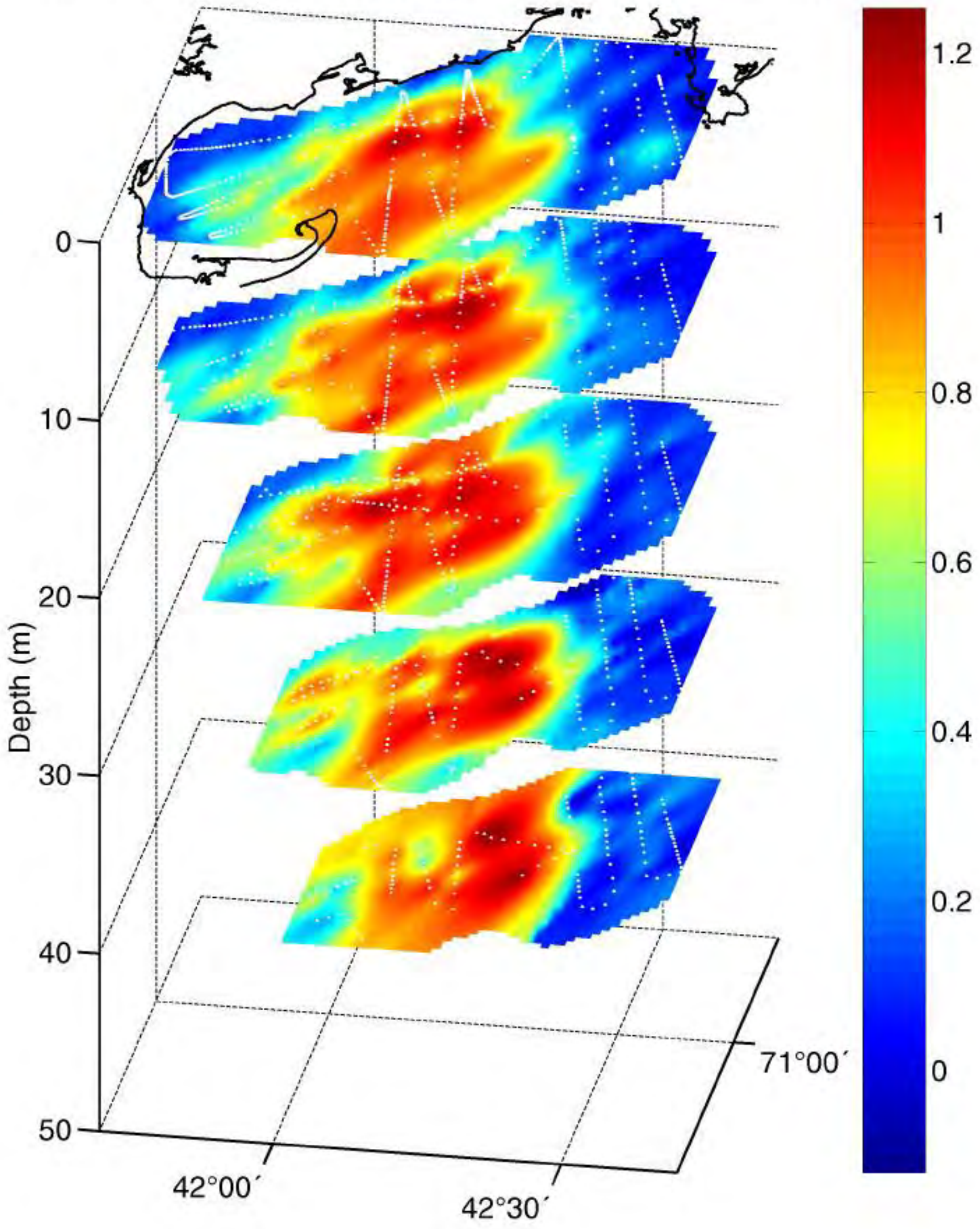
*Chaetoceros* chains (#/liter) March 12–14, 1998

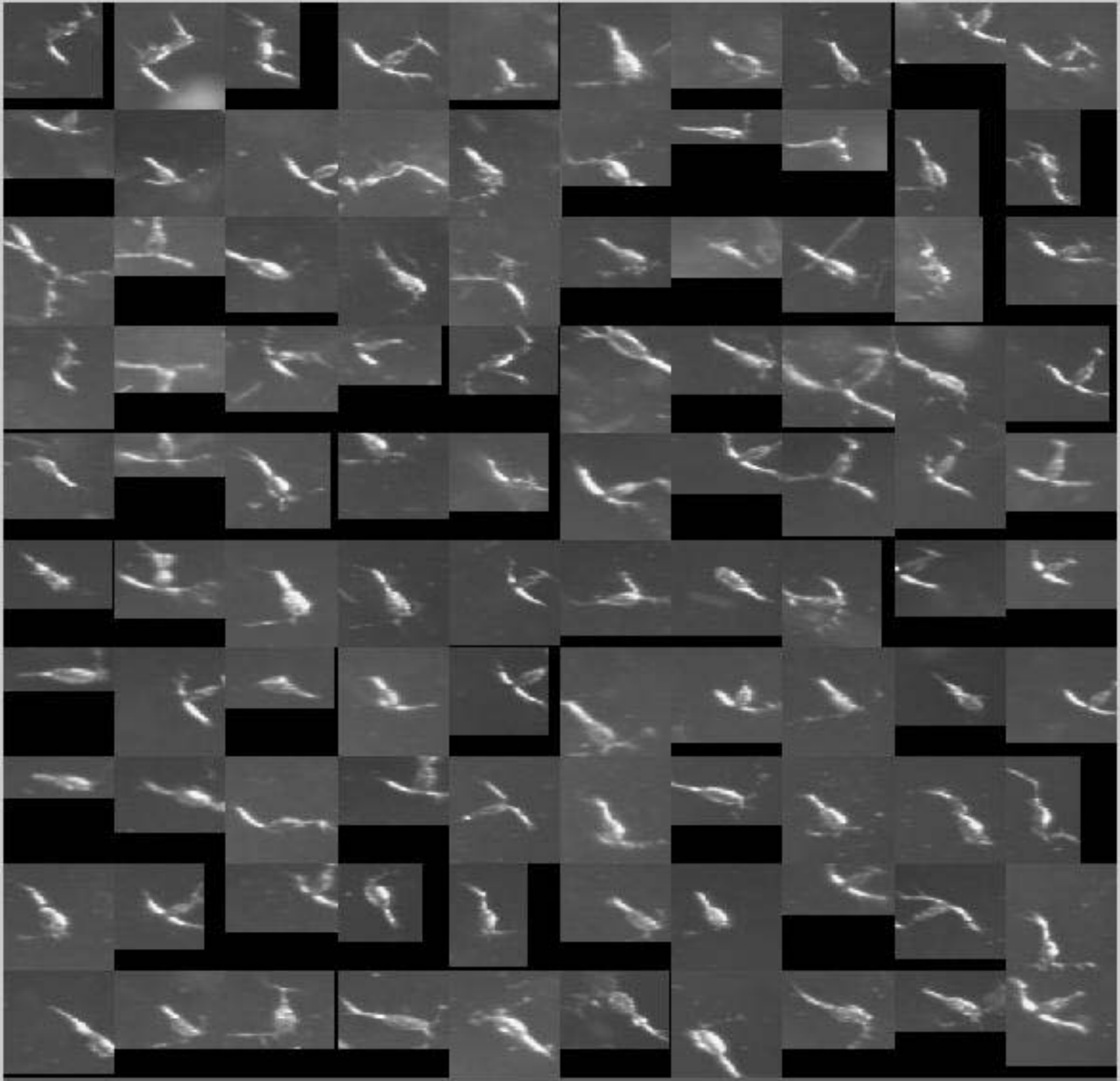


*Chaetoceros* chains (#/liter), March 12–14, 1998



*Chaetoceros* chains ( $\text{Log}_{10}[\#/ \text{liter} + 1]$ ), March 12–14, 1998

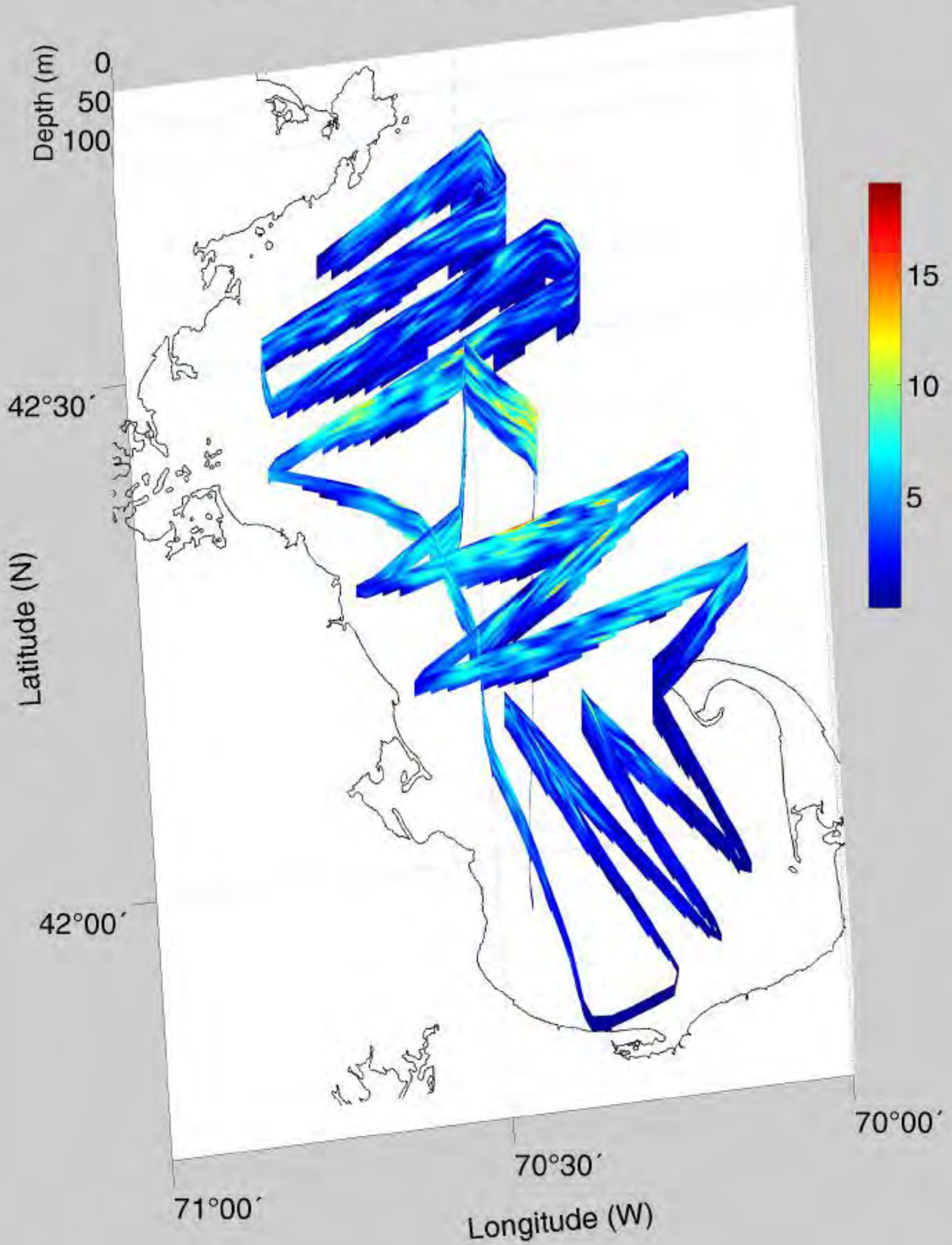




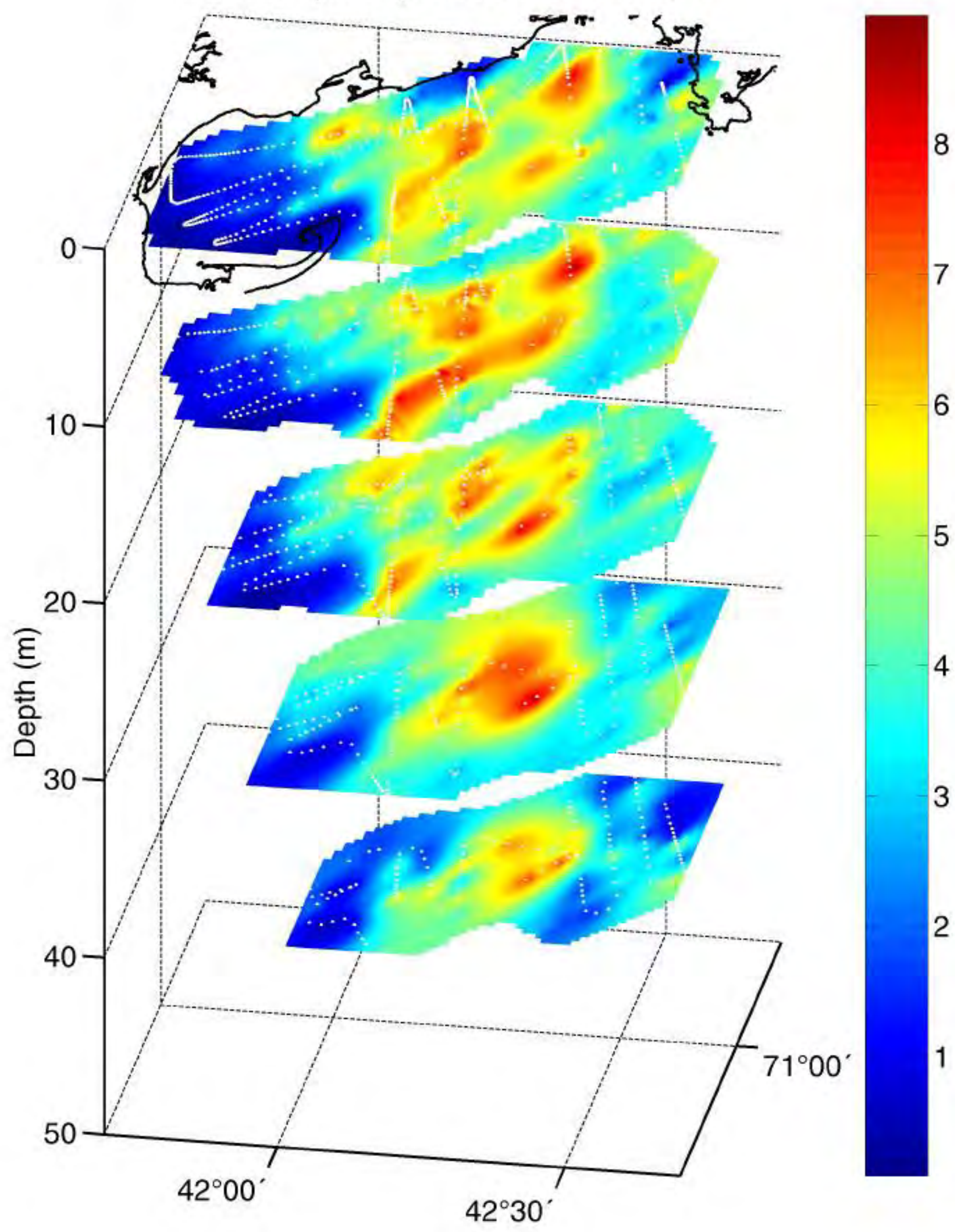
*Oithona*

— ~ 1.0 mm

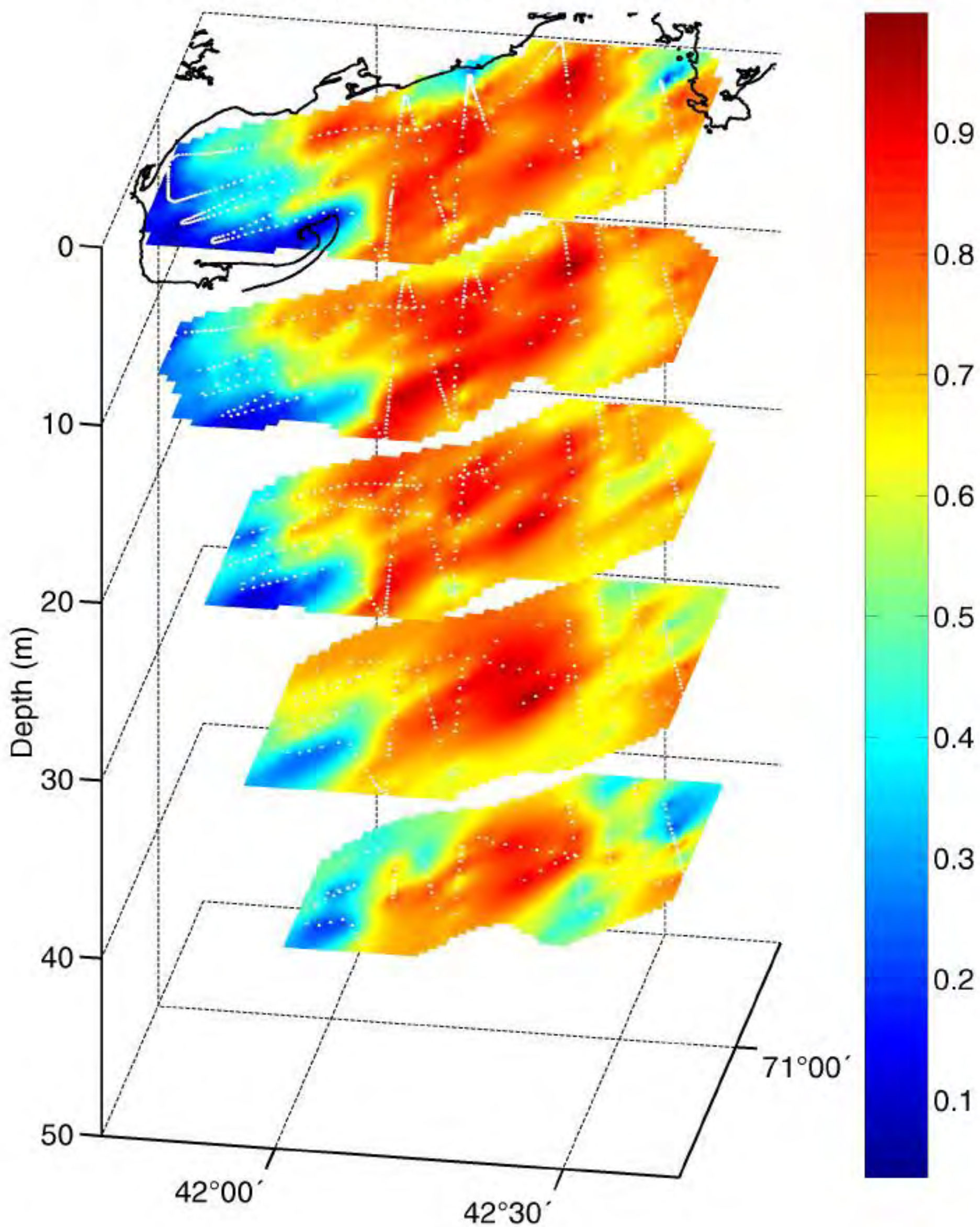
*Oithona* (#/liter) March 12–14, 1998

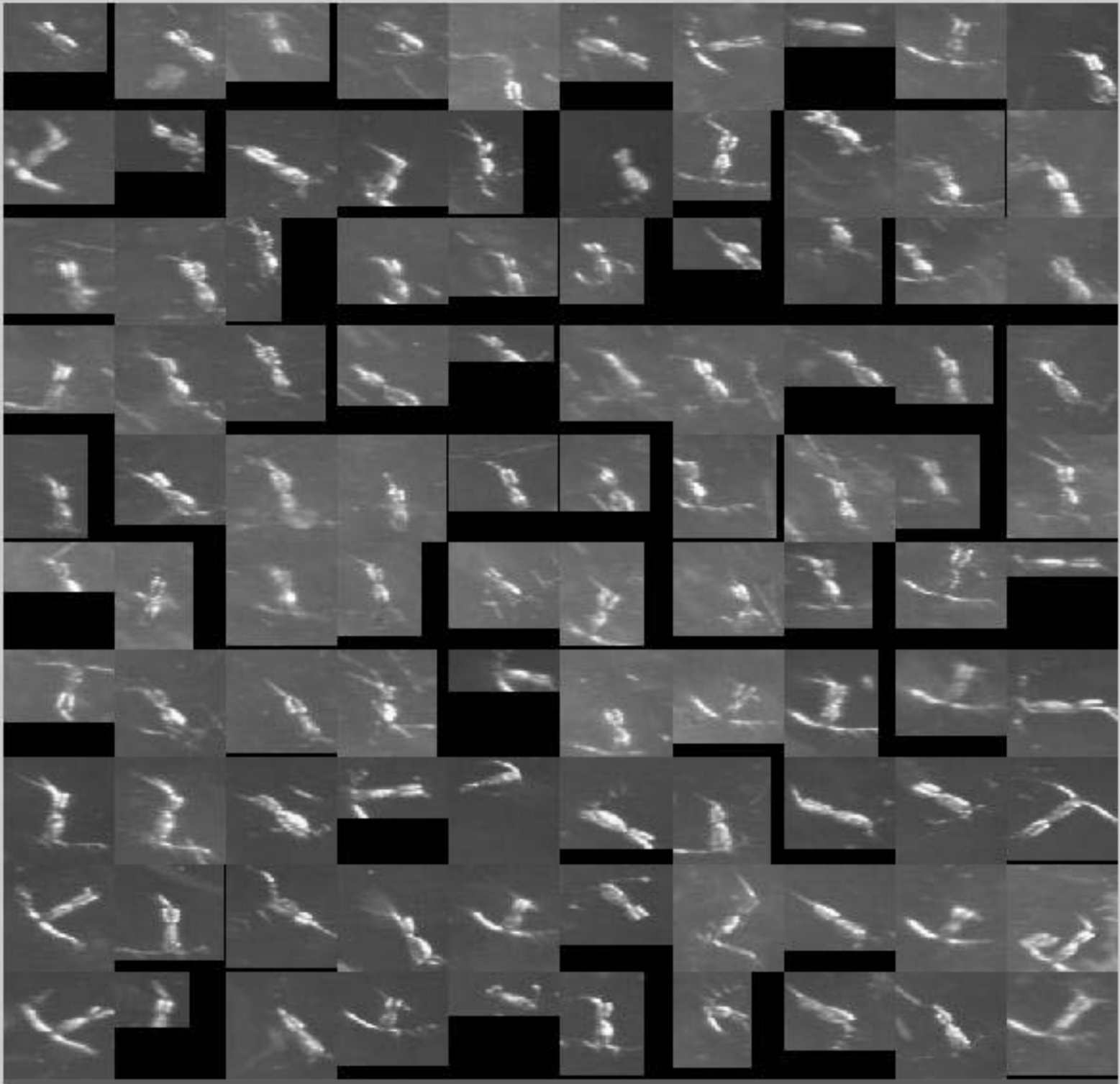


*Oithona* (#/liter), March 12–14, 1998



*Oithona* ( $\text{Log}_{10}[\#/ \text{liter} + 1]$ ), March 12–14, 1998

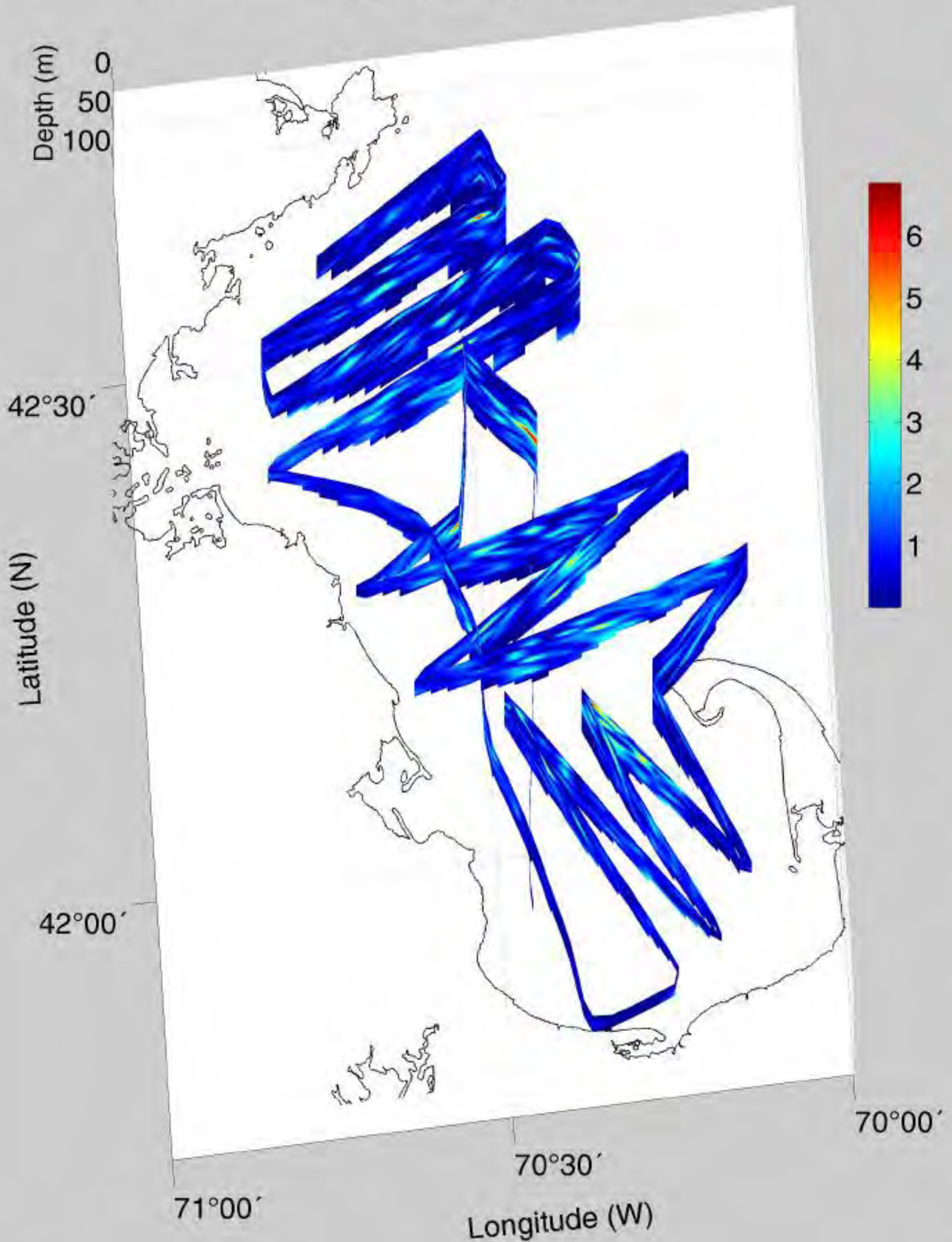




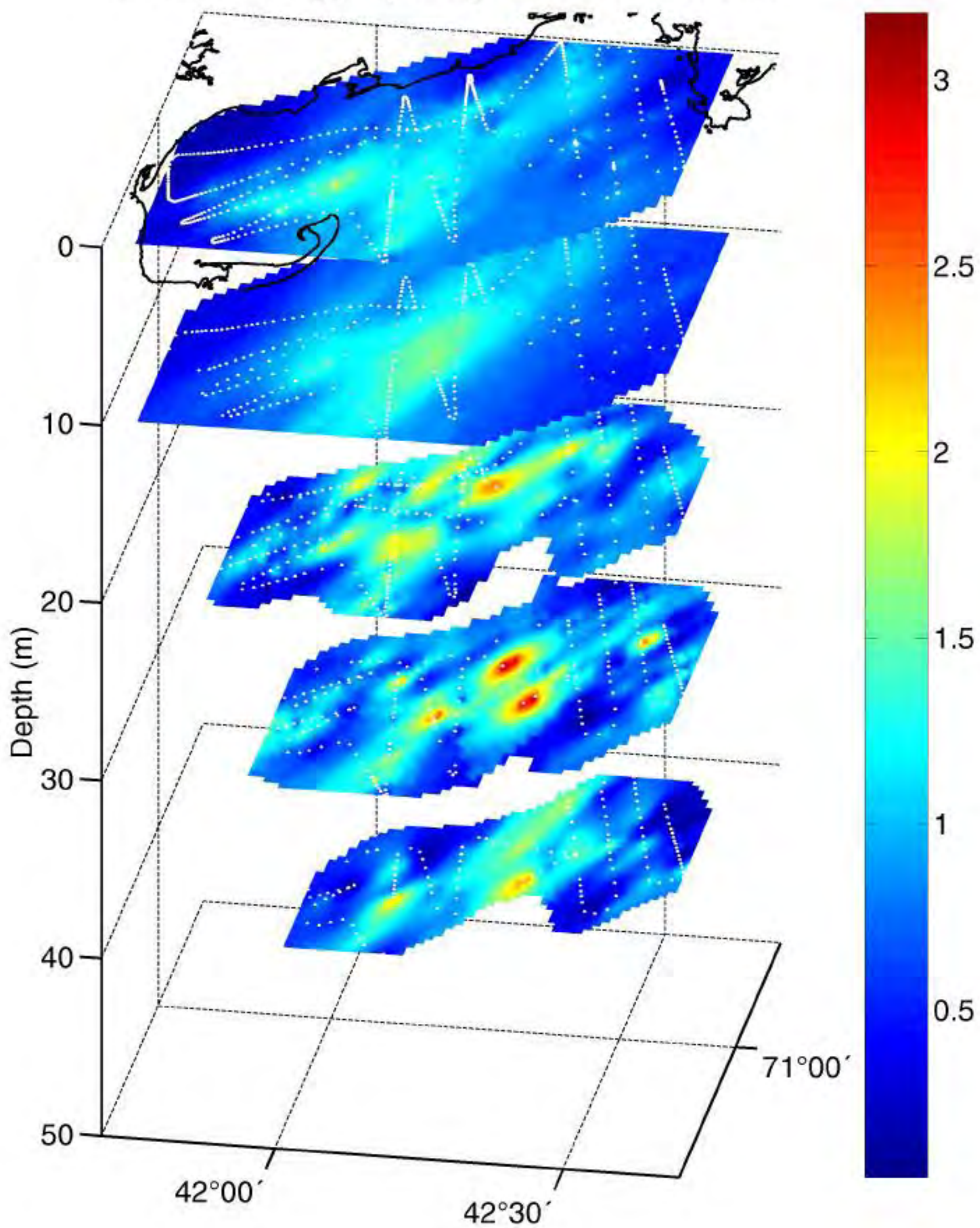
*Oithona* with eggs

— ~ 1.0 mm

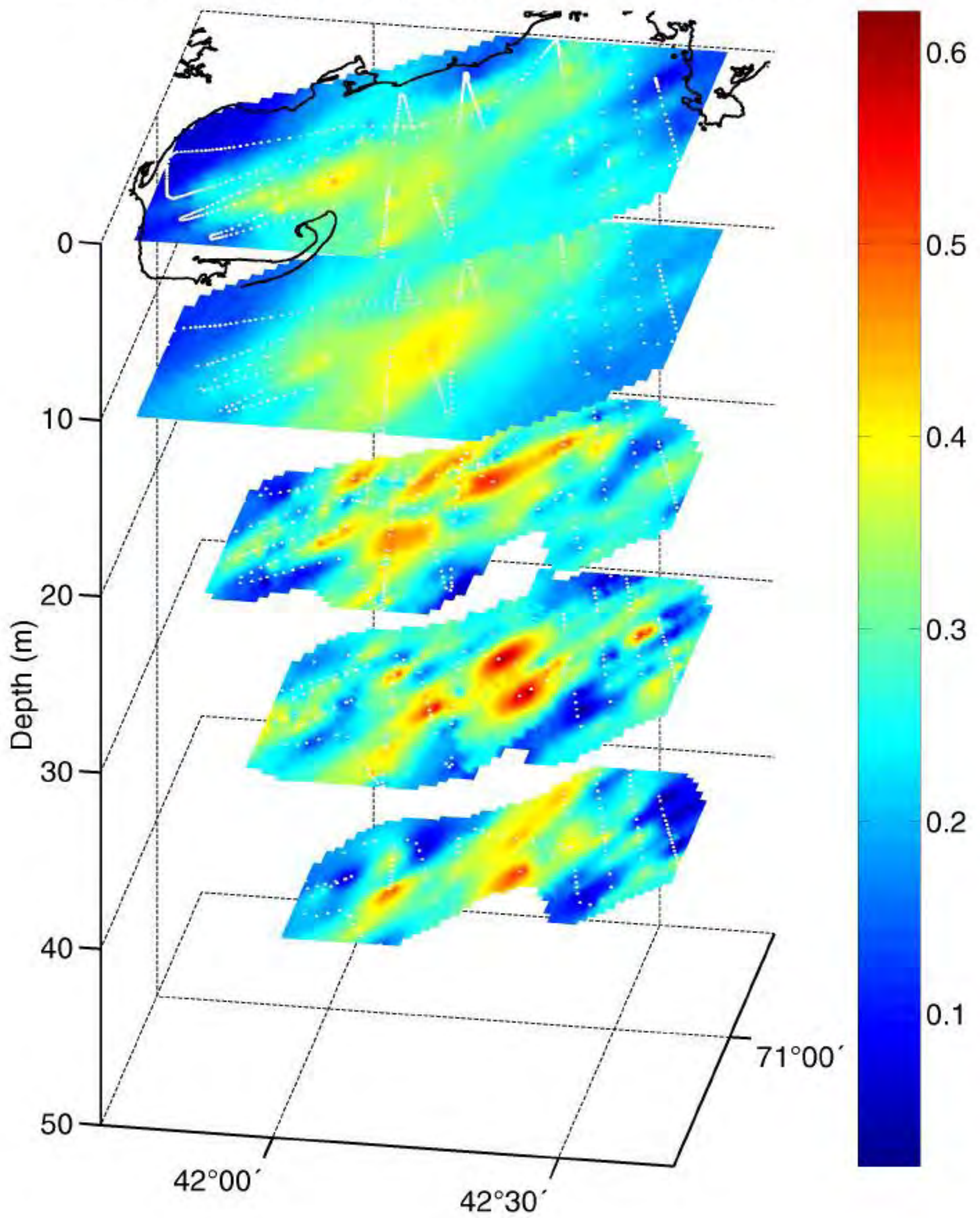
*Oithona* with eggs (#/liter) March 12–14, 1998

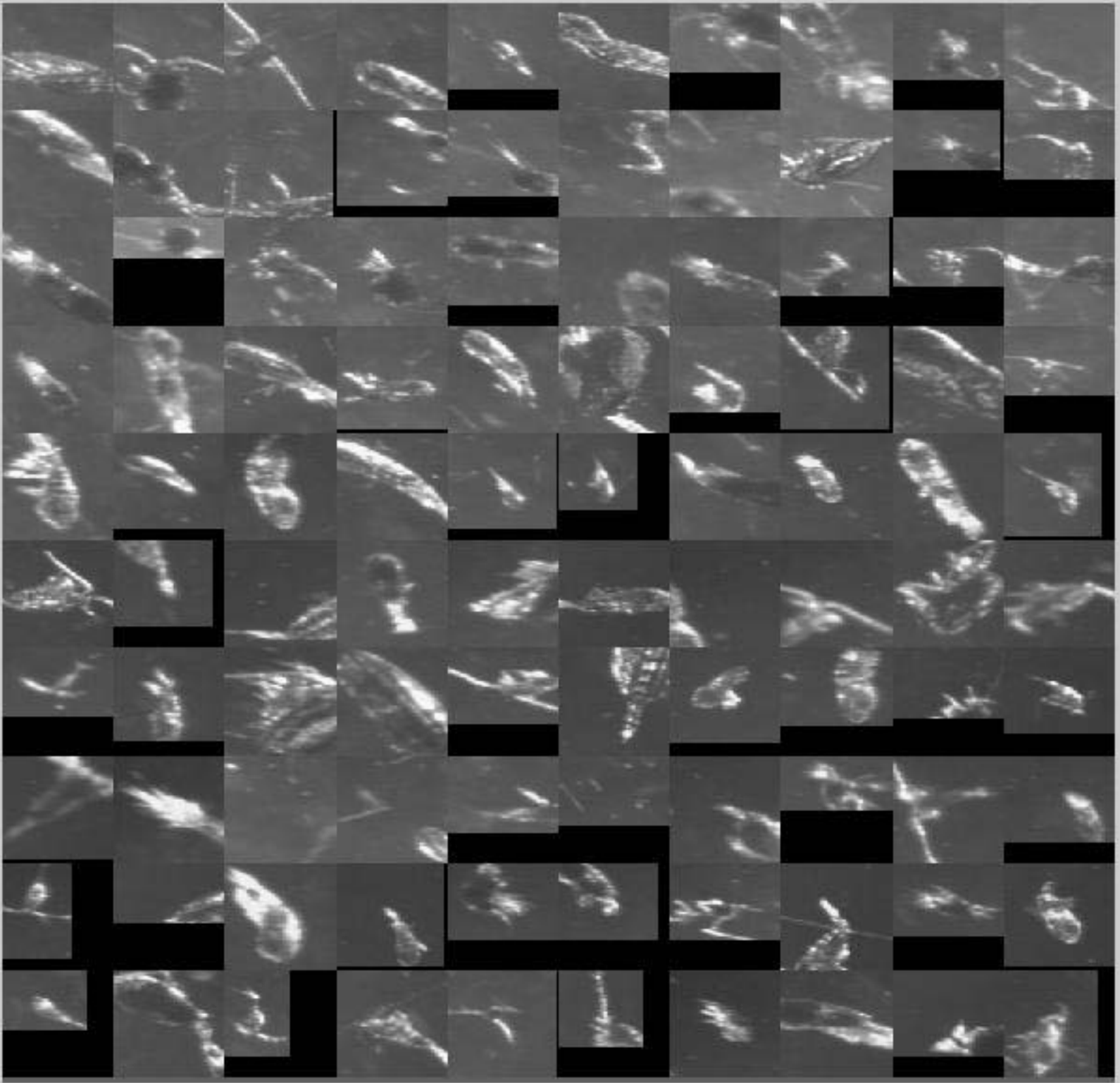


*Oithona* with eggs (#/liter), March 12–14, 1998



*Oithona* with eggs ( $\text{Log}_{10}[\#/ \text{liter} + 1]$ ), March 12–14, 1998

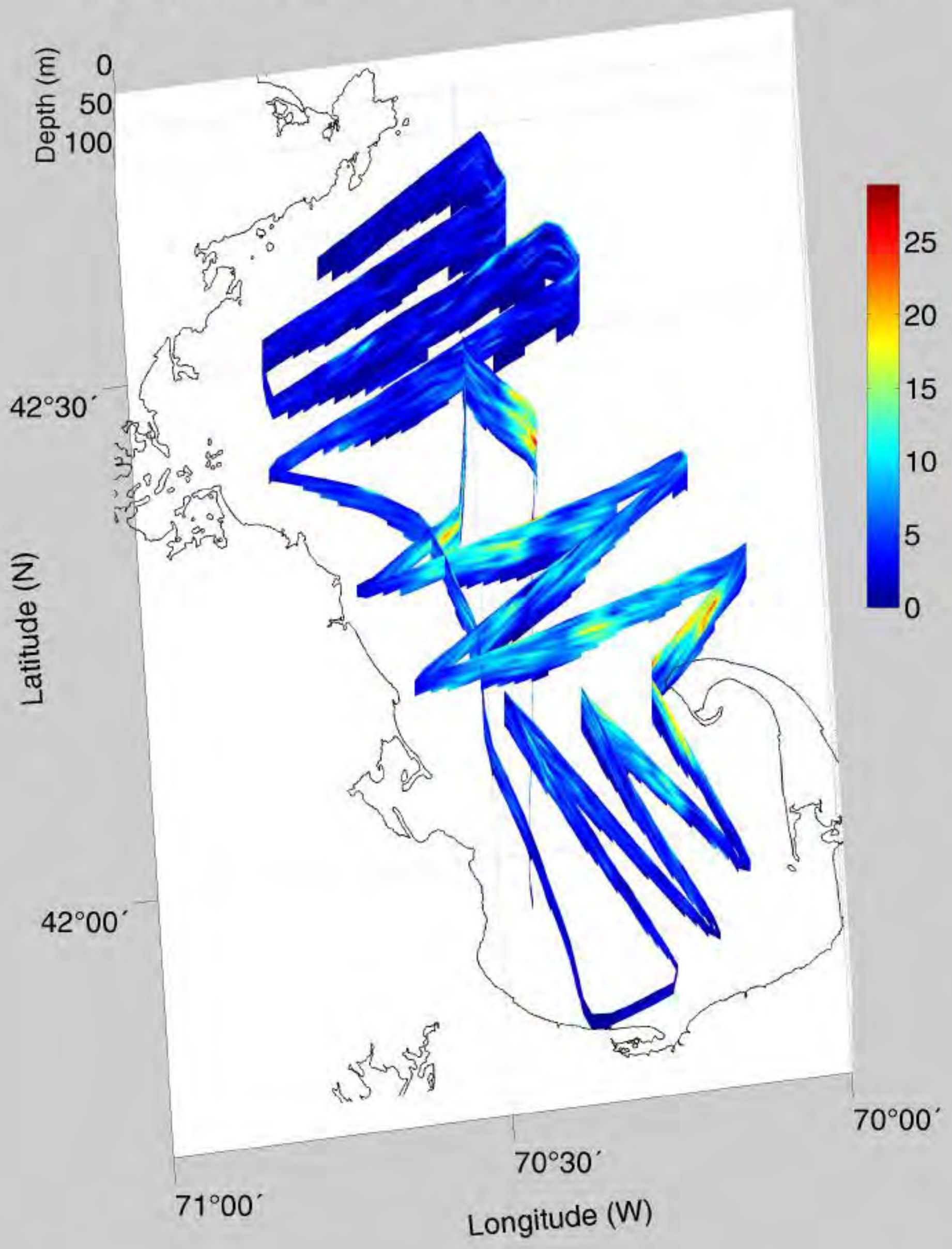




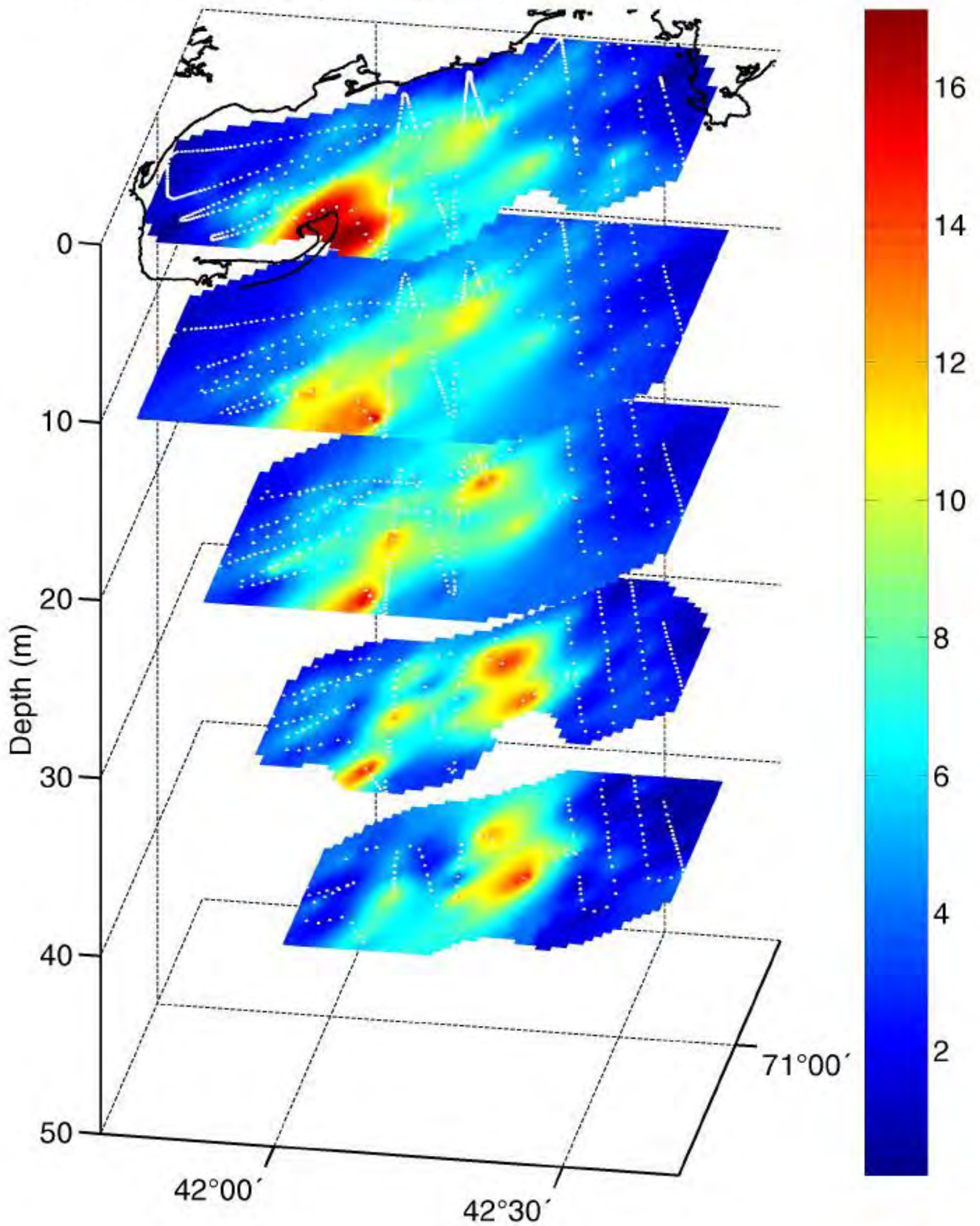
Unidentified copepods

— ~ 1.0 mm

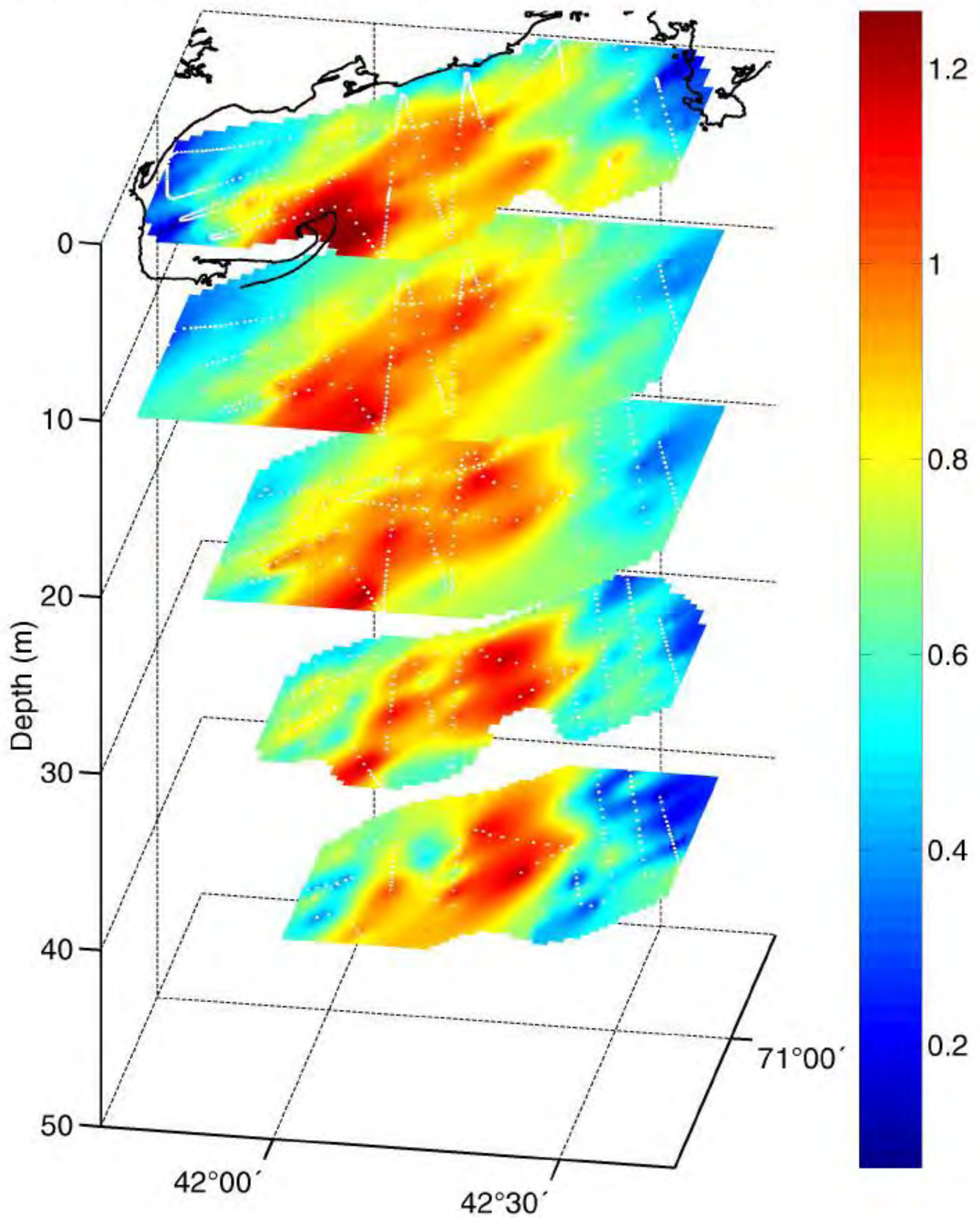
# Copepods – Unidentified (#/liter) March 12–14, 1998

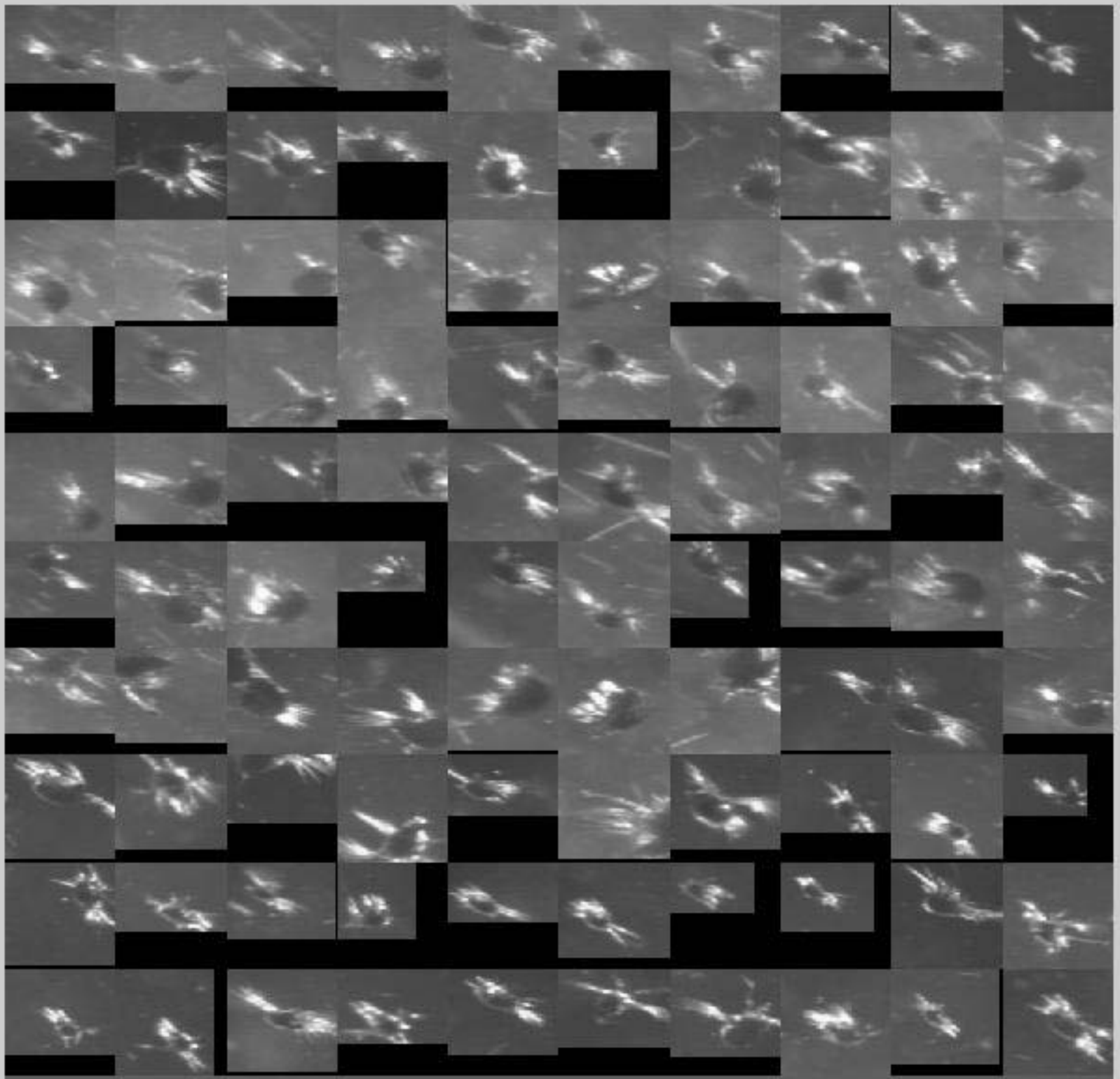


Unidentified Copepods (#/liter), March 12–14, 1998



Unidentified Copepods ( $\text{Log}_{10}[\#/ \text{liter} + 1]$ ), March 12–14, 1998

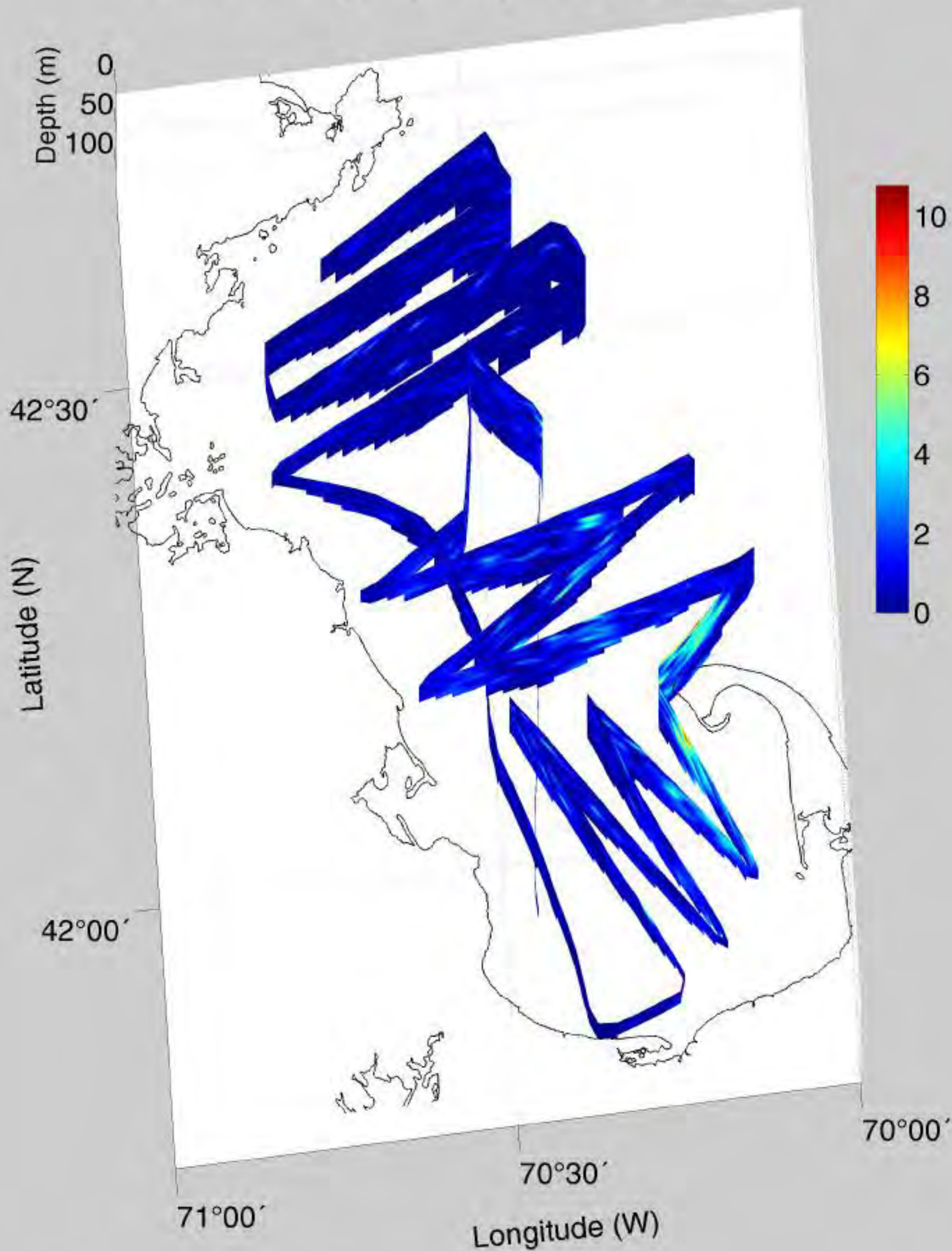




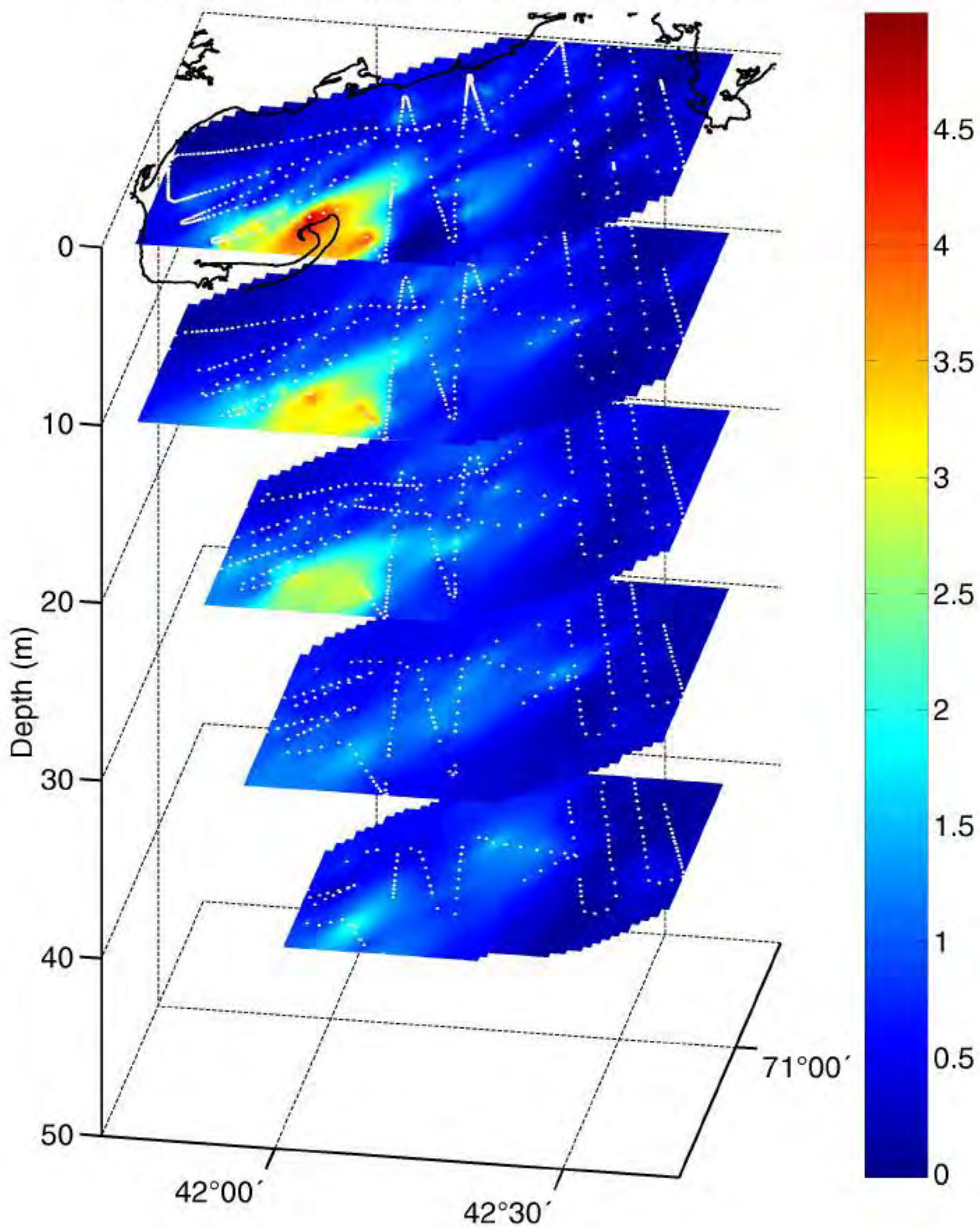
Barnacle larvae

— ~ 1.0 mm

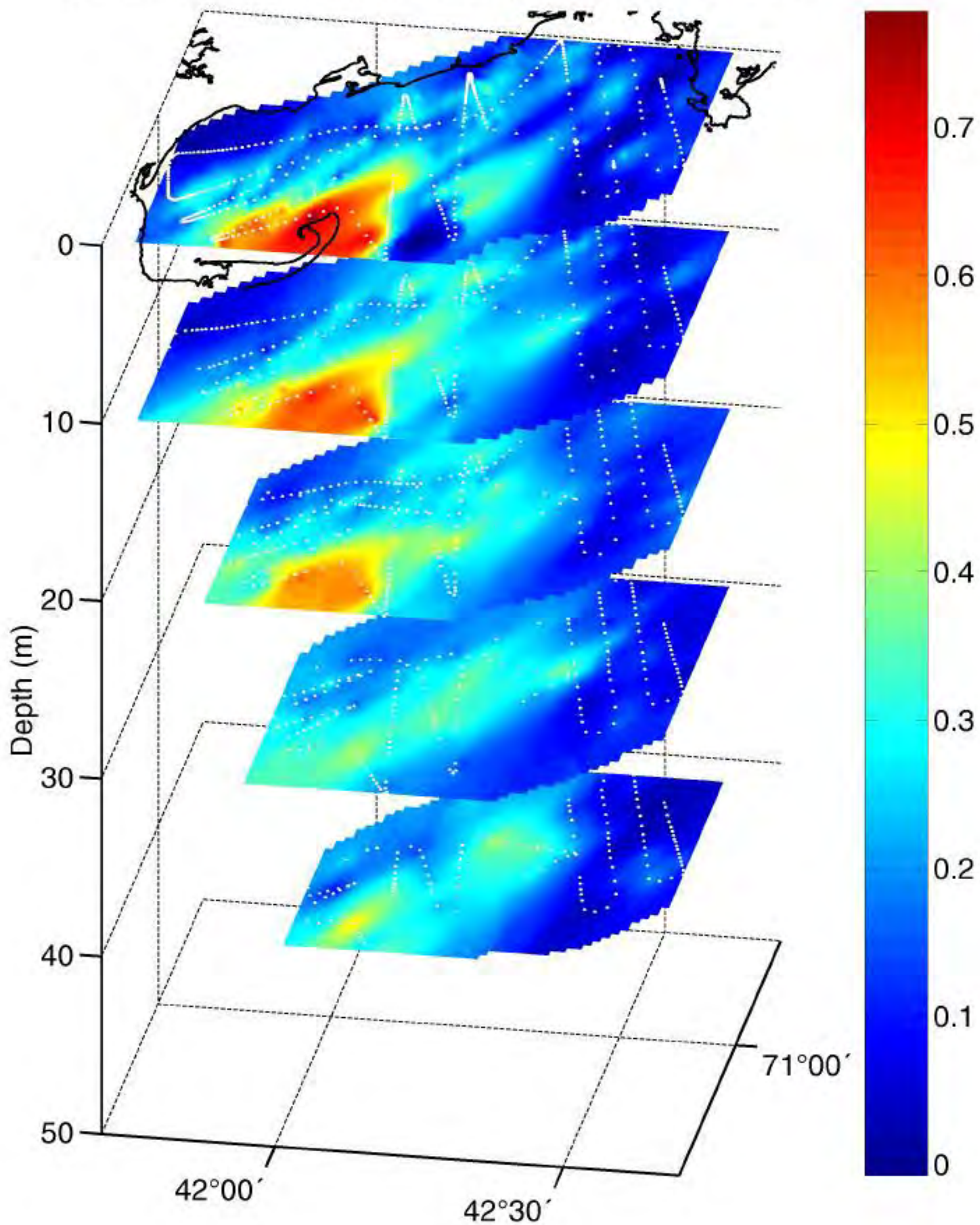
# Barnacle Nauplii (#/liter) March 12–14, 1998

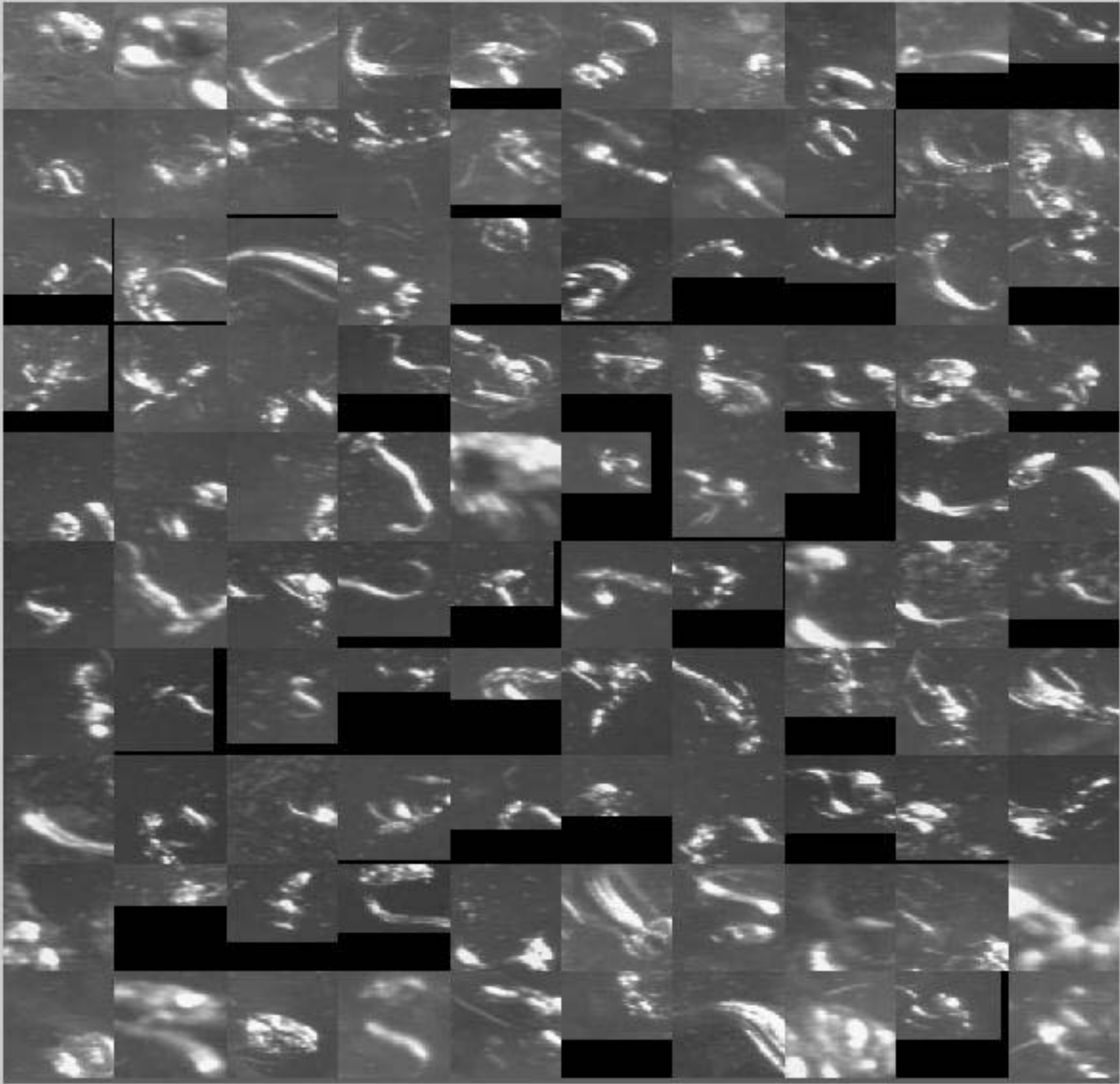


Barnacle Larvae (#/liter), March 12–14, 1998



Barnacle Larvae ( $\text{Log}_{10}[\#/ \text{liter} + 1]$ ), March 12–14, 1998

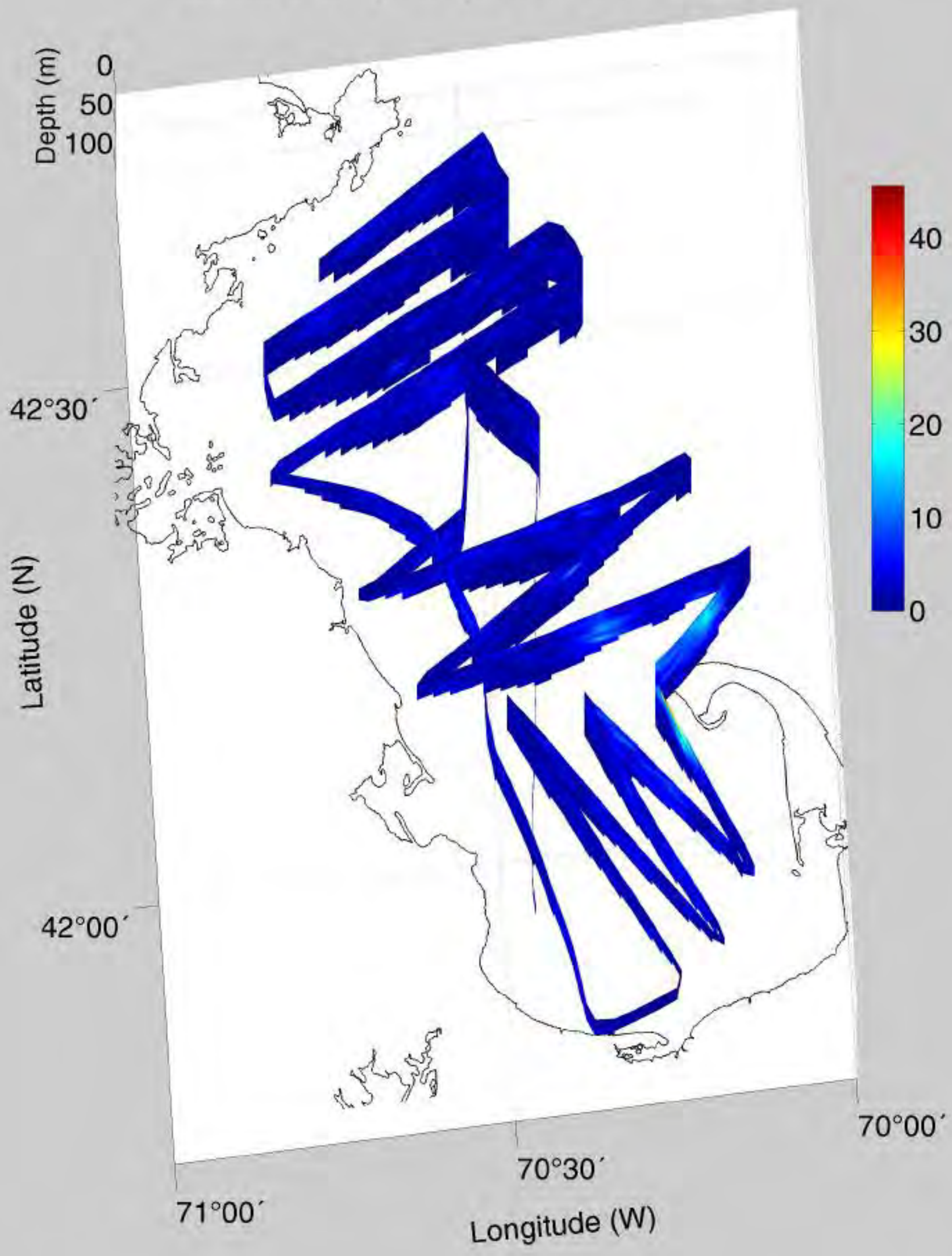




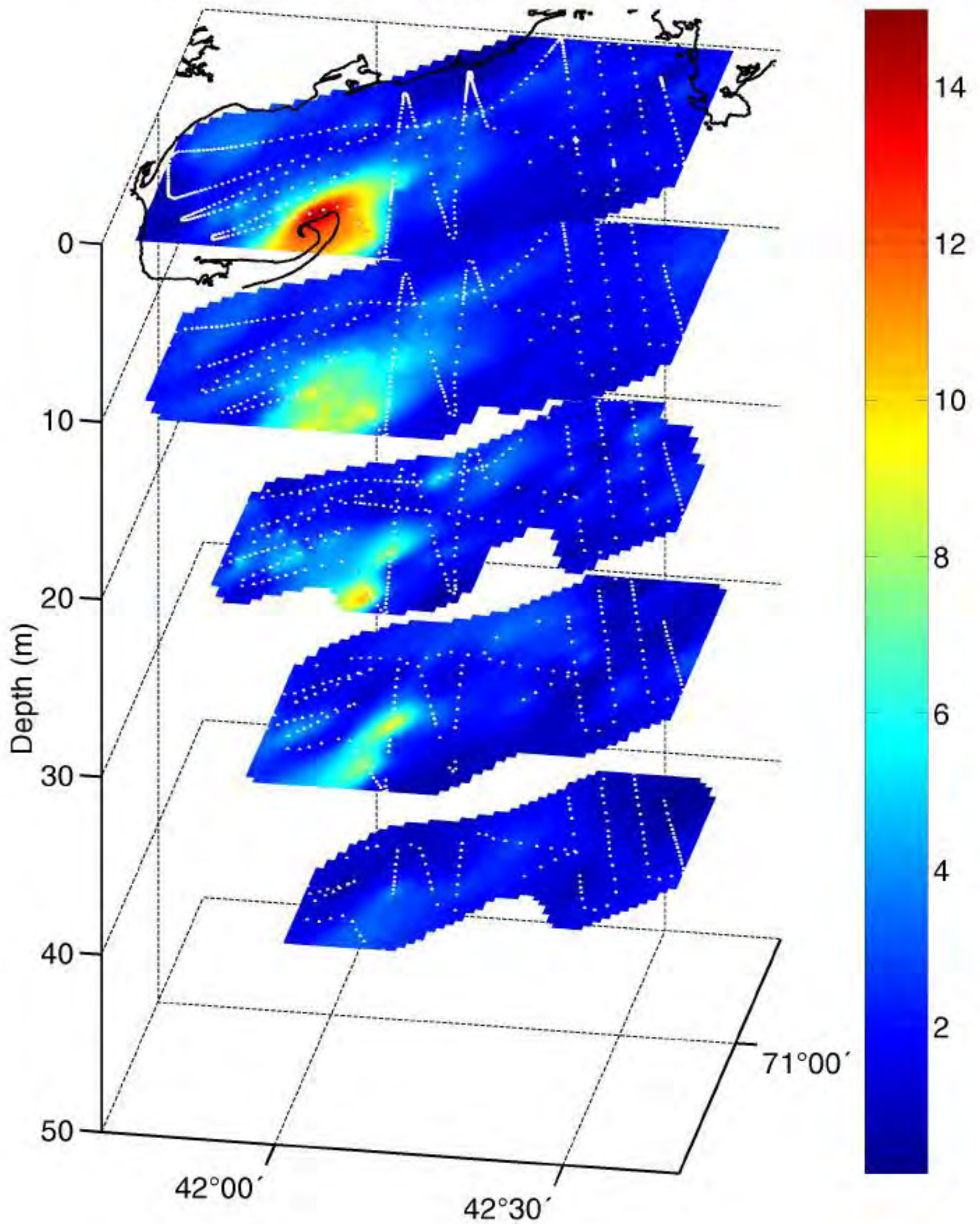
Larvaceans

— ~ 1.0 mm

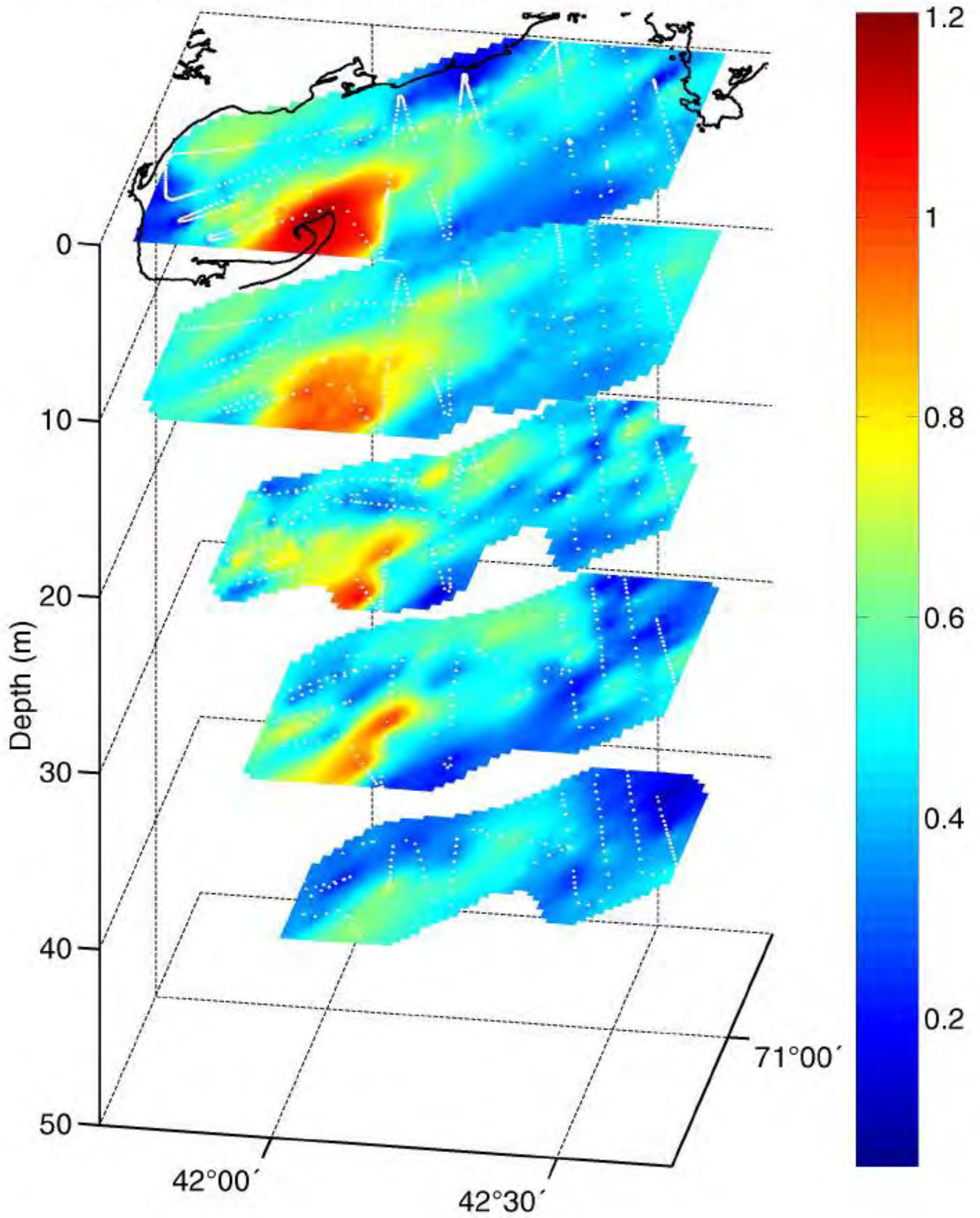
# Larvaceans (#/liter) March 12-14, 1998

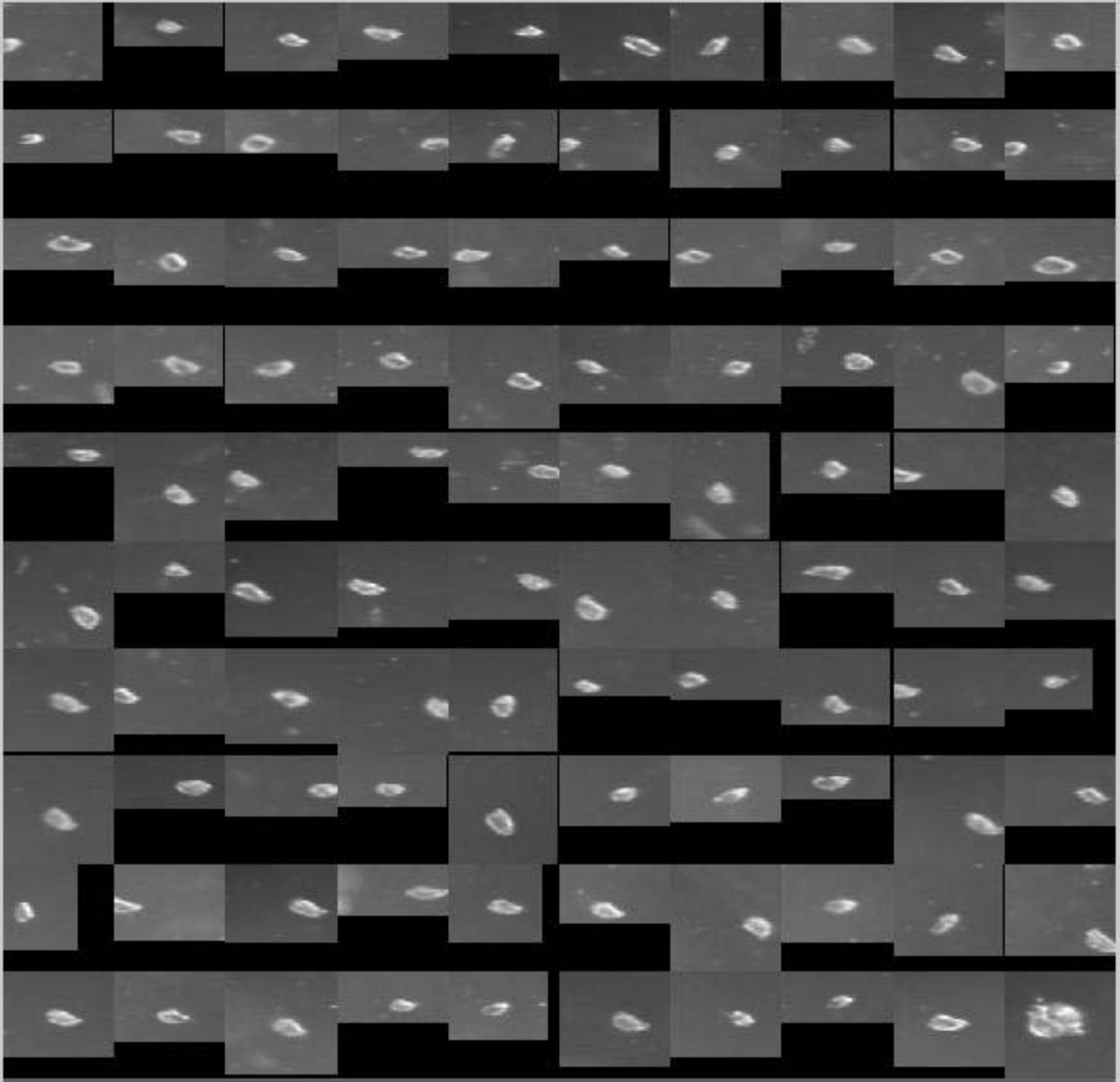


Larvaceans (#/liter), March 12–14, 1998



Larvaceans ( $\text{Log}_{10}[\#/ \text{liter} + 1]$ ), March 12–14, 1998

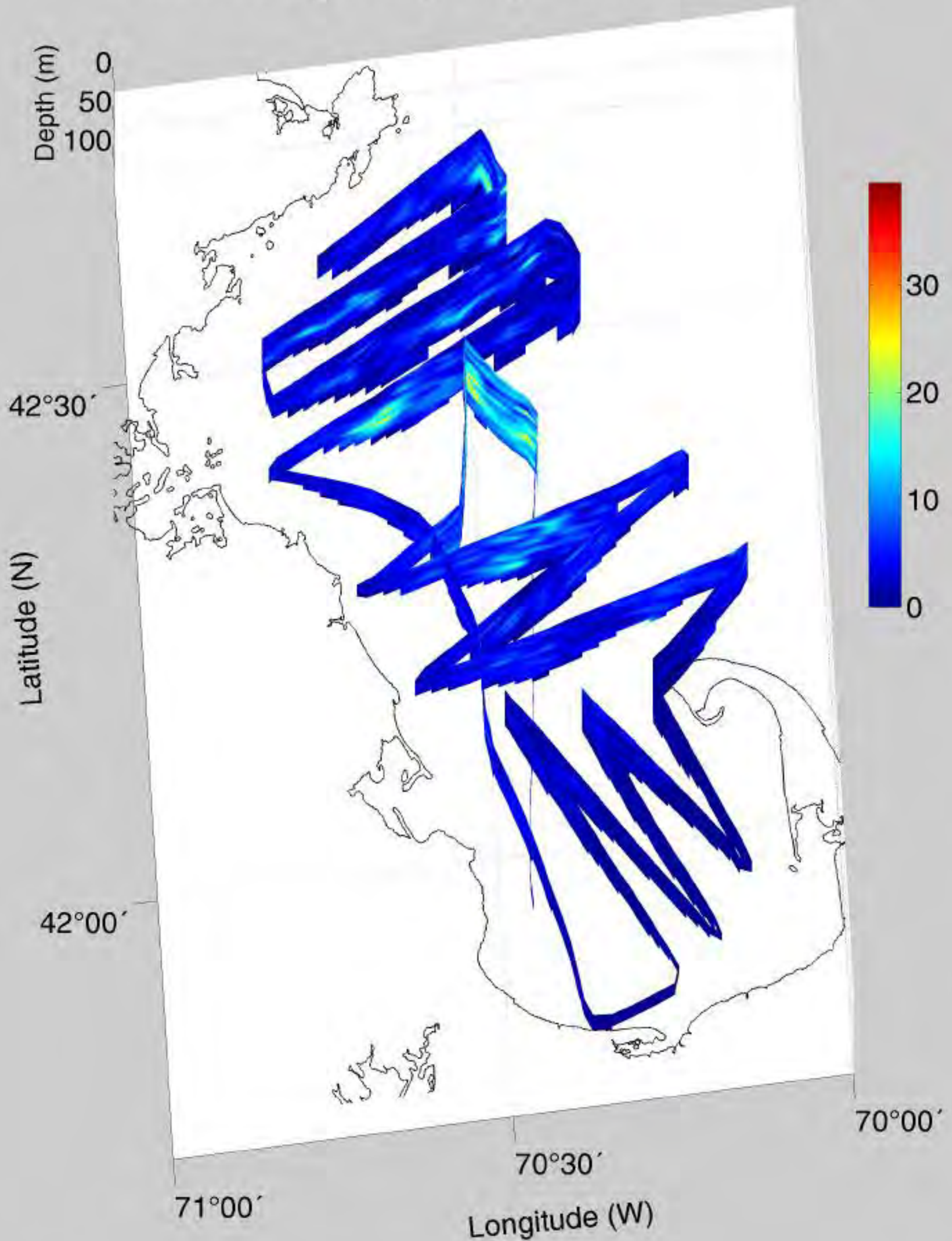




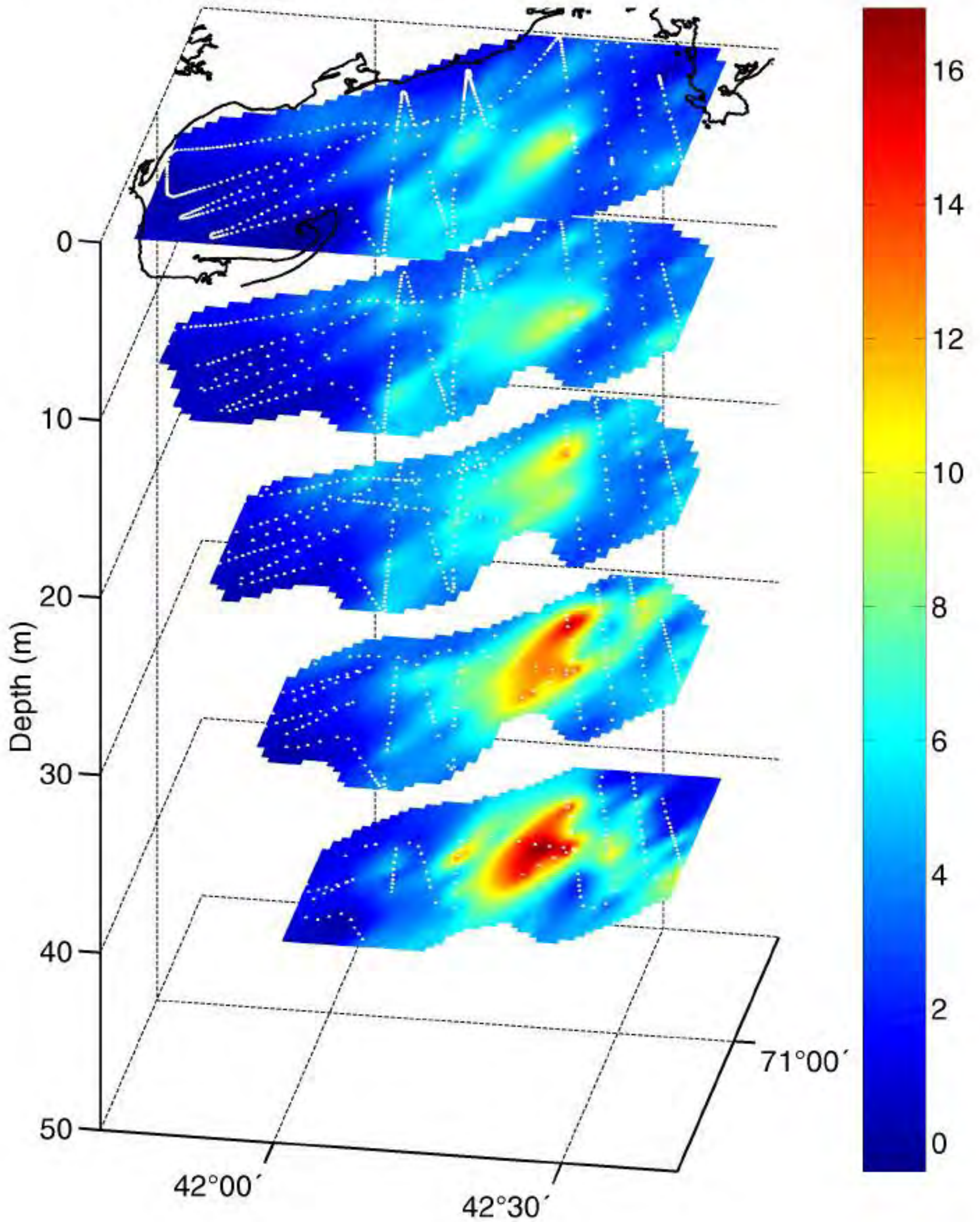
Ostracods /  
Barnacle cyprids

— ~ 1.0 mm

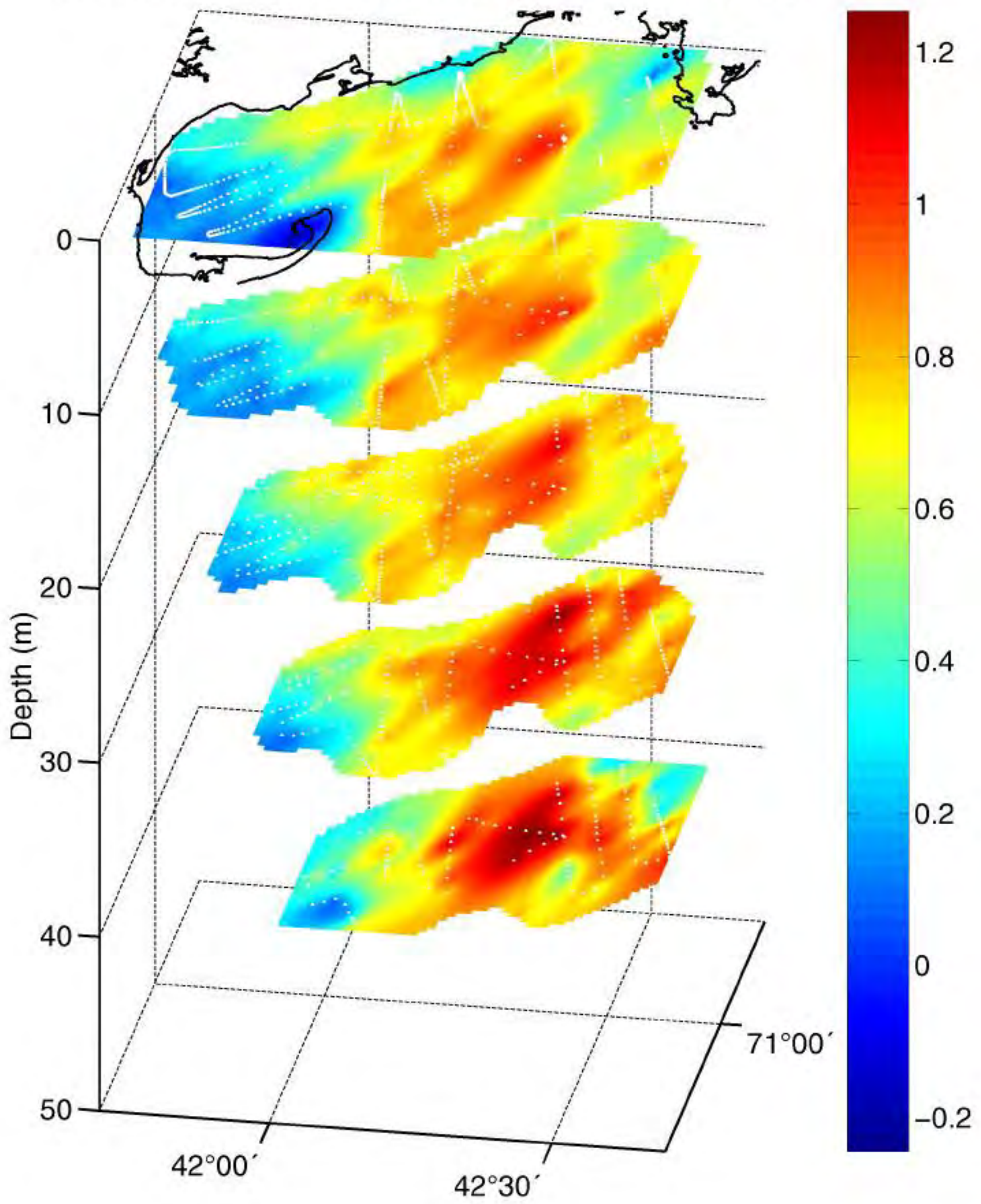
# Ostracods/Cyprids (#/liter) March 12-14, 1998

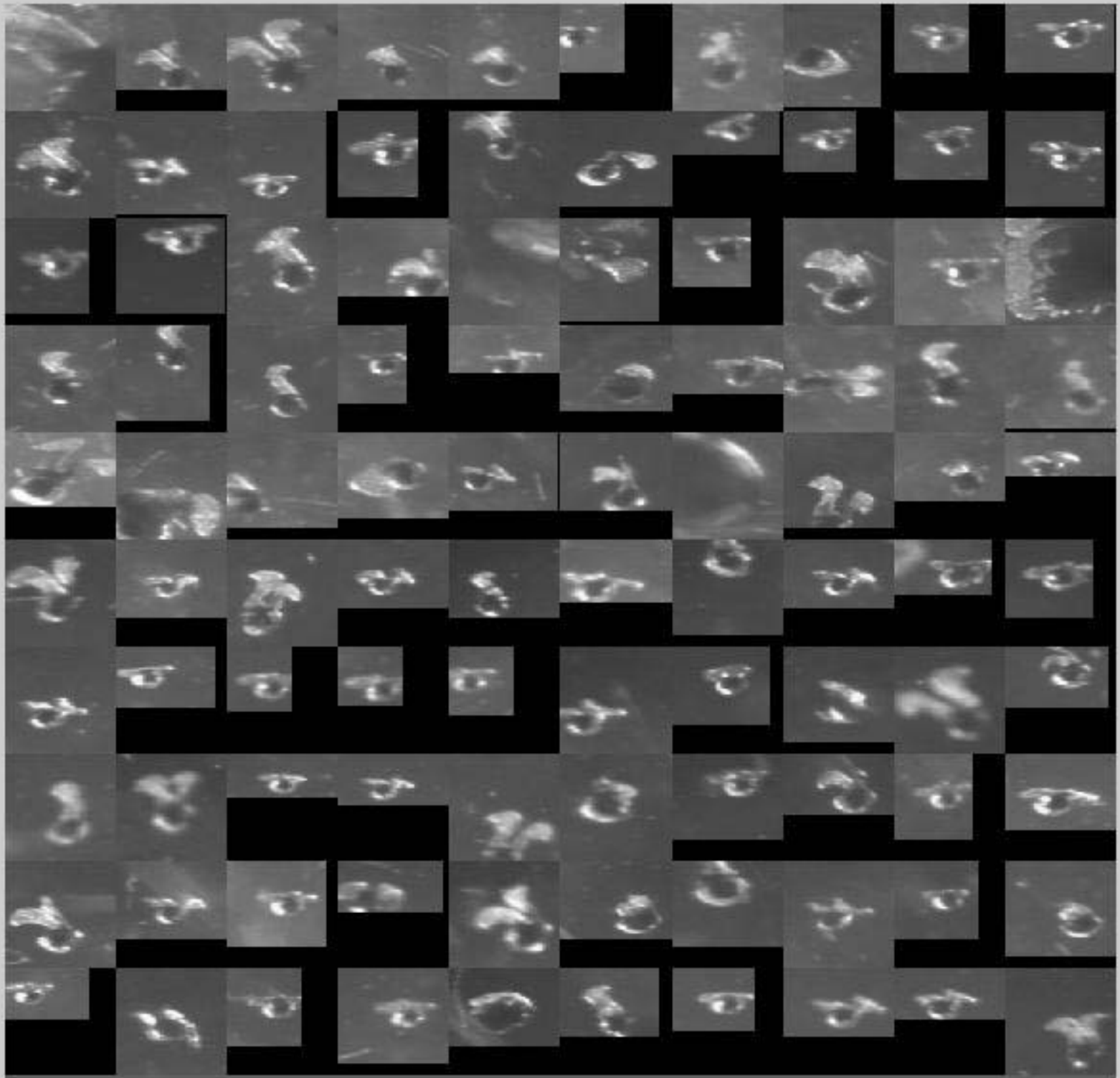


Ostracods/cyprids (#/liter), March 12–14, 1998



Ostracods/cyprids ( $\text{Log}_{10}[\#/ \text{liter} + 1]$ ), March 12–14, 1998

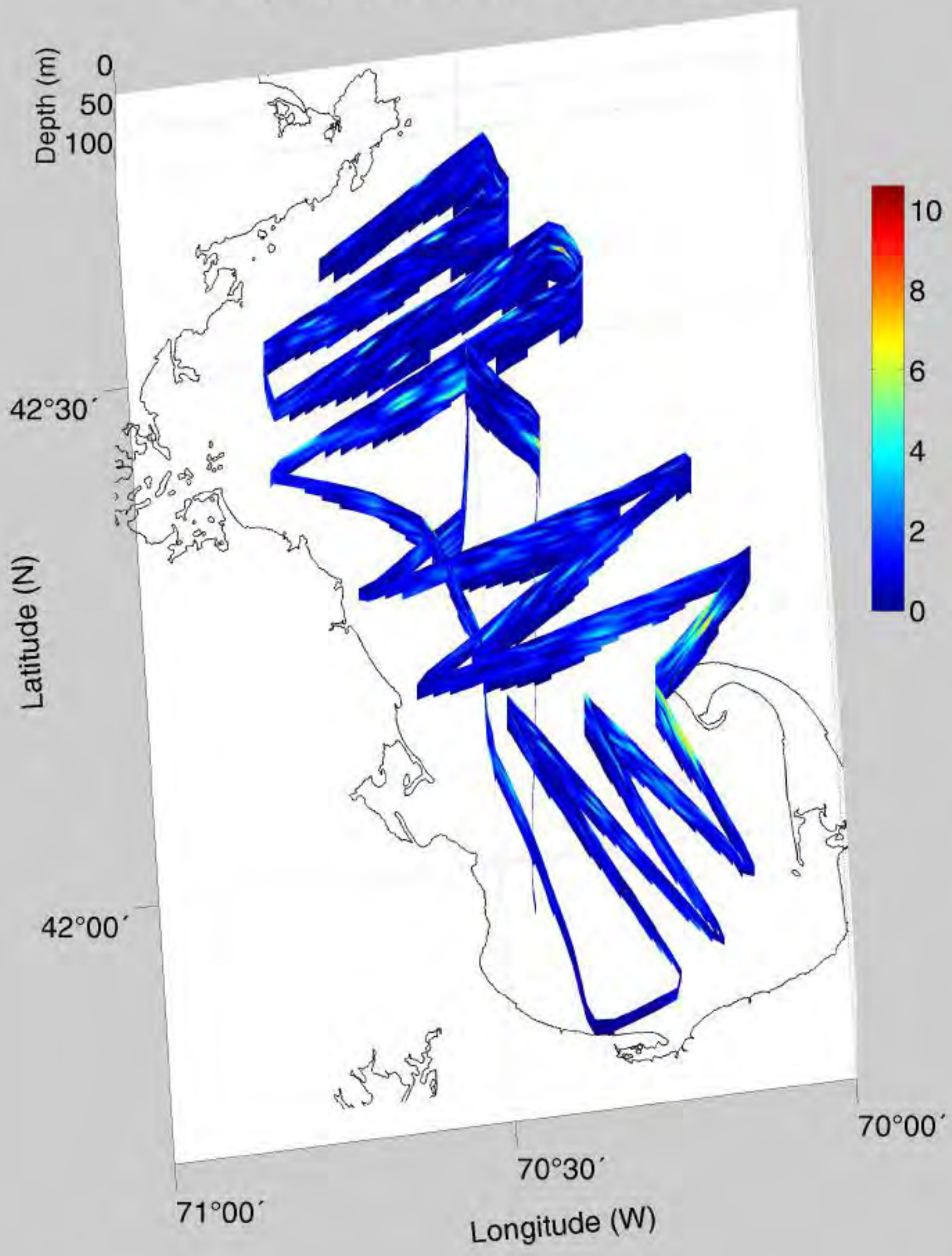




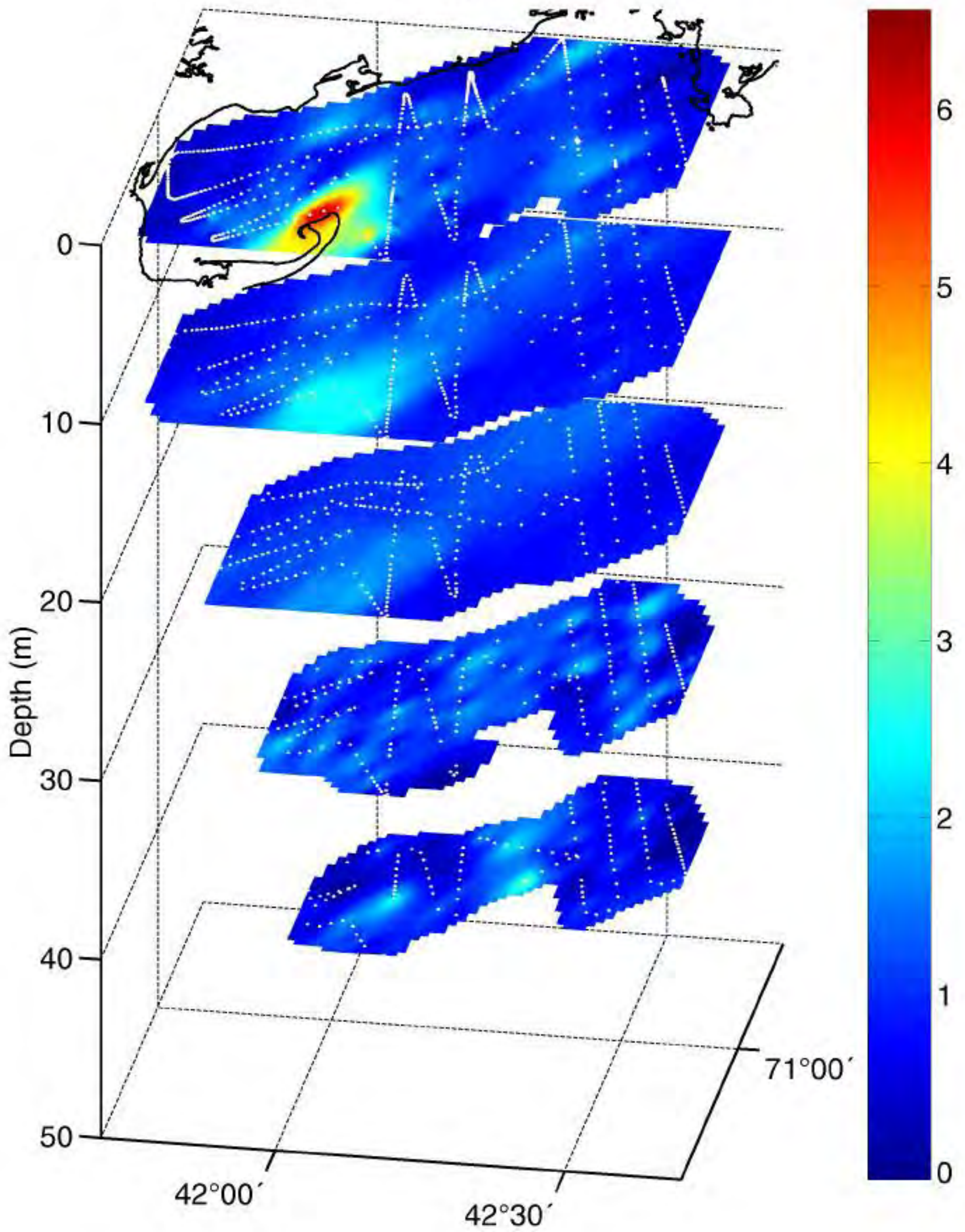
Pteropods

— ~ 1.0 mm

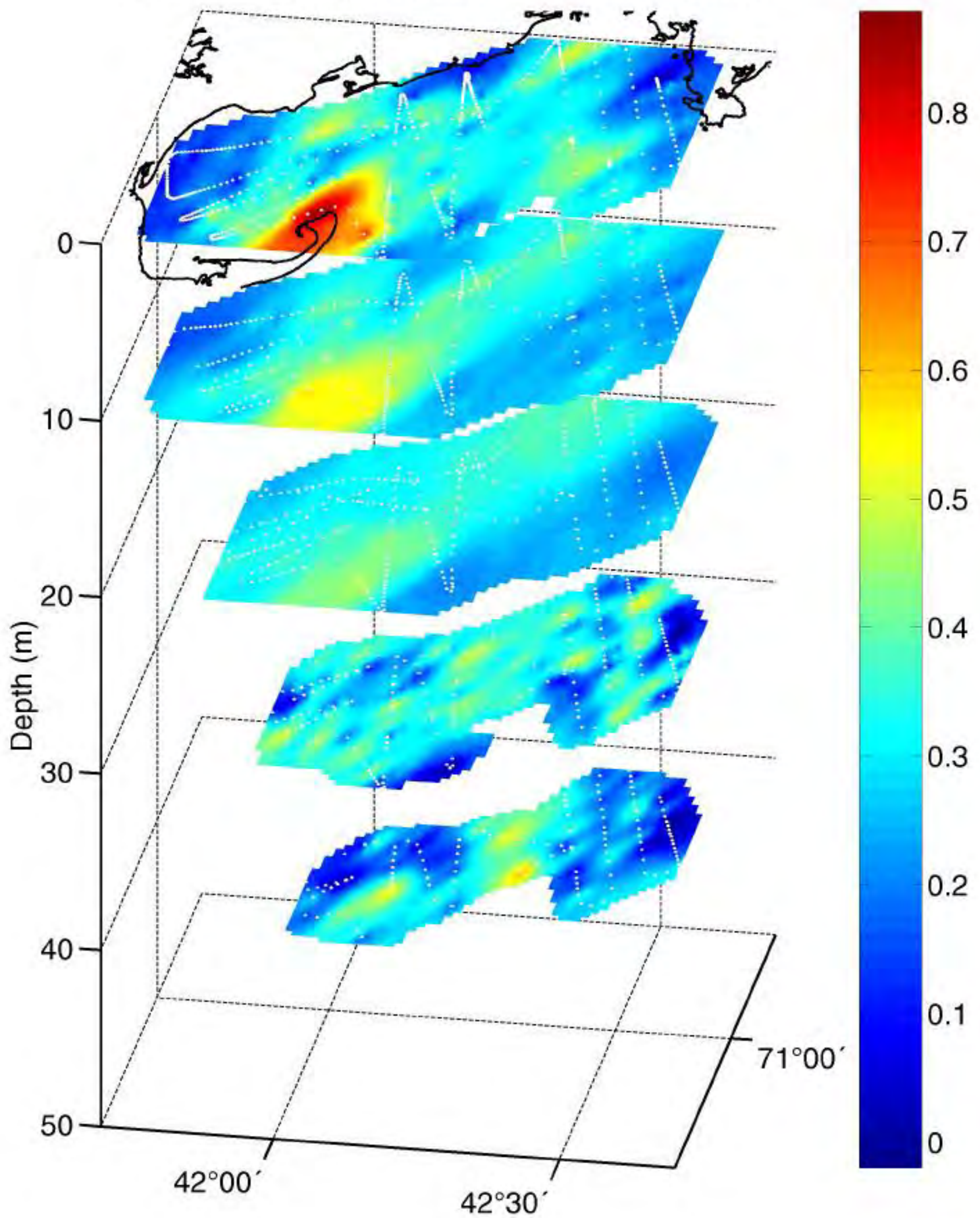
# Pteropods (#/liter) March 12-14, 1998



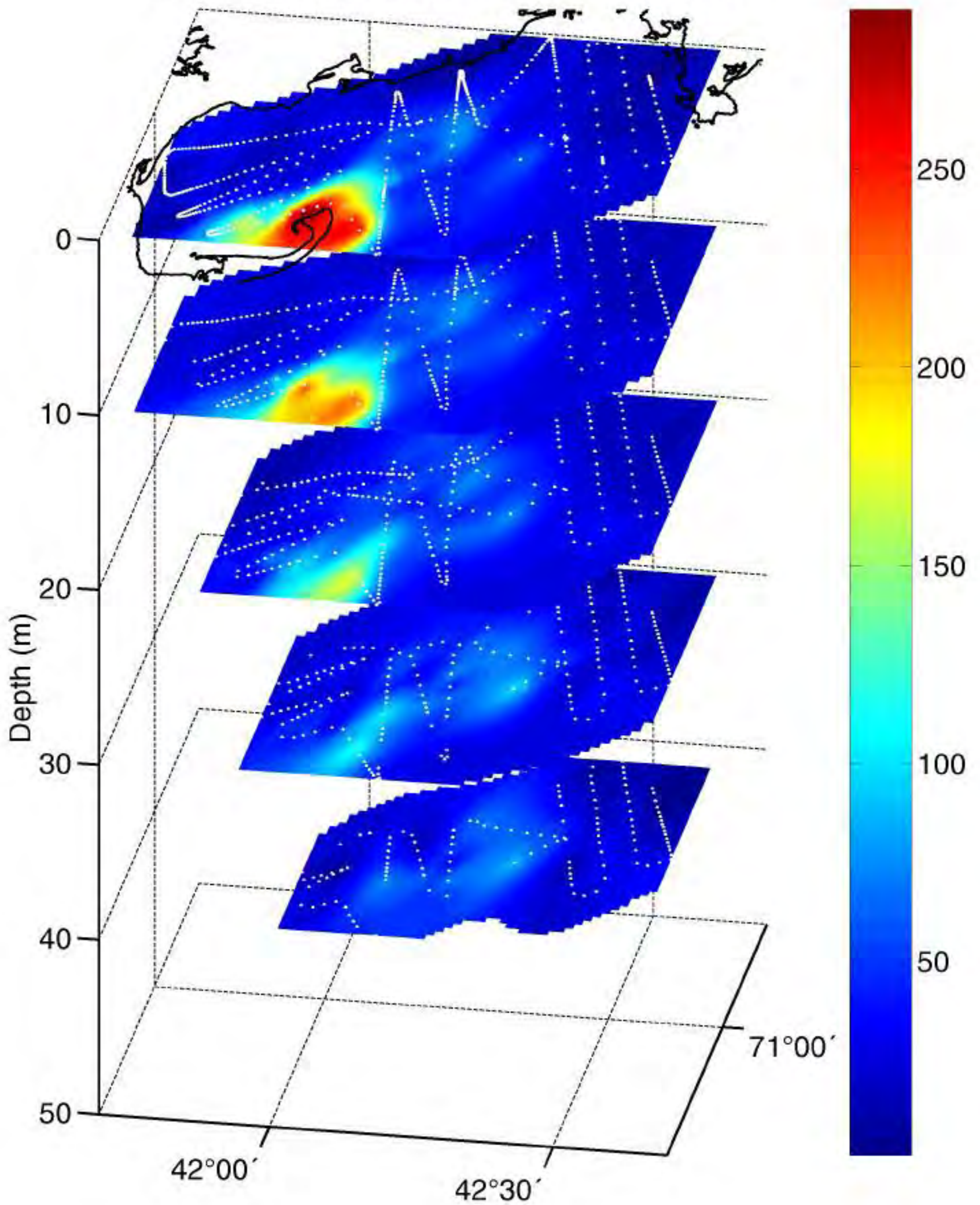
Pteropods (#/liter), March 12–14, 1998



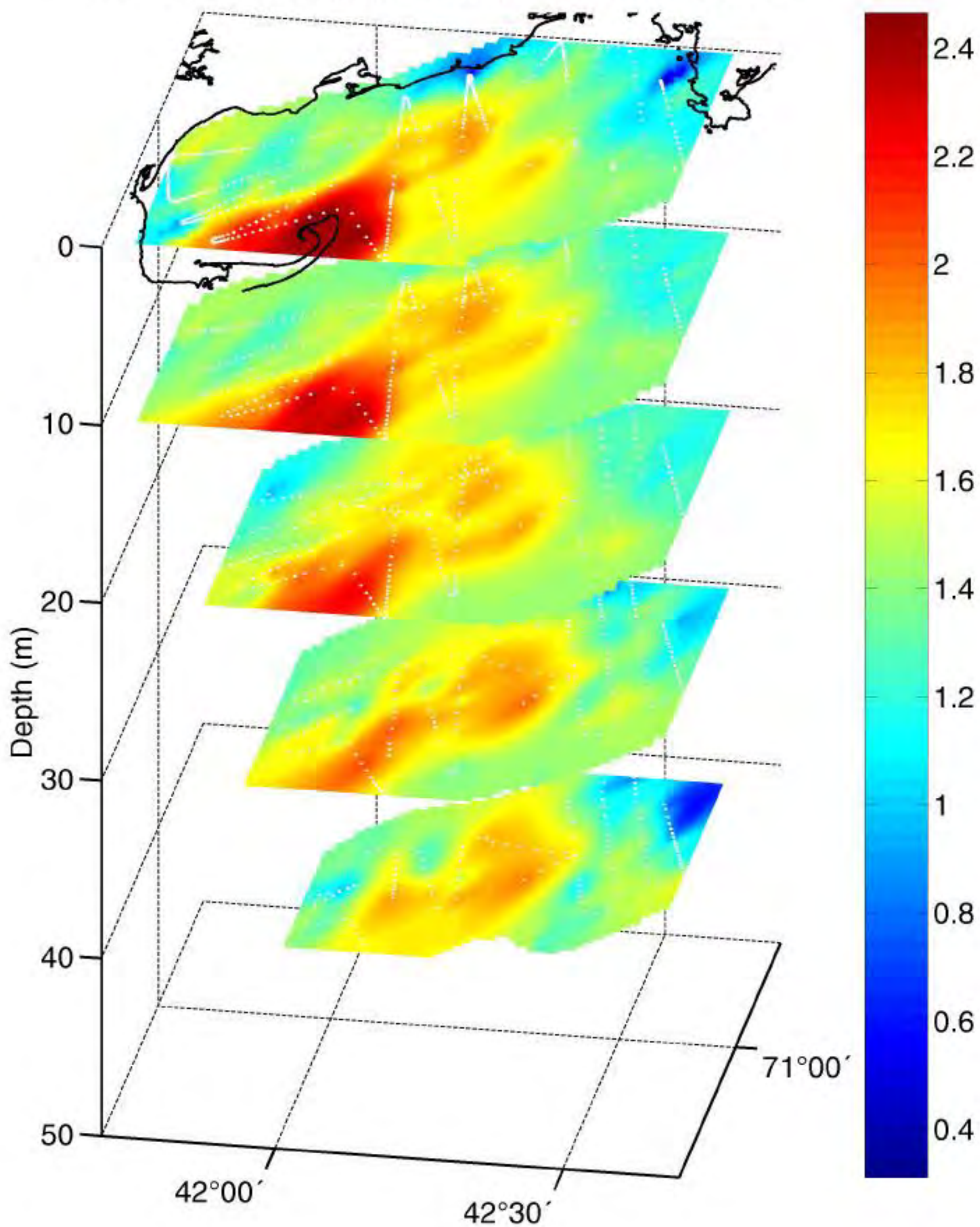
Pteropods ( $\text{Log}_{10}[\#/ \text{liter} + 1]$ ), March 12–14, 1998



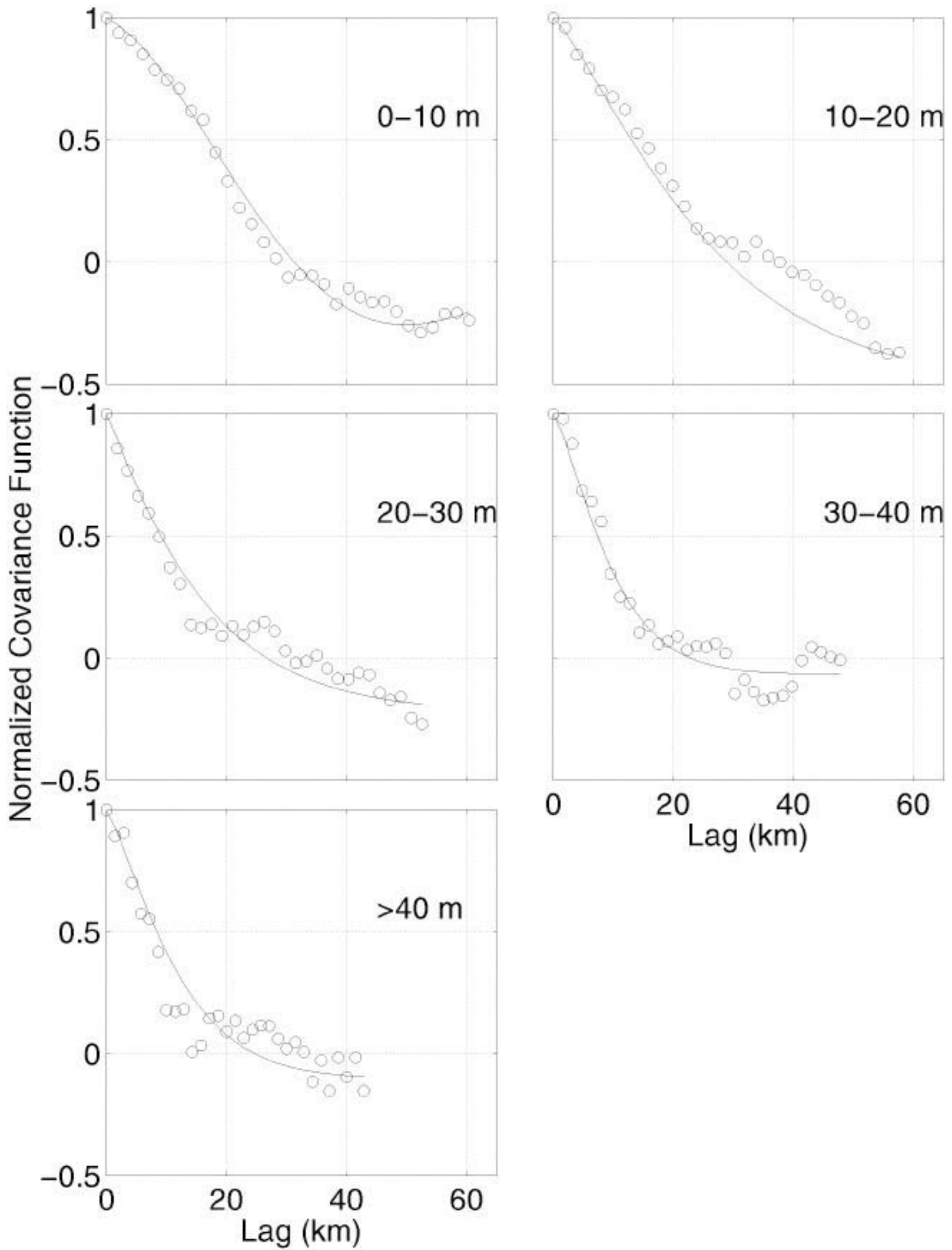
Total Plankton (#/liter), March 12–14, 1998



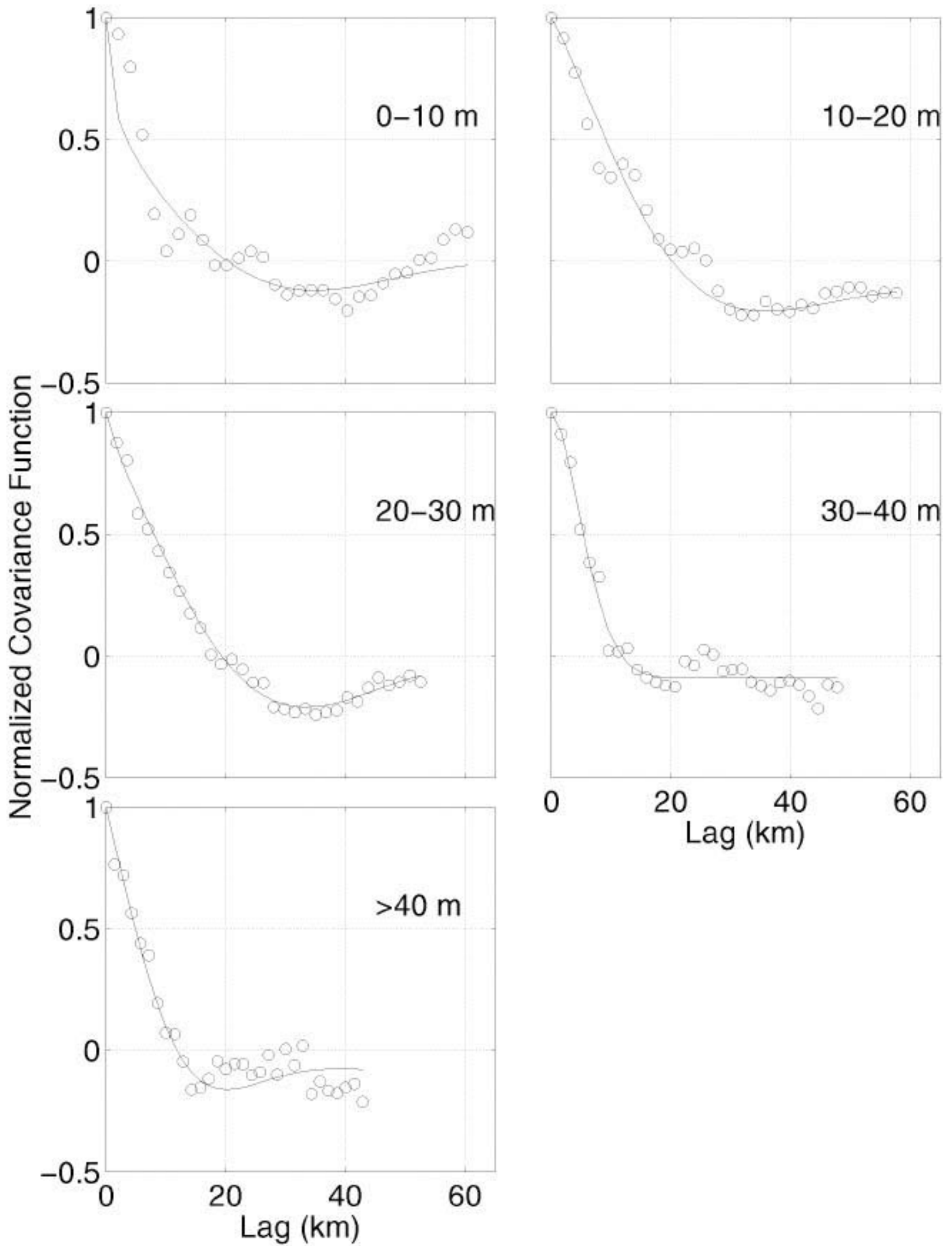
Total Plankton ( $\text{Log}_{10}[\#/ \text{liter} + 1]$ ), March 12–14, 1998



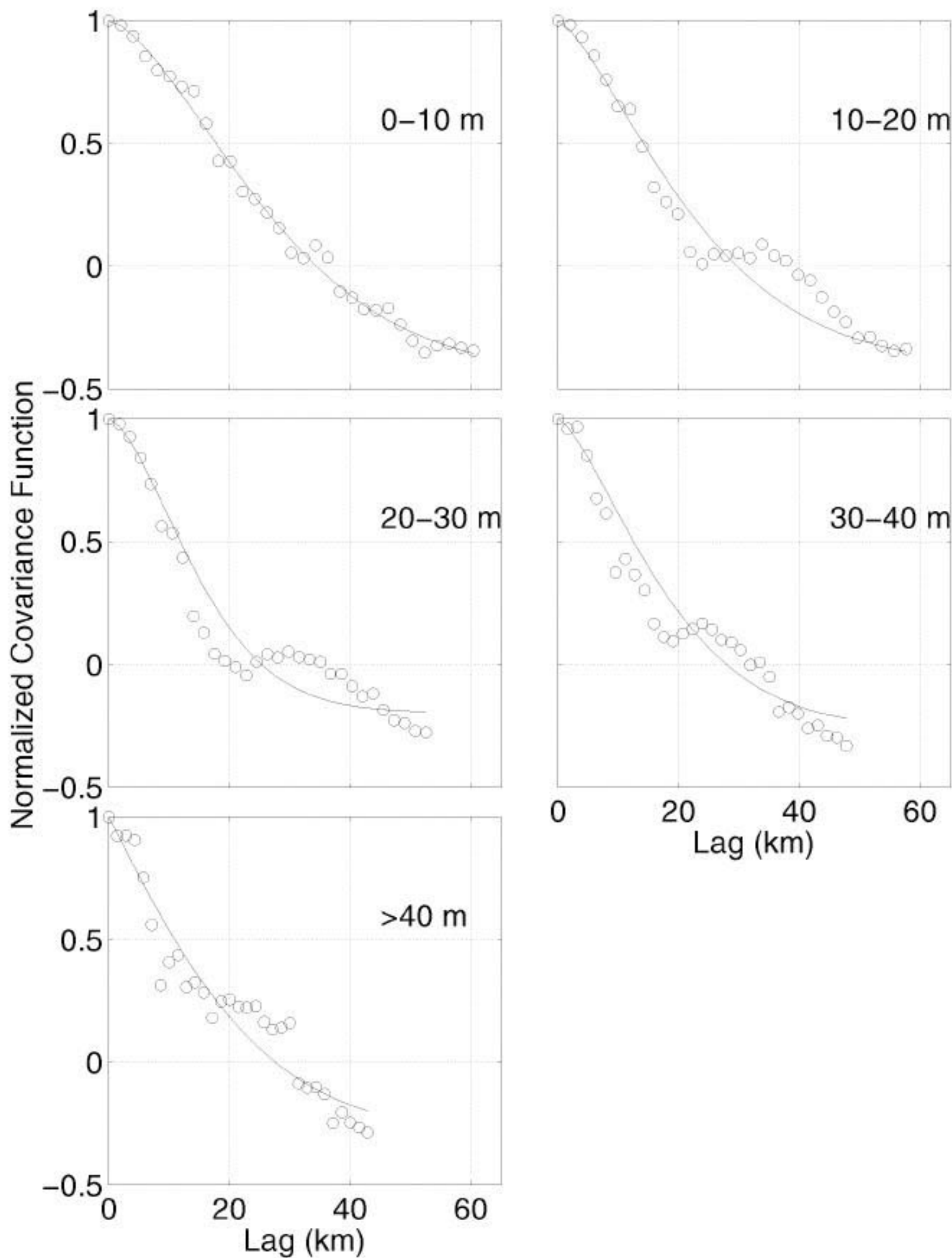
### Correlograms for Temperature (°C)



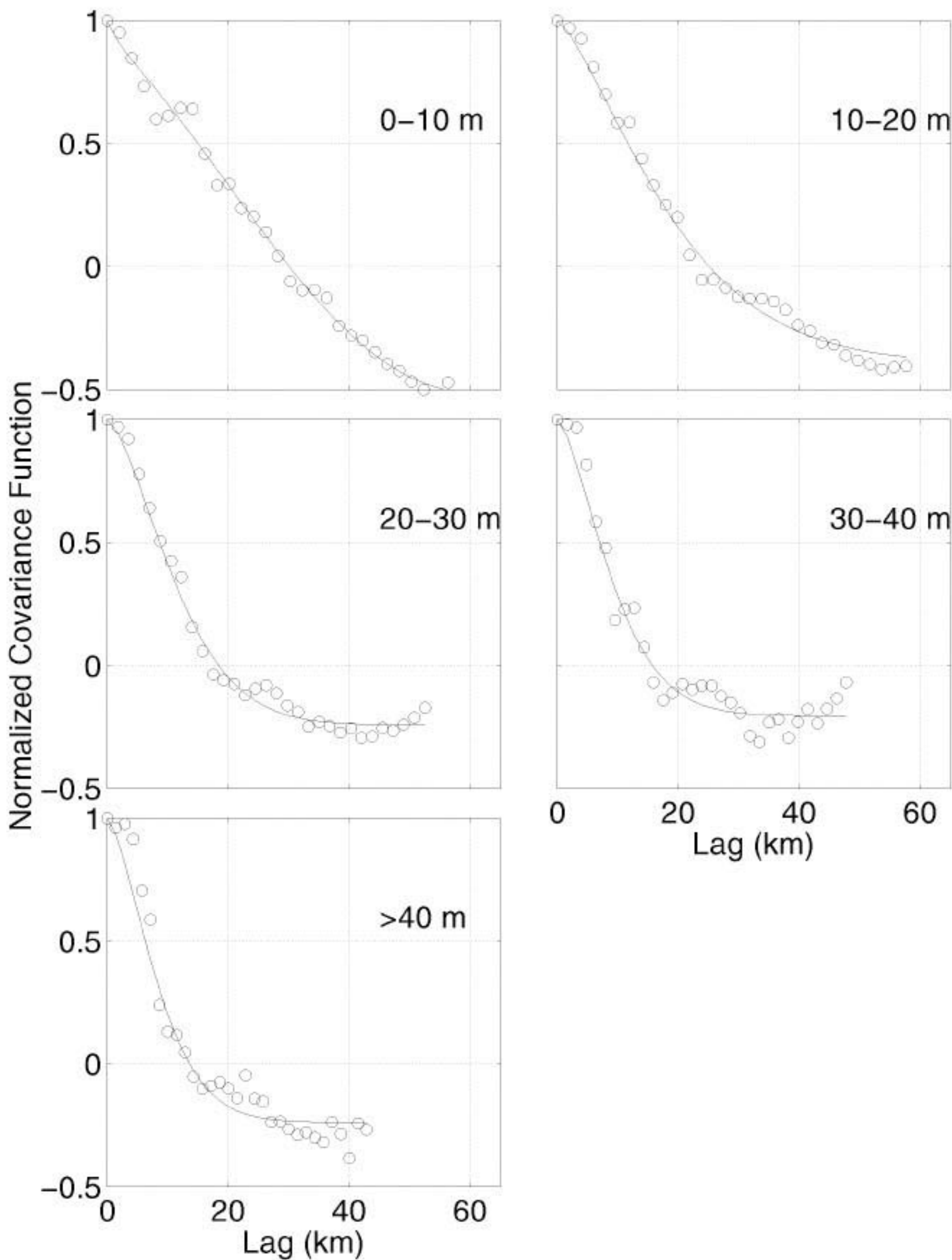
# Correlograms for Salinity (psu)



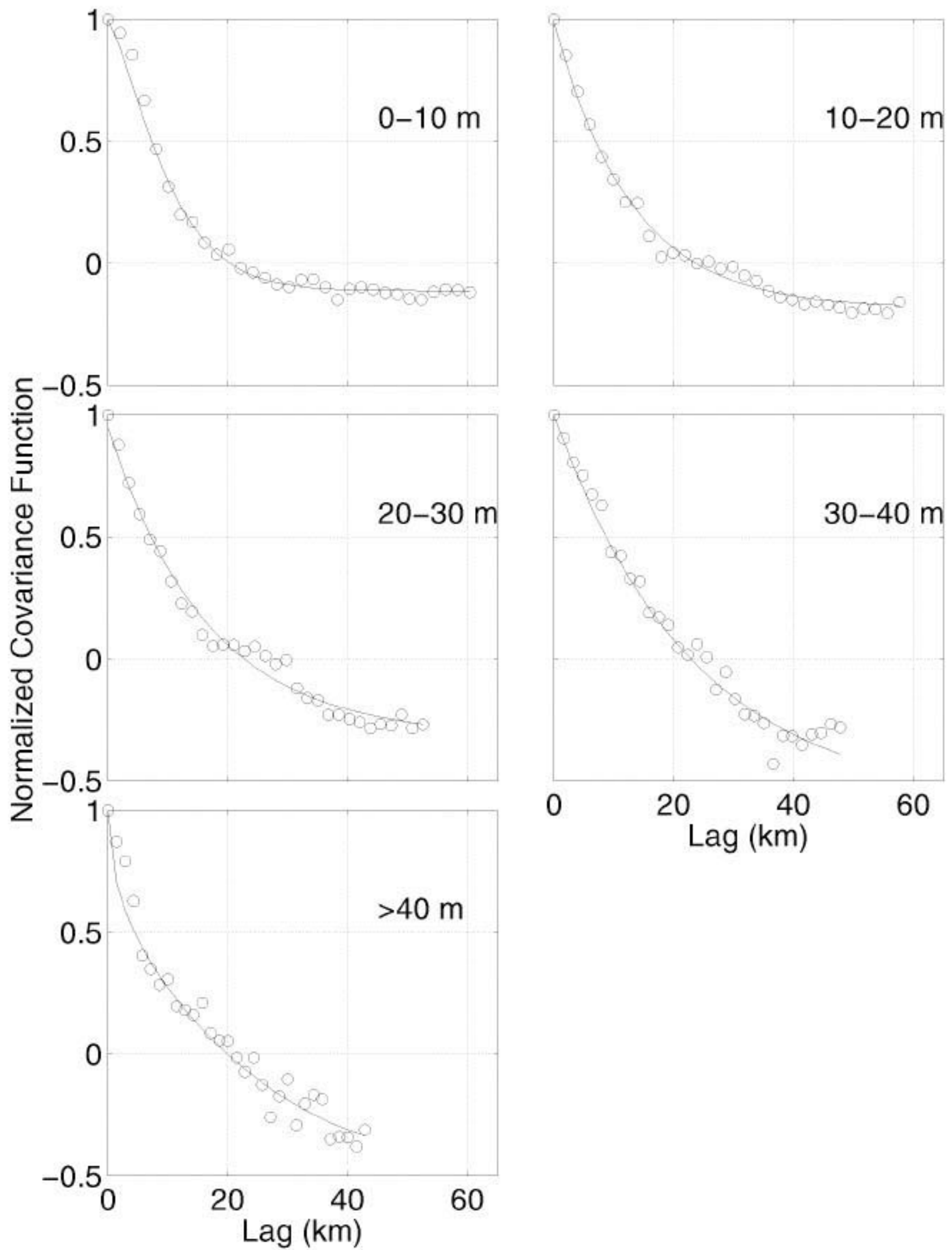
### Correlograms for Fluorescence ( $\mu\text{gChl/liter}$ )



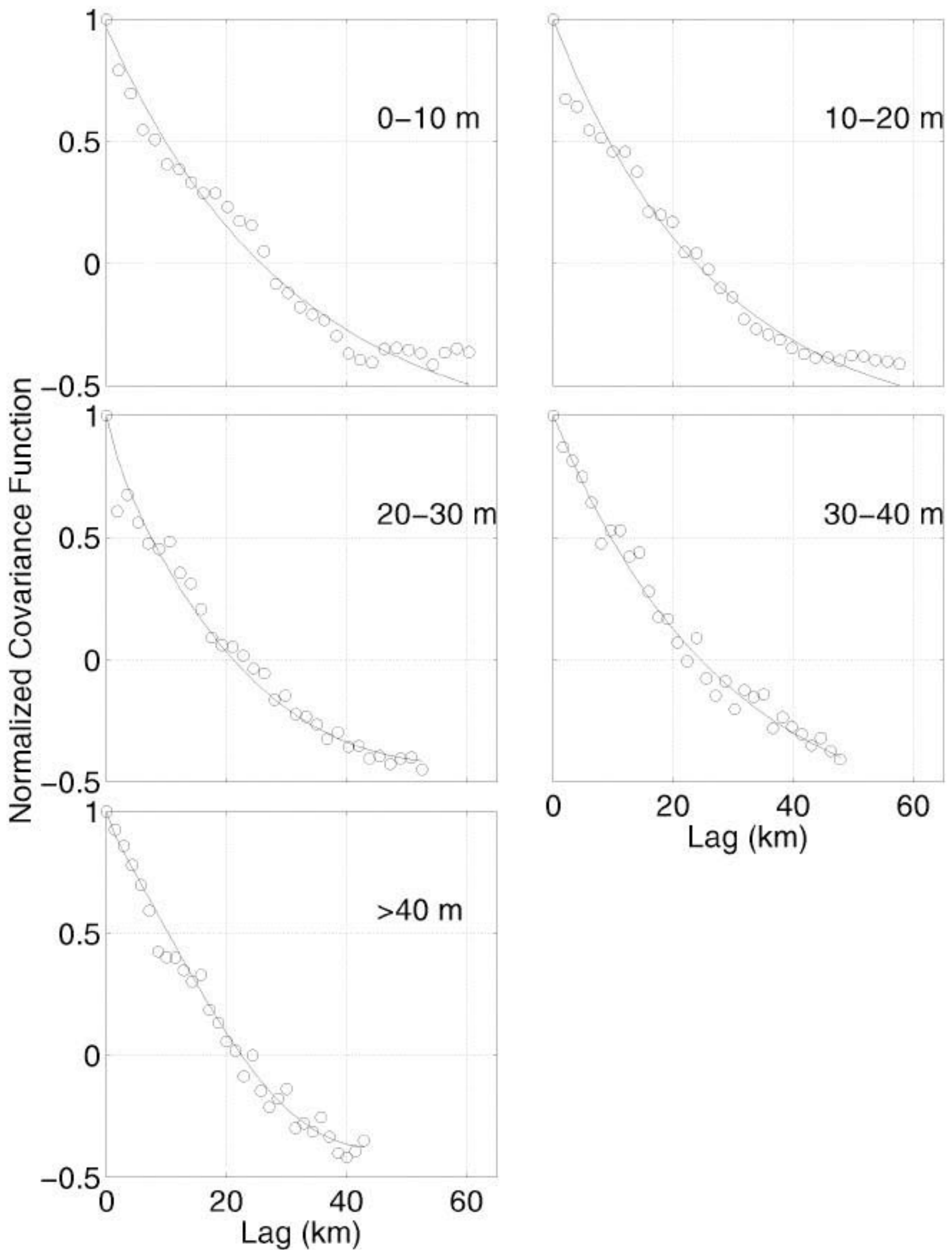
### Correlograms for Attenuation (beam-C)



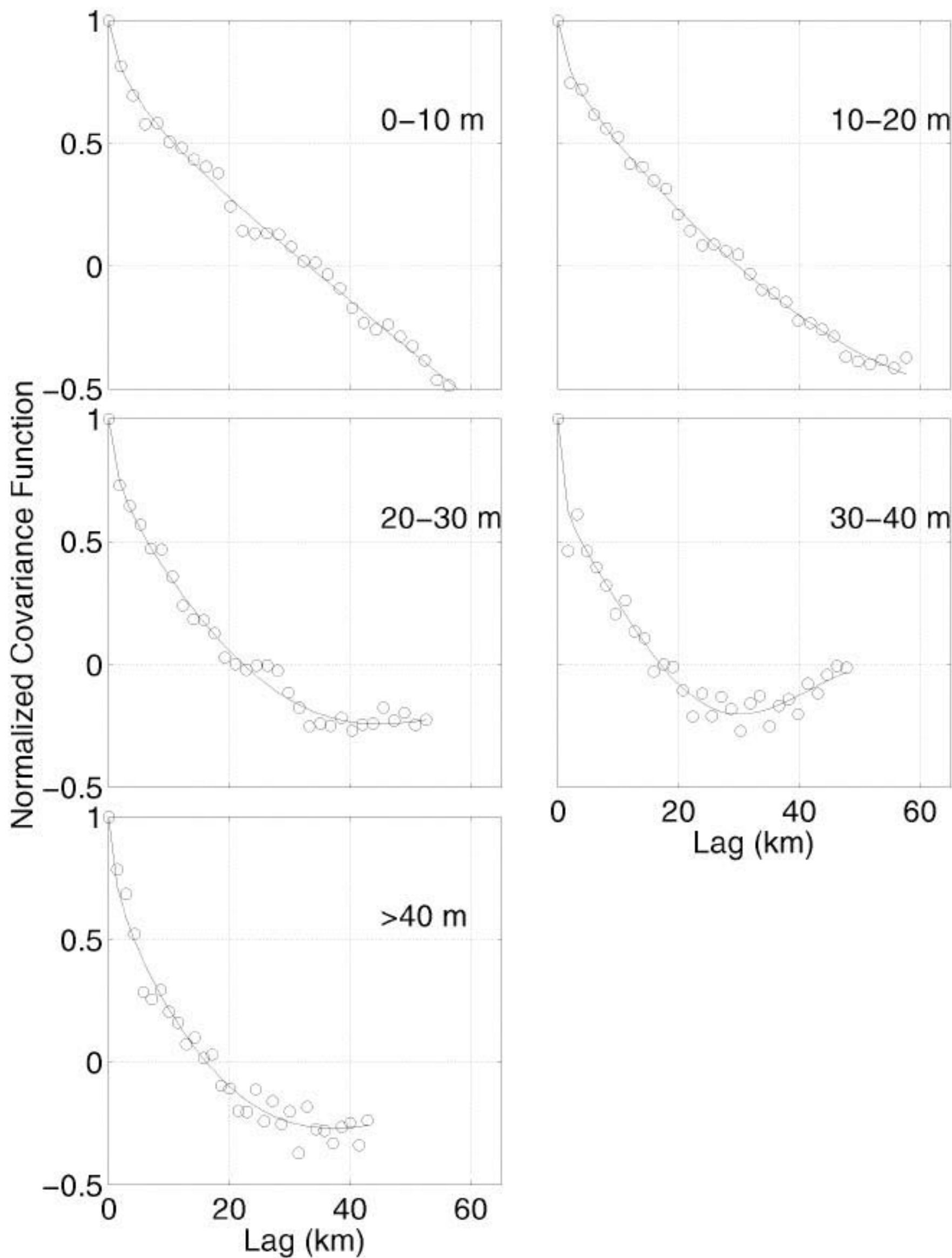
### Correlograms for Rod-shaped Diatoms (#/liter)



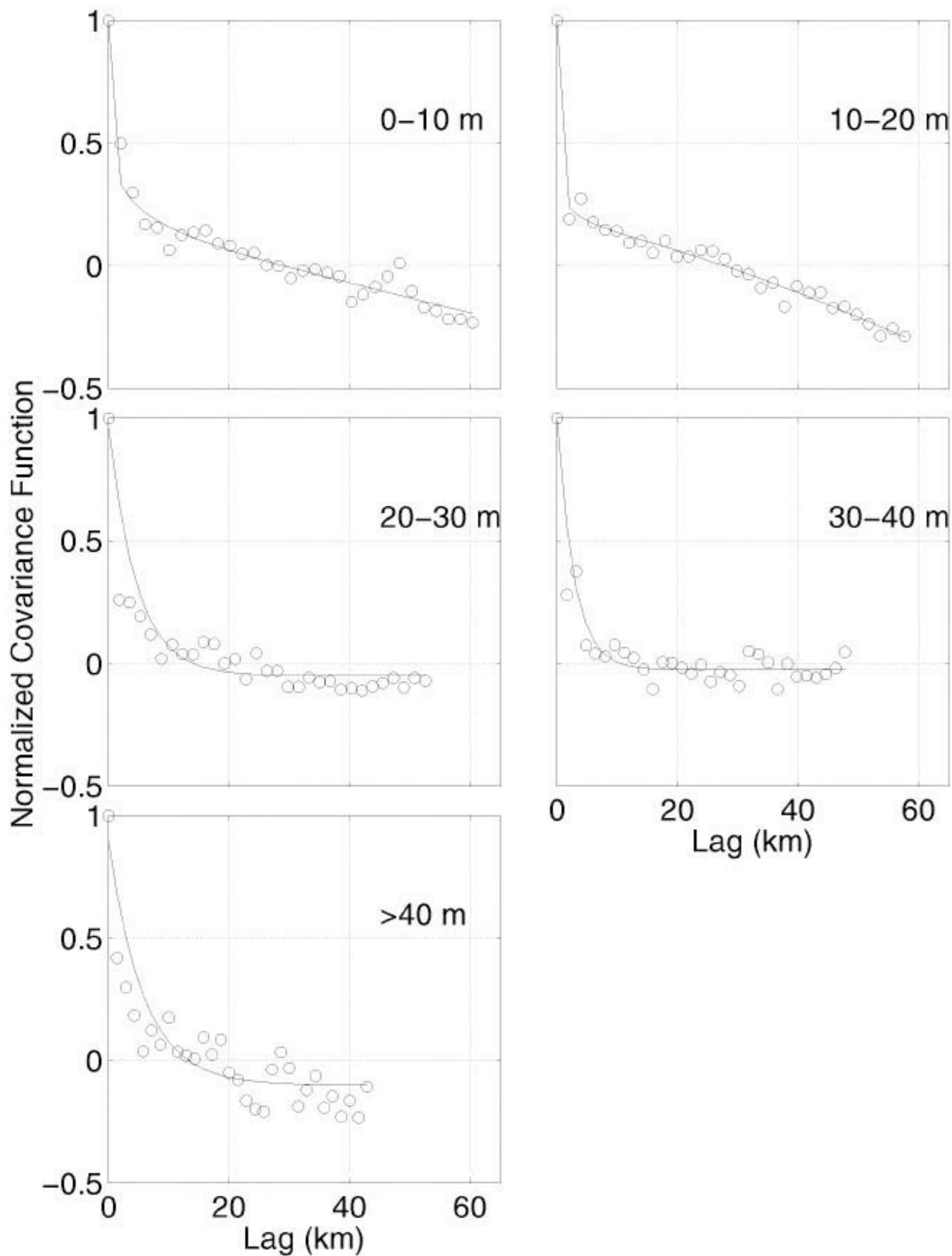
Correlograms for *Chaetoceros* chains (#/liter)



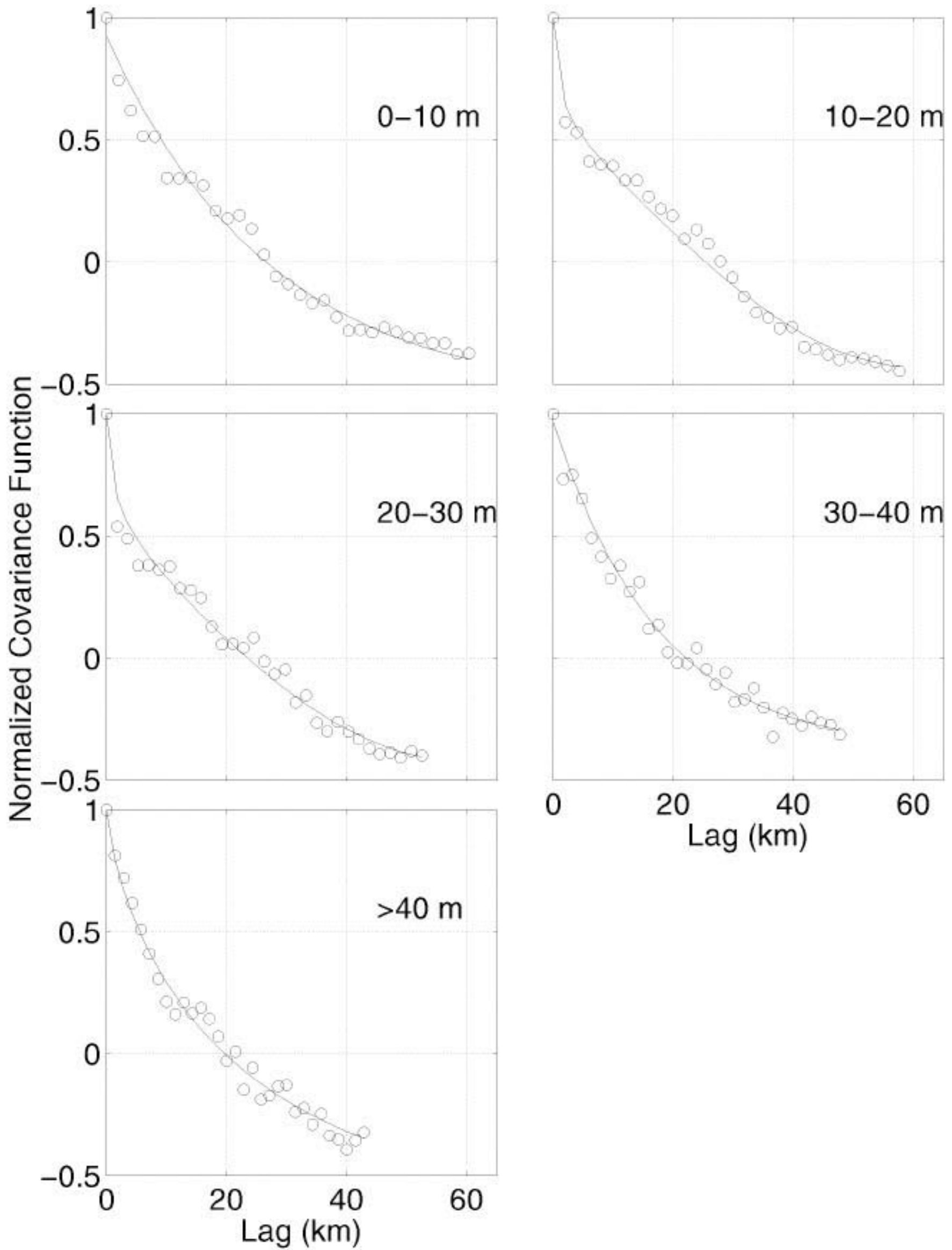
### Correlograms for *Oithona* (#/liter)



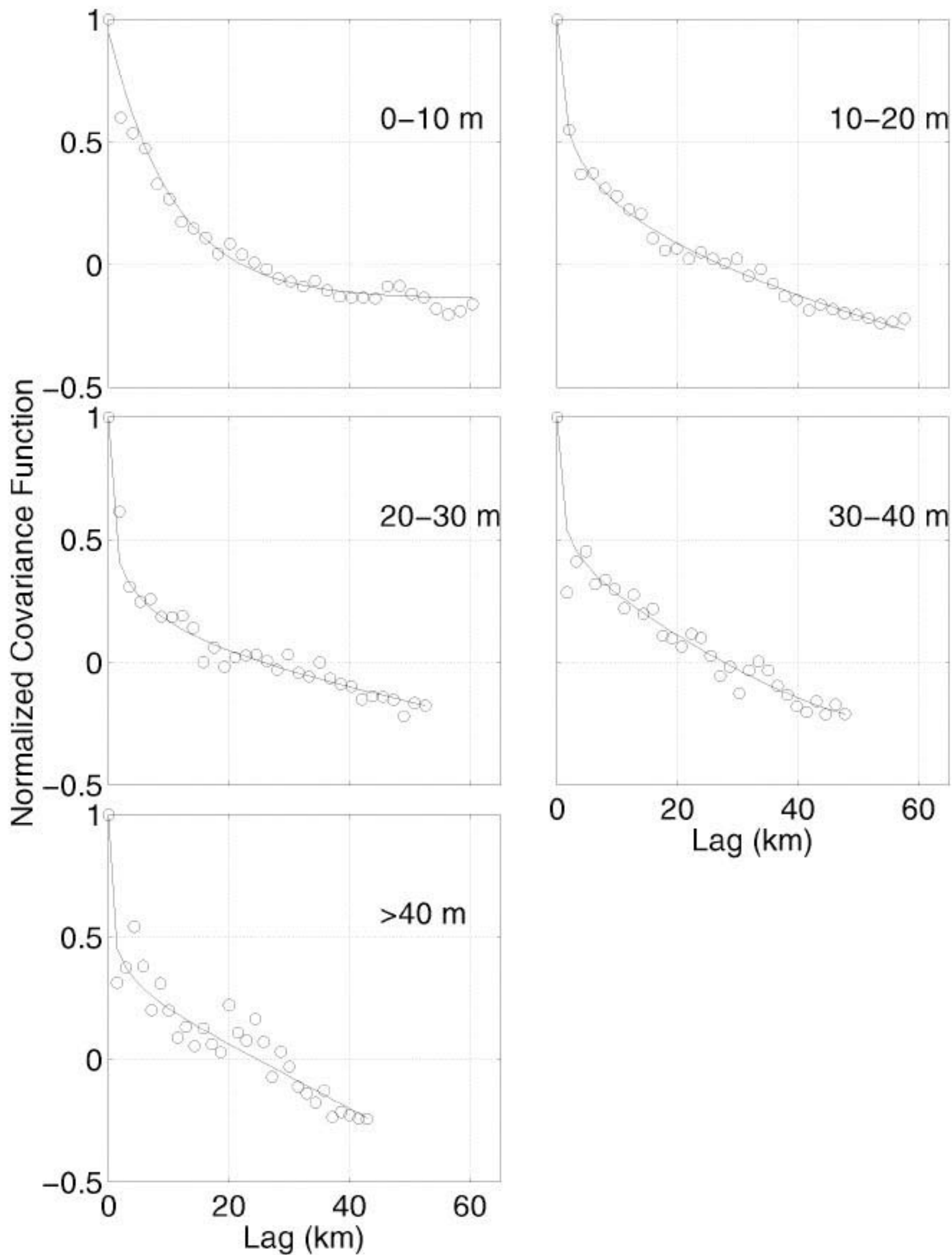
Correlograms for *Oithona* with eggs (#/liter)



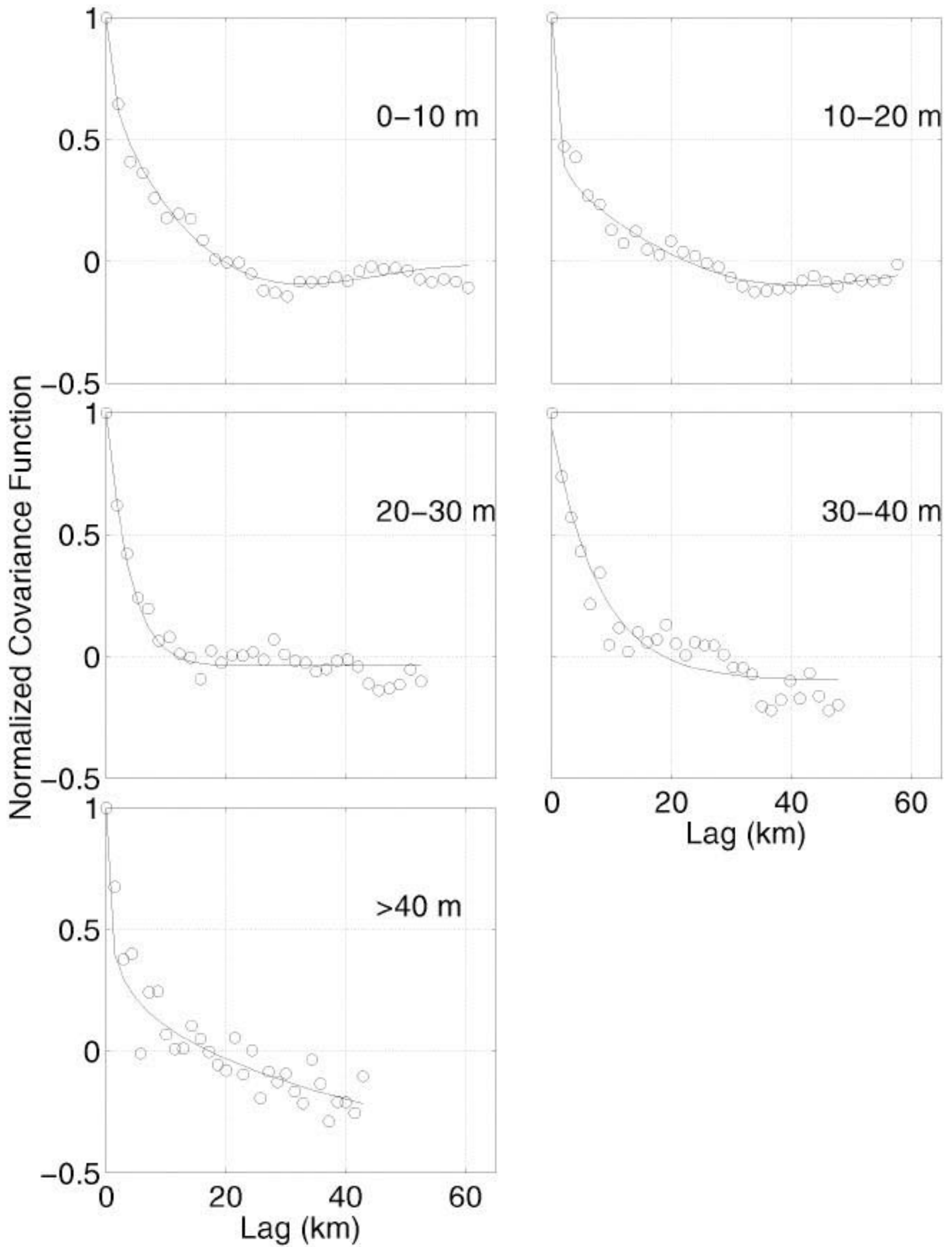
# Correlograms for Unidentified Copepods (#/liter)



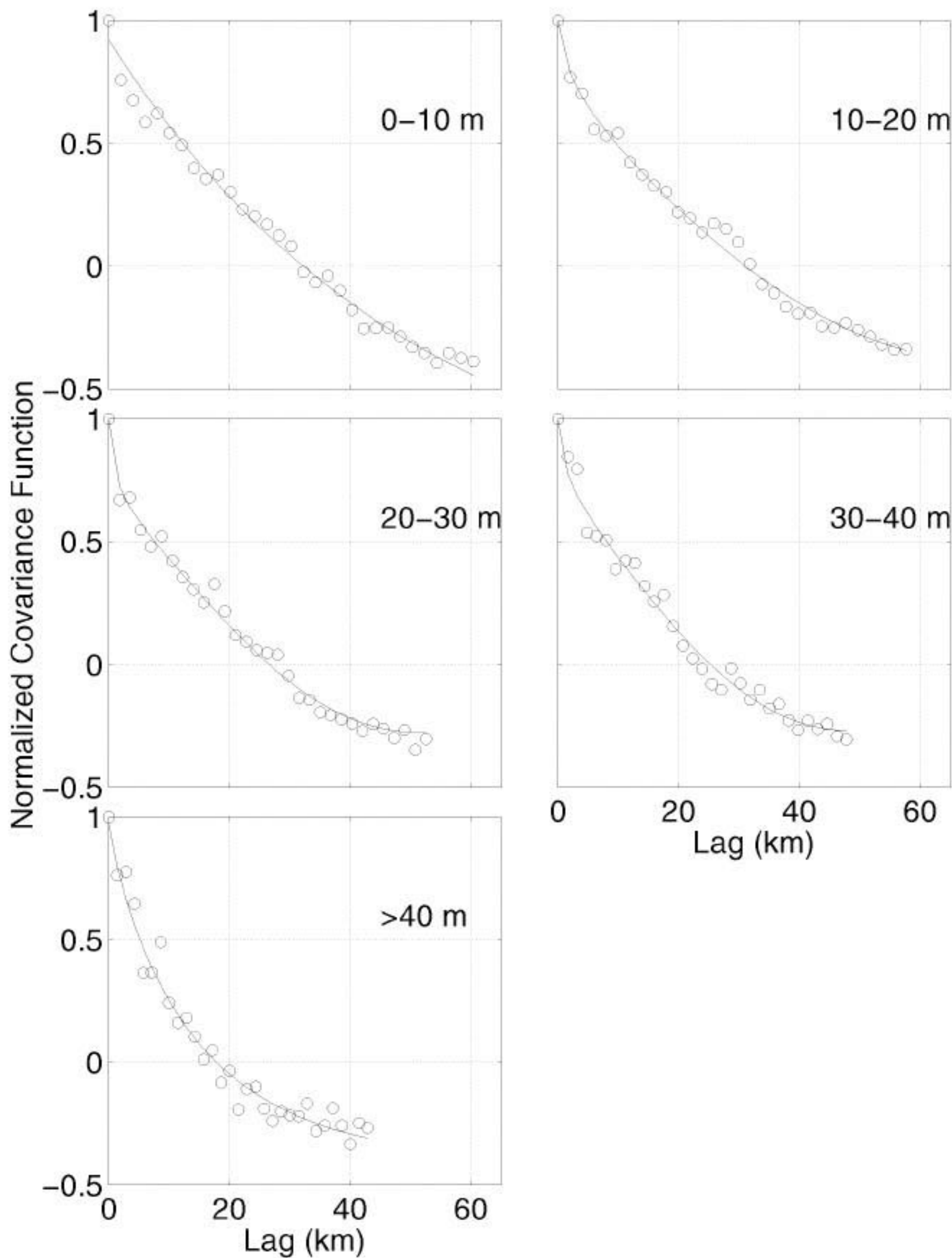
### Correlograms for Barnacle Larvae (#/liter)



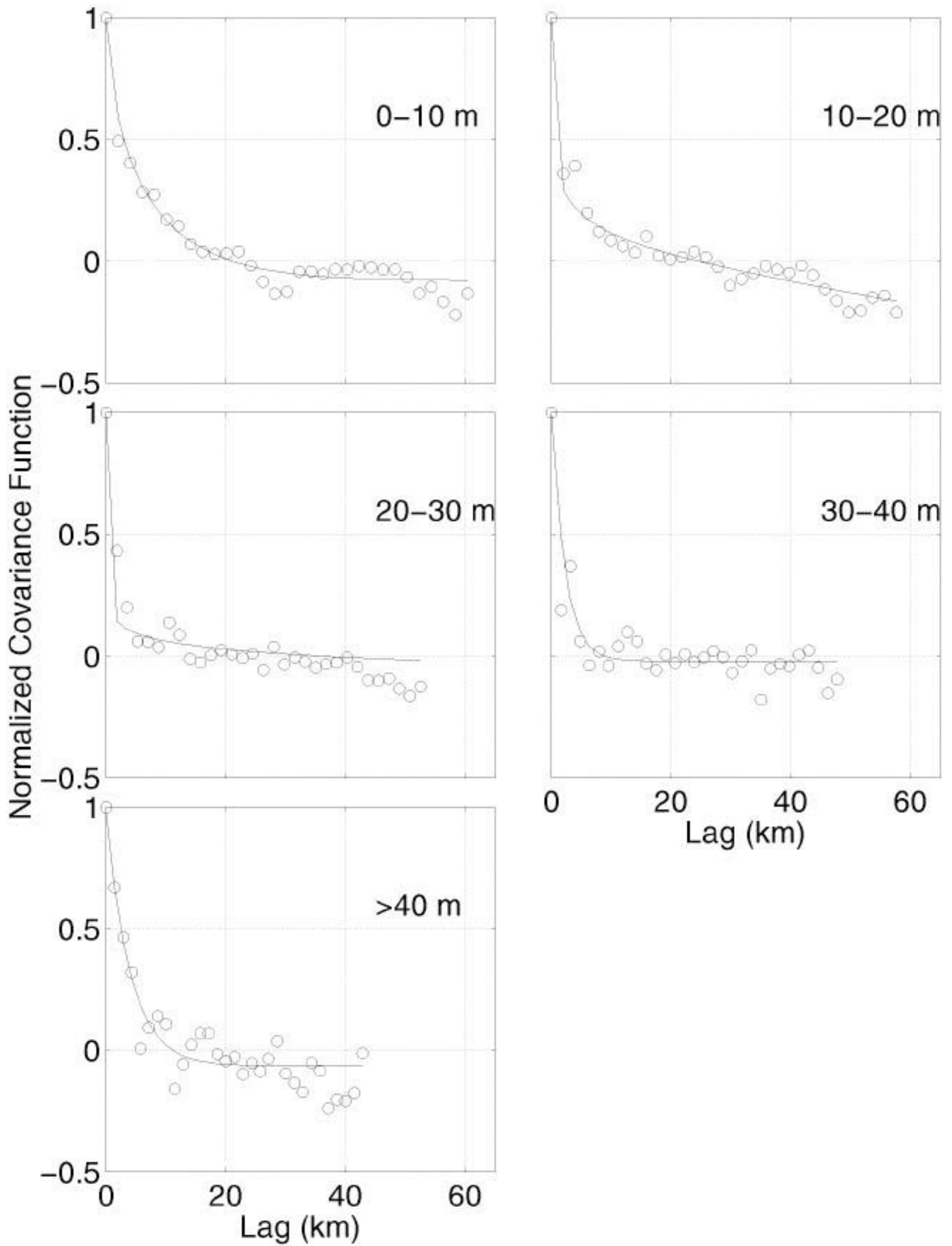
### Correlograms for Larvaceans (#/liter)



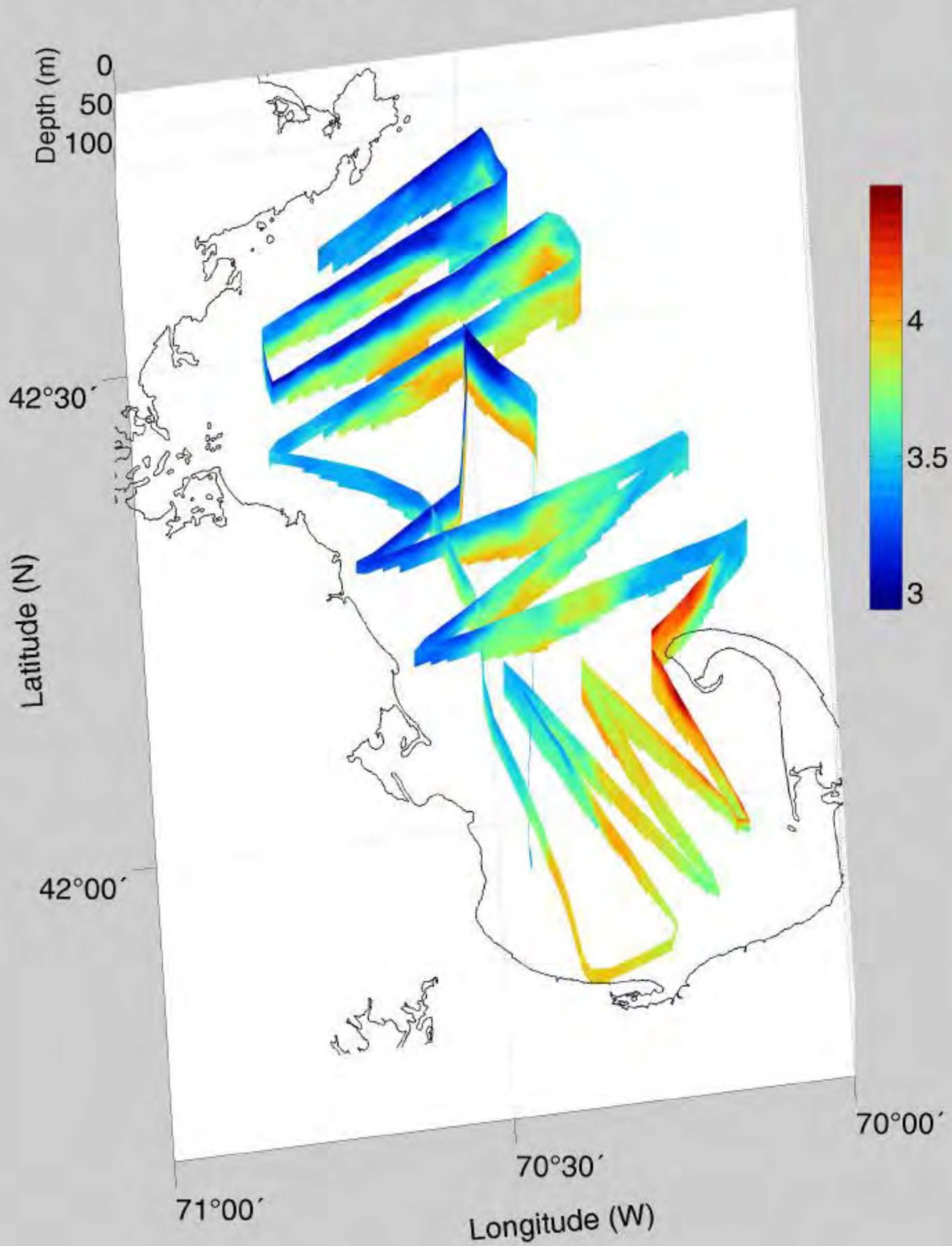
### Correlograms for Ostracods/cyprids (#/liter)



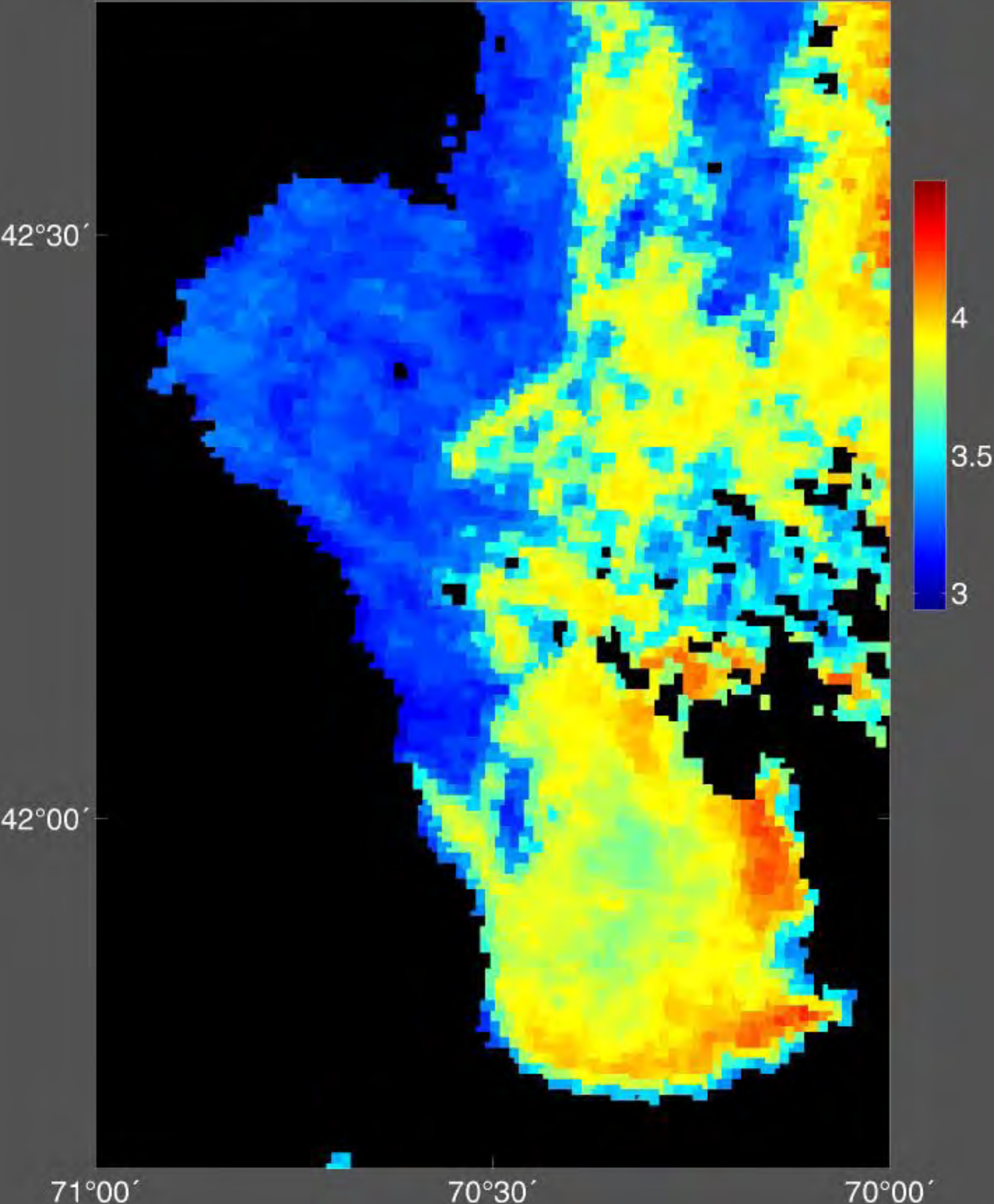
# Correlograms for Pteropods (#/liter)



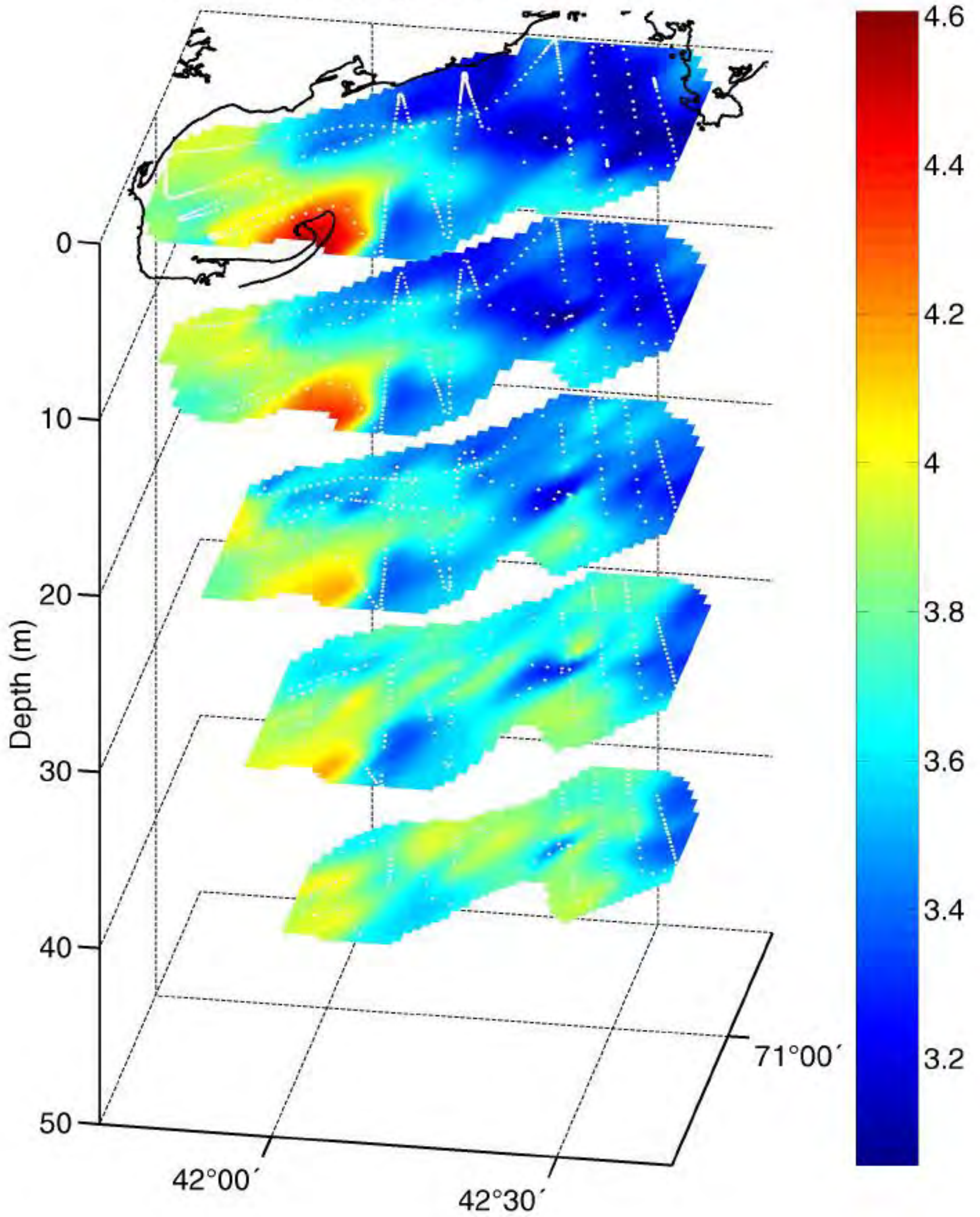
# Temperature (°C) March 12–14, 1998



AVHRR Image, March 13, 1998 (1052GMT) Temperature °C



Temperature ( $^{\circ}\text{C}$ ), March 12–14, 1998





Massachusetts Water Resources Authority  
Charlestown Navy Yard  
100 First Avenue  
Boston, MA 02129  
(617) 242-6000  
<http://www.mwra.state.ma.us>